UNIVERSITÄT ZU LÜBECK

From Lübeck Institute of Experimental Dermatology (LIED),
University of Lübeck
Director: Prof. Dr. Ralf Ludwig

In cooperation with

Institute for Experimental Immunology,

Affiliated to EUROIMMUN Medizinische Labordiagnostika AG

Director: Dr. Lars Komorowski

Characterization of cryptic Antinuclear Autoantibody target Antigens

Dissertation for the Fulfilment of Requirements
for the Doctoral Degree (*Dr. rer. nat.*)
of the University of Lübeck

from the Department of Natural Sciences

Submitted by

Zitao Zeng

from Fujian, China

Lübeck, 2020

First referee: Prof. Dr. Ralf Ludwig

Second referee: Prof. Dr. Rudolf Manz

Date of oral examination: 22.03.2021

Approved for printing: Lübeck, 23.03.2021

Abstract

Antinuclear autoantibodies (ANA) are specific markers of many systemic autoimmune rheumatic diseases (SARD), like systemic lupus erythematosus (SLE) or systemic sclerosis (SSc). The gold-standard screening system for ANA is the indirect immunofluorescence assay (IFA) with the human epithelial cell line HEp-2 as substrate. In serological diagnostic laboratories, unexplained ANA reaction patterns, which cannot be explained by any known autoantibody, occur regularly. The importance of such findings is difficult to evaluate, as studies on the clinical significance cannot be performed by the lack of appropriate monospecific tests. Therefore, this study focused on the identification of novel autoantigens of ANAs, establishment of suitable immunoassays for the candidate antigens and studying their clinical association.

90 sera were applied in fractionated immunoprecipitations with HEp-2 cells to identify unknown nuclear autoantigens (UNA). With the help of mass spectrometry ten candidate antigens were identified as nuclear VCP-like protein (NVL), 5'-3' exoribonuclease 2 (XRN2), interaction partner proline-, glutamic acid- and leucine-rich protein 1 and sentrin-specific protease 3 (PELP1, SENP3), CD2 antigen cytoplasmic tail-binding protein 2 (CD2BP2), transcription factor AP-2-alpha (TFAP2A), matrin-3 (MATR3), TAR DNA-binding protein 43 (TDP43), RuvB-like 1 and RuvB-like 2 homologs (RuvBL1, RuvBL2), replication protein A subunits (RPA1, RPA2, RPA3) and kinesin-like protein KIF11 (KIF11). These ten candidate antigens and other five from a previous project were recombinantly expressed in *E. coli* and/or HEK293 cells, which were applied in the further development of immunoassays. Nine of ten antigens were able to abolish the ANA reaction of the index serum in IFA and all ten reacted with each individual index serum in Western blot whereas healthy controls (N=15) were nonreactive. Additionally, the recombinant HEK293 cells-based IFA was applicable for thirteen candidates. A lineblot based on eight purified recombinant proteins and two recombinant HEK293 cells-based slides containing eleven candidate antigens for IFA were established. The immunoassays were applied to study the prevalence of ANAs against these antigens in a cohort of patients with systemic autoimmune rheumatic diseases (N=488). Autoantibodies against NVL, CD2BP2 and tight junction protein ZO-1 (TJP1) were found in 6/378, 8/378 and 15/378 sera of patients with SSc, respectively. Occasional positive cases

of these ANAs were detected in sera of patients with myositis (2/15, anti-NVL and anti-CD2BP2), mixed connective tissue disease (MCTD) (1/6, anti-CD2BP2) and undifferentiated connective tissue disease (UCTD) (1/10, anti-TJP1).

In conclusion, among ten identified nuclear autoantigens, seven have not been described before. The ten candidate antigens and five other candidate antigens from a previous project were successfully verified with at least one method and the corresponding immunoassays were established. ANAs against NVL, CD2BP2 and TJP1 showed an association with SSc and might be potential SSc markers.

Zusammenfassung

Antinukleäre Autoantikörper (ANA) sind spezifische Marker für viele systemische rheumatische Autoimmunerkrankungen wie systemische Lupus erythematodes (SLE) oder systemische Sklerose (SSc). Der Goldstandard des ANA Nachweis ist die indirekte Immunfluoreszenztest (IFT) mit HEp-2-Zellen als Substrat. In serologischen Diagnostiklaboren treten regelmäßig unaufgeklärte ANA-Reaktionsmuster auf, die durch keinen bekannten Autoantikörper erklärt werden können. Die klinische Relevanz dieser Befunde ist schwer einzuschätzen, da Studien zur Bewertung der klinischen Assoziation ohne monospezifische Tests nicht durchgeführt werden können. Um diese Lücke zu schließen ist die Aufklärung der Reaktionsmuster deshalb von großem Interesse. Ziel der vorliegenden Arbeit war es, diese neue Autoantigene zu identifizieren, geeignete Immunassays zu etablieren und auf klinischen Assoziationen zu charakterisieren.

Zur Identifizierung unbekannter nukleärer Autoantigene (UNA) wurden 90 Seren in fraktionierten Immunpräzipitationen mit HEp-2-Zellen eingesetzt. Mit Hilfe massenspektrometrischer Analysen wurden zehn Kandidatenantigene identifiziert: *nuclear VCP-like protein* (NVL), *5'-3' exoribonuclease 2* (XRN2), Interaktionspartner *proline-, glutamic acid- and leucine-rich protein 1* und *sentrin-specific protease 3* (PELP1, SENP3), *CD2 antigen cytoplasmic tail-binding protein 2* (CD2BP2), *transcription factor AP-2-alpha* (TFAP2A), *matrin-3* (MATR3), *TAR DNA-binding protein 43* (TDP43), *RuvB-like 1* und *RuvB-like 2* Homologe (RuvBL1, RuvBL2), Untereinheiten des *replication protein A* (RPA1, RPA2, RPA3) und *kinesin-like protein KIF11* (KIF11). Diese und weitere fünf Kandidatenantigene aus einem früheren Projekt wurden rekombinant in E. coli und / oder HEK293-Zellen exprimiert und anschließend für die Entwicklung von Immunassays verwendet. Neun von zehn Antigenen konnten die ANA-Reaktion des Indexserums im IFT aufheben und mit allen zehn reagierte das jeweilige Indexserum im Western Blot. Kontrollseren (N=15) gesunder Blutspender waren hingegen nicht reaktiv. Zudem zeigte für dreizehn Kandidatenantigene das jeweilige Indexserum eine positive Reaktion im IFT mit rekombinanten HEK293-Zellen (RC-IFT). Ein Linienblot basierend auf acht aufgereinigten rekombinanten Proteinen sowie zwei Objektträgern mit rekombinanten HEK293-Zellen für elf Kandidatenantigene wurden hergestellt. Mit Hilfe dieser Immunassays wurde die Prävalenz von ANA gegen die Kandidatenantigene in einer

Kohorte von Patienten mit systemischen rheumatischen Autoimmunerkrankungen (N=488) untersucht. Autoantikörper gegen NVL, CD2BP2 und *tight junction protein ZO-1* (TJP1) wurden in 6/378, 8/378 und 15/378 Seren von Patienten mit SSc gefunden. Weitere positive Reaktionen zeigten Seren von Patienten mit Myositis (2/15, anti-NVL und anti-CD2BP2), gemischten Bindegewebserkrankungen/MCTD (1/6, anti-CD2BP2) und undifferenzierten Bindegewebserkrankung/UCTD (1/10, anti-TJP1).

Sieben der zehn identifizierten nukleären Autoantigene wurden bisher nicht in der Literatur beschrieben. Die zehn Kandidatenantigene und die fünf weiteren Kandidatenantigene aus einem früheren Projekt wurden mit mindestens einer Methode erfolgreich verifiziert und die entsprechenden Immunassays wurden etabliert. ANA gegen NVL, CD2BP2 und TJP1 zeigten eine Assoziation mit SSc und stellen somit potenzielle SSc-Marker dar.

Acknowledgement

I would like to gratefully and sincerely thank my supervisors, Prof. Dr. Ralf Ludwig and Dr. Lars Komorowski for their excellent guidance, understanding and patience. During the dissertation period, they encouraged me and assisted me in getting through the difficulties.

I would like to express my in-depth appreciation to Dr. Wolfgang Schlumberger and Prof. Dr. Winfried Stöcker that I have got the opportunity to do my PhD thesis at the EUROIMUN AG. I am very thankful for their support.

I would also like to thank my both mentors, Dr. Ramona Miske and Dr. Madeleine Scharf, for providing with valuable suggestions and assistance during this whole research work, and in keeping my progress on schedule. Their willingness to give their time so generously has been very much appreciated.

I am particularly grateful for the help provided by the DFG funded Research Training Group (RTG) 1727, for getting me associated and many treasurable advices given by the other PhD students, researchers and PIs. The pure friendly scientific atmosphere created by the RTG members makes me feel like academic home. Here, I want to thank especially Prof. Dr. Jennifer Hundt and Prof. Dr. Xinhua Yu for their mentally and practically guidance and encouragement.

My thanks go to the members of the Institute for Experimental Immunology of the EUROIMMUN AG, especially the neuroimmunological and the immunobiochemical research teams in Dassow. They are warmhearted and have helped me with the experimental procedures and instruments. I have so many pleasant memories with them. Special thanks are addressed to Susann Satow, Laura Olejko, Melanie König, Sina Turek and Kristin Tüttenberg for their technical support, friendship and collegiality during the experimental works. Assistance in mass spectrometry provided by Yvonne Denno and Mareike Asmer was greatly appreciated.

I would like to thank external collaborators, Prof. Dr. L. E. C. Andrade from Universidade Federal de São Paulo and Dr. E. Siegert from University Hospital Charité, for providing the sera for this work.

I wish to thank various people for their contribution to this project; Dr. Thomas Nitzsche, for his support in protein purification, his friendship and encouragement;

Acknowledgement

Dr. Christian Probst, Dr. Mandy Unger, Stefanie Brakopp and their team for providing the assistance in recombinant synthesis of proteins; Dr. Milena Lipkowski and colleagues for the advice and support in cell cultures; Viktor Schmalz and Detta Franck, for their great collaboration and assistance; Dr. Iswariya Venkataraman, Dr. Nora Begemann and Dr. Stefanie Hahn, for their advice and support.

Last but not least, I want to express my gratitude to my parents, though there is long physical distance, for their support and care all the way.

Abbreviation

ACR	American college of rheumatology
AchR	Acetylcholine receptor
AD	Autoimmune disease
AIH	Autoimmune hepatitis
ALS	Amyotrophic lateral sclerosis
ANA	Antinuclear autoantibody
APA	Advanced protein assay
AS	Ammonium sulfate
ASS	Anti-synthetase syndrome
BCA	Bicinchoninic Acid
Cat-IEX	Cation exchange chromatography
CAR	chimeric antigen receptor
CAAR	chimeric autoantibody receptor
CBA	Cell based assay
CHT	CHT^{TM} Ceramic Hydroxyapatite
CLIA	Chemiluminescence immunoassay
CV	Column volume
DTT	Dithiothreitol
DM	dermatomyositis
DNA	Deoxyribonucleic acid
dsDNA	Double-strand DNA
Dsg1	Desmoglein 1
Dsg3	Desmoglein 3
ELISA	Enzyme-linked immunosorbent assay
EULAR	European league against rheumatism
FIP	Fractionated immunoprecipitation
FITC	Fluorescein isothiocyanate
FTD	Frontotemporal lobar degeneration
HEp-2	Human epithelial type 2
IAA	Iodoacetamide
IBM	Inclusion body myositis
IFA	Indirect immunofluorescence assay
IgG	Immunoglobulin G

IMAC	Immobilized metal ion affinity chromatography
IP	Immunoprecipitation
FBS	Fetal bovine serum
LE	Lupus erythematosus
MALDI-TOF	Matrix Assisted Laser Desorption/Ionization - Time of Flight
MAGUK	Membrane associated guanylate kinase
MCTD	Mixed connective tissue disease
MS	Mass spectrometry
NP40	Nonidet™ P 40 substitute solution
PAGE	Polyacrylamide gel electrophoresis
PBC	Primary biliary cholangitis
PC	Positive control
PMSF	Phenylmethanesulfonyl fluoride
PMF	Peptide mass fingerprinting
PS	Penicillin-Streptomycin
pSS	Primary Sjögren syndrome
RA	Rheumatoid arthritis
RC-IFA	Recombinant HEK293 cells based indirect immunofluorescence assay
RIPA	Radio immunoprecipitation assay
RNA	Ribonucleic acid
RNP	Ribonucleoprotein
RT	Room temperature
SARD	Systemic autoimmune rheumatic disease
SCLC	Small-cell lung carcinoma
scFv	Single-chain variable fragment
SDS	Sodium dodecyl sulfate
SjS	Sjögren's syndrome
SLE	Systemic lupus erythematosus
SSc	Systemic sclerosis
TRIM	Tripartite-motif protein
TSHR	Thyroid-stimulating hormone receptor
UCTD	Undifferentiated connective tissue disease
UFO	Unknown fluorescence object
UNA	Unknown nuclear autoantigen

Table of contents

Table of contents

1 Introduction

1.1 Autoimmunity and autoimmune diseases

The immune system is a complex network and has important functions in preventing infection. Generally, the immune system is subclassified as innate immunity and adaptive immunity, where the innate immune response reacts relatively fast, but is less specific against the pathogens; the adaptive immune response is subsequently activated and has a high specificity. The ability to distinguish self- and non-self-components is of great importance for the immune system to implement its functions [1]. When an antigen is exposed to the immune system, specific antibodies produced by plasma cells can bind to the antigen and neutralize it, which aids in phagocytosis, or complement-mediated lysis and ultimately results in destruction of the pathogen [1]. Generally, the immune system shows low-level response against self-components. These autoimmune responses are important in maintaining the homeostasis and blocking potential dangers, like clearance of abnormal cells and cancer cells [2, 3]. But with the loss of immunological tolerance, the number of autoreactive B cells and T cells can massively increase [4]. Though low-level autoimmunity is thought to be beneficial, breakdown of immunological tolerance and high-level of autoimmunity lead to autoimmune diseases (AD). More than 80 different autoimmune related chronic disorders are known so far [5, 6]. Approximately 5-8% of the western population are suffering from ADs, of which more than two third are women, and the incidence of ADs increased over the last devades [1, 3]. Depending on the type and the target of autoimmune response, the severity of ADs varies from mild to lethal. Though the exact causes of ADs remain unknown, it is generally accepted that ADs are the result of a complex interaction between genetic and environmental factors [2, 3]. Certain genotypes of human leukocyte antigens (HLA) associate to higher risk of having ADs, for example HLA-DRB1 was reported to represent the major determinant of genetic predisposition to rheumatoid arthritis [3, 7]. Environmental factors, like infections, ultraviolet radiation exposure, nutrition, drug and environmental pollutants, play also important roles in the development of autoimmunity [3].

The adaptive immune response is activated after (auto)antigens are presented to the immune system. Different kinds of mature T cells, including cytotoxic T cells and T

helper cells, are produced through cell-mediated immunity. On the other hand, autoantibodies are produced by plasma cells representing the humoral immunity. Unwanted inflammation appears as the cytotoxic T cells and autoantibodies bind to self-antigens. The autoimmune diseases can be classified into organ-specific or systemic ADs. For organ-specific ADs, the autoimmune response is limited to certain organs. For example in type 1 diabetes, the autoimmune reaction is limited to the pancreas, where pancreatic β cells are attacked and destroyed by cytotoxic T cells [8]. In systemic ADs, like systemic lupus erythematosus (SLE), the autoantibodies bind to released nuclear autoantigens after apoptosis and deposited immunocomplexes cause strong inflammation [9].

1.2 Autoantibodies

Autoantibodies are observed not only in patients with ADs, but also in patients with cancer and even in healthy individuals. Naturally occurring autoantibodies are tightly regulated by regulatory T cells and play important roles in defending the body against infections and removing the waste products, like apoptotic cells [4]. These autoantibodies show low affinity and low specificity to a broad spectrum of antigens including pathogens and autoantigens [10]. Additionally, depending on the class and subclass of the autoantibodies and their post-translational modification, like glycosylation and sialylation, it is been documented that they have a protective role in autoimmune diseases and suppression of inflammation [10]. The generation of autoantibodies can be stimulated by tumor cells that express autoantigens with abnormal modifications. It has been reported that autoantibodies against nuclear antigens are detected in patients with cancer, which is considered as a risk for development of ADs [11]. Infection and acute tissue damage can also trigger the production of autoantibodies. A study showed that liver damage under oxidative stress can result in induction of antimitochondrial autoantibodies [12]. However, because of the different immunological backgrounds, the patients with autoantibodies are not necessarily to develop ADs.

Autoantibodies have an important role in autoimmune diseases. Approximately, 3-5% of the population is affected by autoantibody-driven autoimmune diseases [10], which takes up more than 50% of ADs. Autoantibodies against cell-surface proteins are considered pathogenic as they can directly bind to their target antigens; on the other hand, autoantibodies targeting intracellular proteins are considered non-pathogenic,

but they are markers for T-cell mediated immune responses [13]. Though the pathology of some autoantibodies remains unclear, different pathogenic mechanisms of autoantibodies have been identified, including stimulation or blockage of receptors, or induction of uncontrolled cell lysis and inflammation [10]. Some representative examples are given in Table 1-1. As mentioned above, autoantibodies can also serve as diagnostic marker, but are not contributing to pathogenesis. For example, type 1 diabetes is a T-cell mediated AD. The presence of autoantibodies against intracellular GAD65 is the result of autoimmunity but not pathogenic [14].

Disease	Autoantibody targets	Consequence
Grave's disease	thyroid-stimulating hormone receptor (TSHR)	Stimulation of the TSHR causing hyperthyroidism
Myasthenia gravis	Acetylcholine receptor (AchR)	Blockage of the AchR resulting in degradation of the receptors and complement-mediated cell lysis
Pemphigus vulgaris	Desmoglein 3 (Dsg3) and in cases with skin inflammation also Desmoglein 1 (Dsg1)	Binding to Dsg3 causes destruction of desmosomes and consequently blistering of the skin
Autoimmune hemolytic anemia	Red blood cells	Lysis and destruction of red blood cells by complement and FcR phagocytes
Rheumatoid arthritis	Cyclic citrullinated proteins and IgG-Fc	Deposition of the immunocomplexes in the joints causing inflammation and bone destruction

Table 1-1 Examples of autoantibody-driven autoimmune diseases [4, 10]

1.2.1 Antinuclear autoantibodies (ANA) and associated diseases

ANAs are a group of autoantibodies that targets the nuclear components of mammalian cells. They are mainly associated with systemic autoimmune rheumatic diseases (SARD) and some of the ANAs are biomarkers for certain SARDs. For example, anti-double-strand DNA (dsDNA), anti-Sm and anti-ribosomal P are tightly associated with systemic lupus erythematosus (SLE); while anti-Scl70, anti-centromere and anti-RNA polymerase III are biomarkers for systemic sclerosis (SSc) [15]. Meanwhile, increasing evidence shows that elevated level of ANAs in cancer patients is significant in confronting tumor cells [11, 15, 16]. For example, multiple studies revealed that anti-dsDNA autoantibodies can induce the apoptosis of cancer cells and inhibit the growth of tumors [11, 17, 18, 19]. Some well-established ANAs for SARD are found to be associated with different cancers, for example anti-dsDNA,

anti-Ro/SS-A and anti-Scl70 are presented with gastrointestinal cancer, hematological malignancies and lung cancer respectively [11, 15, 16]. Additionally, ANAs could be detected in approximately 5.9-30.8% of healthy individuals, more frequent in women than in men; and elder people show higher rate of being ANA positive [15]. This increases the complexity of application of ANAs in diagnostic and thus urges the identification of individual ANA and the assessment of their clinical values.

1.3 ANA diagnostics

The immunoassay for the detection of ANA is dated back to 1948, Hargraves et al. discovered and applied lupus erythematosus (LE) cells in order to aid the diagnose of SLE patients, though it was found later that the LE cell test was neither sensitive nor specific enough [20]. In the late 1950s, the indirect immunofluorescence assay (IFA) based on animal tissue substrates, such as kidney from rats, was established. The principle of the test is that the specific ANAs bound to the antigens coated on object slides are detected by fluorescence labeled anti-human antibodies, which can be visualized under a fluorescence microscope. For the better evaluation of the result, the observed positive fluorescence signals are described as different patterns, like homogenous and granular, which is useful in subclassification of the positive results [21]. Another important parameter in the evaluation of the results is the highest serum dilution, with which the patterns are still visible; this is defined as titer. Two decades later, HeLa-derived human epithelial type 2 (HEp-2) cells, which show better sensitivity and specificity, were applied in the IFA. When compared to cryosection of animal tissues, HEp-2 cells have the advantage of a large nucleus and a better visibility of other organelles, high division rate and an expression profile with more than 100 autoantigens, which contributes to easier observation and interpretation of the results. According to the guideline for ANA tests, a negative IFA result indicates a non-SARD condition while a positive result should be further differentiated with available monospecific tests.

Monospecific ANA tests were developed as the corresponding nuclear autoantigens were identified since 1960s [21, 22]. Currently, different kinds of solid phase-based assays, including enzyme-linked immunosorbent assay (ELISA), lineblot, Western blot and chemiluminescence immunoassay (CLIA), are available with native or recombinant antigens. These tests have a similar principle as IFA, where the

secondary anti-human antibodies are labelled with enzymes or chemical compounds that can generate color-change reactions or light emission reactions [10].

1.3.1 Indirect immunofluorescence assay (IFA)

IFA with HEp-2 cells remains the gold standard for ANA screening because of its high sensitivity and specificity. This immunoassay cannot be replaced by others for different reasons. Firstly, the autoantigens are presented in a natural environment; secondly, it is possible to detect unidentified autoantigens and interpret the results by staining patterns; thirdly, a negative outcome is very useful in ruling out the SARD [10]. Due to the complexity of the staining patterns, the standardization of the interpretation of the IFA result was initiated by the international consensus on ANA patterns (ICAP) and is kept updated. So far, 29 different HEp-2 IFA patterns are defined, of which fifteen are nuclear patterns, nine cytoplasmic patterns and five mitotic patterns [23]. The recommended cutoff for IFA with HEp-2 is 1:80 according to the European league against rheumatism (EULAR) and the American college of rheumatology (ACR) [24]. Some representative nuclear patterns are shown in Figure 1-1.

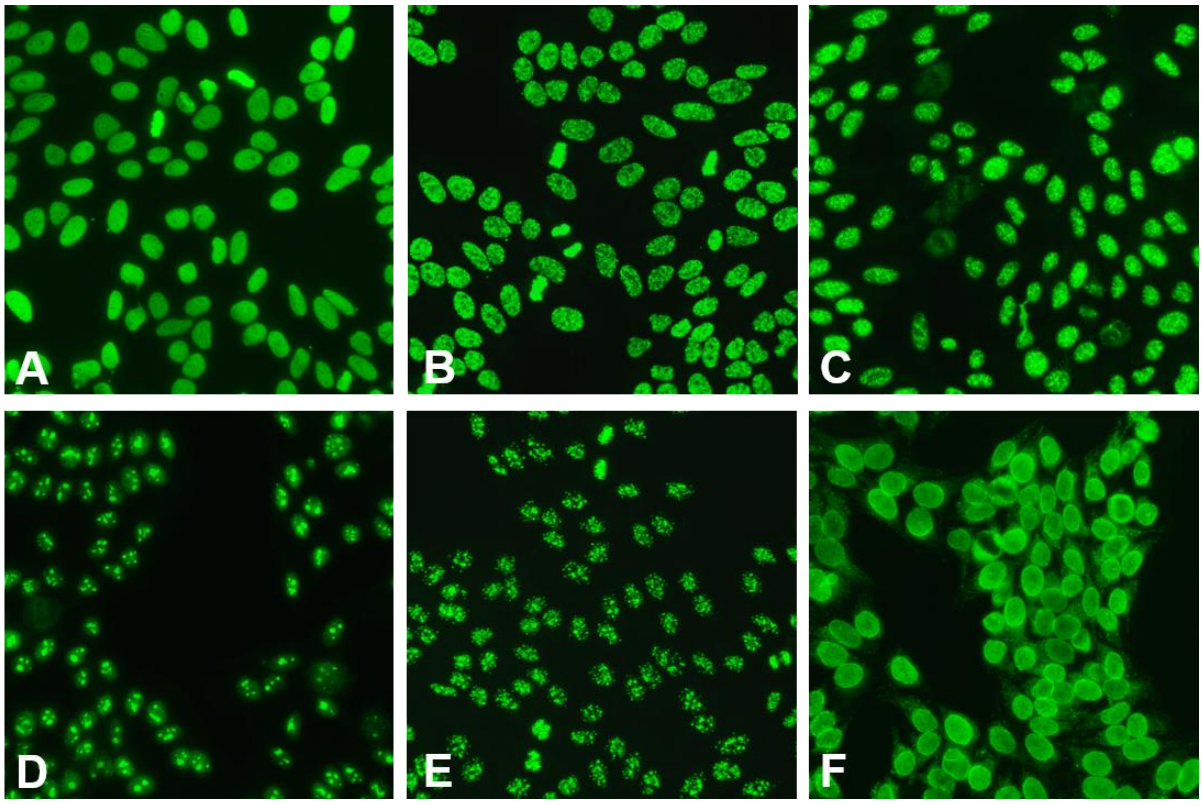

Figure 1-1 Representative IFA ANA pattern on HEp-2 cells
A) Homogenous, **B)** dense fine speckled, **C)** granular, **D)** nucleolar and granular, **E)** centromere, **F)** nuclear envelope.

1.3.2 Solid phase-based immunoassays

ELISA, lineblot, Western blot and CLIA are the most applied semiquantitative solid phase-based immunoassays in detection of ANAs, where ELISA is based on microtiter plates, lineblot and Western blot are based on membrane and CLIA is based on beads. These immunoassays require preparation of purified target autoantigens from native or recombinant resources. Therefore, the prerequisite for establishment of these immunoassays is that the autoantigens should be well-studied and a clear clinical relationship between the relevant ANAs and SARDs is revealed. Currently, tests with approximately 30 different nuclear autoantigens are commercially available for the detection of corresponding ANAs [25, 26]. These immunoassays are of great importance in the further differentiation of ANAs and a positive result helps in clinical diagnostics of a certain disease. When compared to IFA, the immunoassays based on purified antigens have the advantages of increased specificity, easier standardization of the methods and simpler interpretation of results.

1.4 Application of ANA diagnostics in clinical practice

The occurrence of high titers of ANAs may be years before the development of clinical syndromes. Arbuckle and colleagues have reported that ANAs could be detected in 88% of SLE patients in a mean of 3.3 years before onset of the disease [27]. This demonstrates the significance of ANAs in early diagnosis of the disease and a possible specific treatment. However, the utility of ANA diagnostics differs from one to another. Some of ANAs showed high disease specificity and are included in the diagnostic criteria and/or reflecting disease activity, while some others show weak association with SARD or even negative relations. Currently, the relationship between HEp-2 IFA patterns, autoantibodies and clinical symptoms is partly revealed. The five most often observed ANA patterns and their association with ANAs and SARDs are shortly summarized below.

1.4.1 Homogeneous

This pattern (Figure 1-1, A) is found in patients with SLE, autoimmune hepatitis and juvenile idiopathic arthritis. Anti-dsDNA, anti-nucleosome and anti-histone autoantibodies are the most frequent reasons for the presence of a homogenous pattern [23]. Other possible ANAs with less frequency for a homogenous pattern are anti-Scl70 autoantibodies, which can cause granular to homogenous pattern [23, 25]. Anti-dsDNA autoantibodies are the diagnostic marker for SLE, which are present in

43-92% of patients with SLE with a high specificity between 89-99% and sensitivity from 8 to 54% depending on the immunoassays applied. Meanwhile, it was shown that anti-dsDNA autoantibodies correlate with the disease activity and thus are considered as prognostic markers [15, 25].

1.4.2 Dense fine speckled (DFS)

As shown in Figure 1-1, B, the character of this pattern is dense fine granules in nucleus of interphase cells and chromosome area of mitotic cells. The distinction of DFS and homogenous patterns relies on experienced experts. One identified autoantibody that causes this pattern is the anti-DFS70 autoantibody, which targets lens epithelial derived growth factor. However, if the serum of a patient is only anti-DFS70 positive without additional positive reaction against other established ANAs, the patient has a very low probability of having SARD [28]. In another words, anti-DFS70 autoantibody is an exclusion marker for SARD. Anti-DFS70 positive autoantibodies explain 5-11% of ANA reactions in healthy blood donors and are observed in up to 30% of ANA positive sera [25].

1.4.3 Granular

The granular pattern (Figure 1-1, C) is also known as speckled pattern and has different subtypes according to the size of granules observed. This pattern shows low disease specificity and can be found in various SARDs, including SLE, SSc, SjS and dermatomyositis (DM). As a large number of nuclear proteins are located diffuse in the nucleoplasm, ANAs that lead to granular patterns are diverse. The representative well-established ANAs with granular patterns are present in Table 1-2.

ANA	Target antigens	SARD	Prevalence	Remark
Anti-RNP/Sm	snRNP core proteins B/B', D1, D2, D3, E, F and G	SLE	15-55%	Main targets: B/B', D1 and D3; very high specificity (99%); diagnostic and prognostic marker
Anti-Ro60	60 kDa SS-A/Ro ribonucleoprotein	SjS	33-77%	Diagnostic and risk marker for SjS; association with organs involvement in other SARDs
		SLE	36-64%	
		SSc	9%	
		RA	5-15%	
Anti-Ro52	TRIM21	SjS	17-63%	Less specific than anti-Ro60; associated with the risk of interstitial lung disease and pulmonary fibrosis in SARDs
		SLE	23%	
		SSc	20%	
		PBC	28%	
		AIH	17%	
		ASS	30%	
Anti-La/SS-B	Lupus La protein	SjS	23-47%	Diagnostic marker for SjS
		SLE	8-33%	
Anti-Scl70	Topoisomerase I	SSc	30-41%	Very high specificity (>99%); diagnostic, prognostic and risk marker
Anti-Ku	X-ray repair cross-complementing protein 5 and 6	SSc	1-4%	Rarely detected; indicator for overlap syndrome
		SLE	2%	
Anti-RNA polymerase III	Subunits of RNA polymerase III	SSc	3-19%	Often cooccurrence with anti-RNAP I and II; very high specificity (98-100%)
Anti-U1RNP	U1-snRNP 70 kDa, A and C	SSc	10%	MCTD diagnostic criterion: anti-U1-RNP detection without presence of anti-Sm and anti-dsDNA
		SLE	13-32%	
		MCTD	100%	
Anti-Mi-2	Chromodomain-helicase-DNA-binding protein 3 and 4	DM	18-35%	Very high specificity (~99%); diagnostic and prognostic marker
Anti-TIF1	TRIM24, TRIM28 and TRIM33	DM	13-38%	Main target: TRIM33; detected in patients with SLE and PM; strong association with cancer occurrence

Table 1-2 Representative ANAs associated with granular IFA pattern on HEp-2 cells [15, 23, 25]
AIH: Autoimmune hepatitis; DM: Dermatomyositis; MCTD: Mixed connective tissue disease; PBC: Primary biliary cholangitis; RNP: ribonucleoprotein; RA: Rheumatoid arthritis; SLE: Systemic lupus erythematosus; SjS: Sjögren's syndrome; SSc: Systemic sclerosis; TRIM: Tripartite-motif protein

1.4.4 Nucleolar

The nucleolar pattern (Figure 1-1, D) is most often associated with SSc. Until now, four nucleolar associated ANAs are well-established: anti-U3RNP/Fibrillarin, anti-NOR90/hUBF, anti-PM-Scl and anti-Th/To (Table 1-3).

ANA	Target antigens	SARD	Prevalence	Remark
anti-U3RNP/Fibrillarin	Fibrillarin	SSc	4-10%	Diagnostic and prognostic marker
anti-NOR90/hUBF	Human upstream binding factor	SSc	4-6%	Rarely detected; not particular associated with certain SARD
anti-PM-Scl	Exosome component 10 and RRP45	PM-Scl	24-55%	Diagnostic and prognostic marker for myositis overlap syndrome and SSc
		SSc	3-13%	
		PM/DM	8-12%	
anti-Th/To	Ribonucleases P/ Ribonucleases MRP protein complex	SSc	2-5%	Main targets: Rpp25 and hPop1; marker for SSc

Table 1-3 Four established nucleolar autoantibodies [15, 23, 25, 29]
PM-Scl: Polymyositis and scleroderma overlap syndrome; PM/DM: polymyositis/dermatomyositis; SSc: Systemic sclerosis; hPop1: Ribonucleases P/MRP protein subunit POP1; Rpp25: Ribonucleases P protein subunit p25

1.4.5 Centromere

The centromere pattern (Figure 1-1, E) is commonly found in patients with SSc and primary biliary cholangitis (PBC) [23, 25]. It is strongly associated with anti-CENP-B autoantibodies. The other related ANAs are anti-CENP-A and -C, which are often co-presented with anti-CENP-B [25]. Anti-CENP-B and -A autoantibodies are diagnostic marker for SSc with a prevalence of 20-40%, while approximately 10-30% patients with PBC present with anti-centromere autoantibodies [25, 29]. About half of these PBC patients have concomitant SSc or SSc related syndromes [25]. Anti-CENP-B and -A autoantibodies are rarely detected in other SARDs [25].

1.5 Current issues in ANA diagnostics

ANAs are important diagnostic and prognostic markers. With the current strategy and techniques, the patient samples are first analysed in IFA with HEp-2 cells and then further differentiated with various available monospecific tests, which are helpful tools in the diagnosis and classification of the patients [15, 25]. However, regardless of

more than a half century of study and experience, there are still some gaps remaining in ANA diagnostics that urge to be resolved.

Nowadays, more physicians, rather than just rheumatologists, are ordering ANA tests for preventive medicine and precision health, which leads to increasing numbers of positive result of ANA tests, especially positive IFA with HEp-2 cells, with unclear clinical value. However, it is not only important to report the ANA patterns and titers on HEp-2 cells but also to further distinguish ANAs for the correct diagnosis. Some ANAs, like anti-Scl70, are highly specific but with a limited prevalence in the patients with SARD; on the other hand, certain ANAs like anti-DFS70 are negatively related with SARD. Moreover, it is reported that many ANAs could not give consistent patterns on HEp-2 cells and different ANAs could reveal similar or the same pattern [26, 30]. Therefore, additional effort is required to identify the unknown ANAs and to study the corresponding clinical association.

Another point is that in the last years several novel autoantigens was identified but they were not further validated nor applied in the clinical practice. For example, more than 180 different autoantibodies are reported in SLE patients, but only a few of them are applied in diagnostic assays, which may be due to multiple reasons, like a restriction of the technique in the past, limitations in access to proper patient groups for further validation or very low prevalence of the autoantibodies [26, 31]. Thus, it is crucial to establish applicable immunoassays for the identified autoantigens and carefully evaluate their clinical utility.

1.6 Aim of this study

In the routine screening of the Clinical Immunological Laboratory of Prof. Dr. med Winfried Stöcker, some sera with certain ANA pattern on HEp-2 cells, like DFS and granular, showed negative results in monospecific tests with the established nuclear autoantigens. One can speculate that these sera contain autoantibodies against unknown nuclear autoantigens. As it is mentioned above, the spectrum of monospecific ANA diagnostics is limited. It is of our interest to improve current ANA tests by expanding the spectrum of known ANAs and to build associations between IFA patterns with specific nuclear antigens, thereby narrowing the gaps in ANA diagnostics. With the developed strategy for identification of ANA target antigens in a previous master thesis [32], this work continues with identification and verification of ANA targets, as well as the optimization of the identification methods for individual

candidate antigens. Moreover, the prevalence of ANAs against candidate antigens will be studied with a SARD cohort to assess the clinical association.

The three goals are: a) to identify and verify unknown autoantibody targets, b) to establish suitable immunoassays with verified candidate antigens and c) to analyse the clinical associations of the novel autoantibodies.

2 Materials and methods

2.1 Material list

2.1.1 Chemicals and reagents

Chemicals and reagents	Supplier	Catalog No.
Acetic acid	Merck KGaA, Germany	8187552500
Acetone	Merck KGaA, Germany	1000220500
Acetonitrile	Merck KGaA, Germany	100016100
Advanced protein assay reagent	Tebu-bio GmbH, Germany	ADV01
Aluminum sulfate hydrate	Sigma-Aldrich Corporation, USA	368458
Albumin bovine serum	Th. Geyer GmbH & Co. KG, Germany	A9647-100G
Ammonium hydrogen carbonate	Merck KGaA, Germany	1011315000
Ammonium phosphate monobasic	Sigma-Aldrich Corporation, USA	A1645
Benzonase®	VWR International GmbH, Germany	1.01656.0001
Bicinchoninic acid solution	Sigma-Aldrich Corporation, USA	B9643-1L
Bio-Scale Mini CHT-II, 40 µm	Bio-Rad Laboratories, Inc., USA	732-4334
Blot casein sample buffer	EUROIMMUN AG, Germany	ZD1120-0010
Blot wash buffer (10x)	EUROIMMUN AG, Germany	ZW1100-1010
Blot wash buffer Plus (10x)	EUROIMMUN AG, Germany	ZW1110-1005
Blot NBT/BCIP substrate solution	EUROIMMUN AG, Germany	ZW1020-0150
Bovine serum albumin	Sigma-Aldrich Corporation, USA	A9647
Coomassie® Brilliant blue G 250	Merck KGaA, Germany	1154440025
Copper (II) sulfate pentahydrate	Th. Geyer GmbH & Co. KG, Germany	1.027.900.250

α-Cyano-4-hydroxycinnamic acid (HCCA)	Bruker Corporation, USA	201344
2-Deoxycytidine	Sigma-Aldrich Corporation, USA	D3897
Dimethyl sulfoxide	Sigma-Aldrich Corporation, USA	D2650
Dithiothreitol (DTT)	Gerbu Biotechnik GmbH, Germany	1008.0250
Dulbecco's Modified Eagle Medium (DMEM), high glucose, GlutaMAX™ Supplement, pyruvate	Thermo Fisher Scientific Inc., USA	31966047
Dynabeads® Protein G for Immunoprecipitation	Thermo Fisher Scientific Inc., USA	1004D
Ethanol	Merck KGaA, Germany	1009800500
Ethylenediaminetetraacetic acid (EDTA)	Gerbu Biotechnik GmbH, Germany	1034.0250
Fetal Bovine Serum	Thermo Fisher Scientific Inc., USA	10270106
Glycerol/PBS (embedding medium for IFA)	EUROIMMUN AG, Germany	ZF1200-0103
Glycerol 99,5%	Gerbu Biotechnik GmbH, Germany	2006.5000
Guanidine Hydrochlorid Standard Grade	Gerbu Biotechnik GmbH, Germany	1057.2500
Imidazole	Sigma-Aldrich Corporation, USA	I-2399
Iodoacetamide (IAA)	Bio-Rad Laboratories, Inc., USA	163-2109-MSDS
Isopropanol	SERVA Electrophoresis GmbH, Germany	39559.02
Methanol	Merck KGaA, Germany	1060020500
Magnesium chloride hexahydrate	Sigma-Aldrich Corporation, USA	M9272

2-(N-morpholino)ethanesulfonic acid (MES)	Gerbu Biotechnik GmbH, Germany	1080
NICKEL RAPID RUN™	Agarose Bead Technologies, USA	6NIRR-1000
Nitro blue tetrazolium chloride/ 5-Bromo-4-chloro-3-indolyl phosphate (NBT/BCIP): Chromogen/Substrate	EUROIMMUN AG, Germany	ZW1020-0150
Nonidet™ P 40 Substitute solution	Sigma-Aldrich Corporation, USA	74388
NuPAGE® LDS sample buffer (4x)	Thermo Fisher Scientific Inc., USA	NP0007
NuPAGE® MES SDS Running Buffer (20X)	Thermo Fisher Scientific Inc., USA	NP0002
NuPAGE® MOPS SDS Running Buffer (20X)	Thermo Fisher Scientific Inc., USA	NP0001
NuPAGE® Transfer Buffer (20X)	Thermo Fisher Scientific Inc., USA	NP0006-1
n-Octyl-β-D-glucopyranoside	Carl Roth GmbH & Co. KG, Germany	CN23.2
ortho-Phosphoric acid	Merck KGaA, Germany	1005731000
Penicillin-Streptomycin (10,000 U/mL)	Thermo Fisher Scientific Inc., USA	15140122
Peptide Calibration Standard II	Bruker Corporation, USA	222570
Phenol red	Sigma-Aldrich Corporation, USA	P3532
Phenylmethanesulfonyl fluoride (PMSF)	Sigma-Aldrich Corporation, USA	P7626-5G
Phosphate buffered saline (PBS)	EUROIMMUN AG, Germany	ZF1100-1000
Ponceau S	Sigma-Aldrich Corporation, USA	P3504
Potassium chloride	Merck KGaA, Germany	1049360250
Protease Inhibitor Cocktail	Sigma-Aldrich Corporation, USA	P8340

SDS Sediments	Carl Roth GmbH & Co. KG, Germany	CN30.2
Sodium azide	Sigma-Aldrich Corporation, USA	S2002
Sodium chloride	Merck KGaA, Germany	1064045000
0.9% Sodium chloride injection solution	Fresenius Kabi Deutschland GmbH, Germany	B23042A
Sodium deoxycholate monohydrate	Th. Geyer GmbH & Co. KG, Germany	AB125126
Sodium hydroxide	Gerbu Biotechnik GmbH, Germany	20200001
SP-Sepharose Fast Flow	GE-Healthcare Europe GmbH,	17-0729-04
Spectra™ Multicolor Broad Range Protein Ladder	Thermo Fisher Scientific Inc., USA	26623
Thymidine	Sigma-Aldrich Corporation, USA	T9250
TO-PRO®-3 Iodide (642/661)	Thermo Fisher Scientific Inc., USA	T3605
Trifluoroacetic acid (25% solution in water) for protein sequenation	Merck KGaA, Germany	1082180050
Tris(hydroxymethyl)aminomethane (Tris)	Gerbu Biotechnik GmbH, Germany	12181000
Trypsin-EDTA (0.5%) (10x)	Thermo Fisher Scientific Inc., USA	15400054
Trypsin (Sequencing Grade Modified)	Promega GmbH, Germany	V5111
Tween 20	EUROIMMUN AG, Germany	ZF1110-0102
Triton™ X-100	Sigma-Aldrich Corporation, USA	X100
Urea	Gerbu Biotechnik GmbH, Germany	10440004
Water for chromatography	Merck KGaA, Germany	1153332500

2.1.2 Antibodies

Antibody	Supplier	Catalog No.
Alexa Fluor® 488 AffiniPure Goat Anti-Human IgG, Fcγ fragment specific, **anti-human-IgG-alexa488**	Jackson ImmunoResearch Inc., USA	109545008
Cy™3 AffiniPure Goat Anti-Mouse IgG (H+L), **Anti-mouse-IgG-Cy3**	Jackson ImmunoResearch Inc., USA	115165062
Fluorescein isothiocyanate (FITC) - labelled anti-human-IgG (goat), **anti-human-IgG-FITC**	EUROIMMUN AG, Germany	AF102-0160
Alkaline phosphatase-labelled anti-human IgG, **anti-human-IgG-B/E-AP**	EUROIMMUN AG, Germany	AE142-1030
Monoclonal Anti-polyHistidine−Alkaline Phosphatase antibody produced in mouse, **anti-His-tag-AP**	Sigma-Aldrich Corporation, USA	A5588
His•Tag® Monoclonal Antibody produced in mouse, **anti-His-tag**	Merck KGaA, Germany	70796-3
Alkaline Phosphatase AffiniPure Goat Anti-Mouse IgG (H+L), **anti-mouse-IgG-AP**	Jackson immunoresearch Inc., USA	115055062
ZO-1 Monoclonal Antibody (ZO1-1A12) produced in mouse, **anti-TJP1**	Thermo Fisher Scientific Inc., USA	33-9100
Mouse monoclonal cyclin B1 Antibody (GNS1), **anti-Cyclin B1**	Santa Cruz Biotechnology, Inc., USA	sc-245
Actin Monoclonal Antibody (mAbGEa) produced in mouse, **anti-actin**	Thermo Fisher Scientific Inc., USA	MA1-744

2.1.3 Buffers

AU
50 mM Acetic acid pH 4.5
8 M Urea

A50
50 mM Acetic acid pH 4.5

BSA standard stock
5 mg/ml BSA
0.9% (w/v) NaCl

Benzonase reaction buffer
20 mM Tris HCl pH 7.4
150 mM NaCl
2 mM $MgCl_2$
1 mM PMSF

Blue Silver- Destaining solution
10% (v/v) Ethanol
2% (v/v) ortho-Phosphoric acid

Blue Silver- Fixing solution
50% (v/v) Methanol
10% (v/v) Acetic acid

Blue Silver- Staining solution
0.02% (w/v) Coomassie® Brilliant blue G 250
5% (w/v) Aluminum sulfate hydrate
10% (v/v) Ethanol
2% (v/v) ortho-Phosphoric acid

Complete medium
1x DMEM
10% (v/v) FBS
1% (v/v) PS

HEK293 lysis buffer
20 mM Tris HCl pH 8
600 mM NaCl
20 mM MgCl2
20 mM Imidazol
1 mM PMSF

HEp-2 lysis buffer
20 mM Tris HCl pH 7.4
50 mM KCl
5 mM EDTA
1 mM PMSF

HEp-2 harvest buffer
20 mM Tris-HCl pH 7.4
2 mM $MgCl_2$
1 mM PMSF

MALDI-Extraction solution
5 mM n-Octyl-β-D-glucopyranoside
50% (v/v) Acetonitrile
0.3% (v/v) Trifluoroacetic acid
Water for chromatography

MALDI-Destaining solution 1
30% (v/v) Acetonitrile
25 mM Ammonium hydrogen carbonate
Water for chromatography

MALDI-Destaining solution 2
50% (v/v) Acetonitrile
10 mM Ammonium hydrogen carbonate
Water for chromatography

MALDI-Trypsin stock solution
10 µg/ml Trypsin
3 mM Tris-HCl pH 8.5

MALDI-Peptide calibration II
Peptide calibration standard II
1 % (v/v) Trifluoroacetic acid

MALDI-Peptide calibration/Matrix
10% (v/v) Peptide calibration II
1.26 mg/ml α-Cyano-4-hydroxycinnamic acid
76.5% (v/v) Acetonitrile
0.1% (v/v) Trifluoroacetic acid
0.9 mM Ammonium dihydrogen phosphate

MALDI-Matrix solution
1.4 mg/ml α-Cyano-4-hydroxycinnamic acid
85% (v/v) Acetonitrile
0.1% (v/v) Trifluoroacetic acid
1 mM Ammonium dihydrogen phosphate

PBS-Tween
1x PBS pH 7.2
0.2% (v/v) Tween 20

PBS1000(U)
1x PBS pH 7.4
1 M NaCl
8 M Urea

Ponceau-S solution
0.2% (w/v) Ponceau S
7% (v/v) Acetic acid

RIPA lysis buffer
1x PBS pH 7.4
0.1% (v/v) Nonidet™ P 40 substitute solution
1% (w/v) Deoxycholate
0.1% (w/v) SDS
1 mM Protease inhibitor cocktail

RIPA-2U buffer
1x PBS pH 7.4
2 M Urea
0.1% (v/v) Nonidet™ P 40 substitute solution
1% (w/v) Deoxycholate
0.1% (w/v) SDS
1 mM Protease inhibitor cocktail

RIPA-4U buffer
1x PBS pH 7.4
4 M Urea
0.1% (v/v) Nonidet™ P 40 substitute solution
1% (w/v) Deoxycholate
0.1% (w/v) SDS
1 mM Protease inhibitor cocktail

Sucrose buffer
20 mM Tris-HCl pH 7.4
10% (w/v) Sucrose
5 mM EDTA
1 mM PMSF

TI500- Eq buffer
10 mM Tris-HCl pH 8.0
500 mM Imidazole

0.1% Triton-X-100 lysis buffer
100 mM Tris pH 7,4
150 mM NaCl
1 mM EDTA
0,1% Triton-X-100
1 mM Protease inhibitor cocktail

TN buffer
50 mM Tris-HCl pH 8.0
300 mM NaCl
10 mg/L Phenol red
1 mM PMSF
25 mM DTT

TNETD buffer
100 mM Tris-HCl pH 7.4
150 mM NaCl
2.5 mM EDTA
1 % Triton-X-100
0.5 % Deoxycholate
1 mM Protease inhibitor cocktail

TNTDI-20 buffer
20 mM Tris HCl pH 8
600 mM NaCl
0.015% (w/v) Triton-X-100
0.5 mM DTT
20 mM Imidazol
1 mM PMSF

TNTDI-20Pi250 buffer
20 mM Tris HCl pH 8
600 mM NaCl
0.015% (w/v) Triton-X-100
0.5 mM DTT
20 mM Imidazol
250 mM NaH_2PO_4
1 mM PMSF

TNTDI-150 buffer
20 mM Tris HCl pH 8
600 mM NaCl
0.015% (w/v) Triton-X-100
0.5 mM DTT
150 mM Imidazol
1 mM PMSF

TNTMDl buffer
20 mM Tris HCl pH 8
600 mM NaCl
0.1% (w/v) Triton-X-100
20 mM MgCl2
0.5 mM DTT
20 mM Imidazol
1 mM PMSF

TNUDI-150 buffer
10 mM Tris-HCl pH 8.0
300 mM NaCl
8 M Urea
0.5 mM DTT
150 mM Imidazole

TNUDI-20 buffer
10 mM Tris-HCl pH 8.0
300 mM NaCl
8 M Urea
0.5 mM DTT
20 mM Imidazole

2.1.4 Serum samples

190 anonymized serum samples were collected from the Clinical Immunological Laboratory of Prof. Dr. med. Winfried Stöcker. In accordance with the Helsinki Declaration, all patients had written informed consent. The patient sera were sent to the reference diagnostic laboratory to determine ANA. The serum samples showed distinct ANA patterns in HEp-2 cell IFA but revealed negative results in the requested antigen-specific tests which implied that there were unknown antinuclear autoantibodies.

Additionally, ten anonymized serum samples with distinct HEp-2 cell patterns were received from the Fleury Medicine and Health Laboratories in Brazil. They were collected by L. E.C. Andrade's group and aimed at identification of target antigens, which was under protocol approved by the Ethics Committee CAAE: 64912216.7.3001.5474.

A cohort of patients with systemic autoimmune rheumatic disease (SARD) was recruited for an exploratory prevalence study. It was received from E. Siegert, Rheumatology and Clinical Immunology, University Hospital Charité, Germany and consisted of 529 serum samples from 488 patients, of which 378 patients had systemic sclerosis (SSc) and 110 patients had other rheumatic diseases. The repeated sera were taken from the same patients at different time points. The patients provided informed consent for this study. The number of patients per indication is given in Table 2-1.

Serum samples from healthy blood donors used as controls for the study were received from the EUROIMMUN internal serum collection.

Diagnosis	Patient Number
Systemic sclerosis (SSc)	378
Anti-synthetase syndrome (ASS)	10
Inclusion body myositis (IBM)	4
Mixed connective tissue disease (MCTD)	6
Myositis	15
Primary Sjögren syndrome (pSS)	11
Rheumatoid arthritis (RA)	24
Systemic lupus erythematosis (SLE)	30
Undifferentiated connective tissue disease (UCTD)	10

Table 2-1 Clinical information of systemic autoimmune rheumatic disease (SARD) cohort

2.1.5 Instruments

Instruments	Supplier	Catalog No.
Analytical balance ACJ/ACS	KERN & SOHN GmbH, Germany	ACJ 120-4M
Autoflex™ III Smartbeam MALDI-TOF/TOF 200	Bruker Corporation, USA	3079094
Centrifuge Hettich ROTANTA 460 R	Hassa GmbH, Germany	5660
Confocal laser scanning microscope LSM700	Carl Zeiss Microscopy GmbH, Germany	Axio Imager M2
CO2 Incubator BBD 6220	Thermo Fisher Scientific Inc., USA	51020241
Dounce tissue grinder set, 1 ml, 15 ml and 60 ml	Sartorius Stedim Biotech GmbH, Germany	8530718 8530912
Eppendorf® Thermomixer Compact	Eppendorf AG, Germany	5350 000.013
Fluorescence microscope EUROStar II	EUROIMMUN AG, Germany	YG_0301

Heraeus Fresco 21 Centrifuge, Refrigerated	Thermo Fisher Scientific Inc., USA	75002426
High Performance centrifuge Avanti J-E	Beckman Coulter GmbH, Germany	369003
Inverted microscope Axio Vert.A1	Carl Zeiss Microscopy GmbH, Germany	491237-0018-000
Lab pH meter inoLab® pH 7110	Xylem Analytics Germany Sales GmbH & Co. KG, WTW, Germany	1AA110
Magnetic stirrer IDL ME-1	IDL GmbH & Co KG, Germany	5100140100
Mini LabRoller™ Dual Format Rotator	Axon Labortechnik GmbH, Germany	27787
PowerPac™ Basic Power Supply	Bio-Rad Laboratories, Inc., USA	1645050
Precision balance PES/PEJ	KERN & SOHN GmbH, Germany	PES 2200-2M
Rocking shaker BIOMETRA® WT16	Biometra GmbH, Germany	042-500
Sonicator Branson 250 Sonifer	Branson ultrasonics corporation, USA	100132868
Sterile station Heraeus® HERAsafe® HS 15	Kendro Laboratory Products, Germany	51012198
TE22 Mighty Small Transfer Tank	Hoefer Inc., USA	80-6204-26
TECAN Reader Sunrise	Tecan Trading AG, Switzerland	16039400
TECAN HydroFlex microplate washer	Tecan Trading AG, Switzerland	30022011
Vortex mixer IKA® MS 3 basic	IKA®-Werke GmbH & Co. KG, Germany	0003617000
Water bath WB14	Memmert GmbH + Co.KG, Germany	1495.0849
XCell SureLock® Mini-Cell	Thermo Fisher Scientific Inc., USA	EI0001

2.2 Characterization of serum samples

The collected serum samples were initially characterized with Euroline ANA profile 23 (IgG) (EUROIMMUN AG, Germany) and indirect immunofluorescence assay (IFA) with HEp-2 cells and monkey liver (EUROIMMUN AG, Germany). Both experiments were carried out following the manufacturer's instruction:

2.2.1 Euroline

Using Euroline ANA profile (IgG) 23, the 23 most common ANAs can be determined (Figure 2-1). The highly purified antigens were coated on the strip. Each strip contains 23 different antigens, which means that the known ANAs can be identified in one single incubation with a small sample volume.

The experiments were performed as described in the standard procedure [33]. All reagents were brought to room temperature before use. Strips were incubated in incubation trays on a rocking shaker with 1 ml casein sample buffer for 5 minutes and then in 1:101 diluted serum sample for 30 minutes. Afterwards, each strip was washed three times with 1.5 ml washing buffer for 5 minutes each time prior to incubation with 1 ml diluted enzyme conjugate (alkaline phosphatase-labelled anti-human IgG) for 30 minutes.

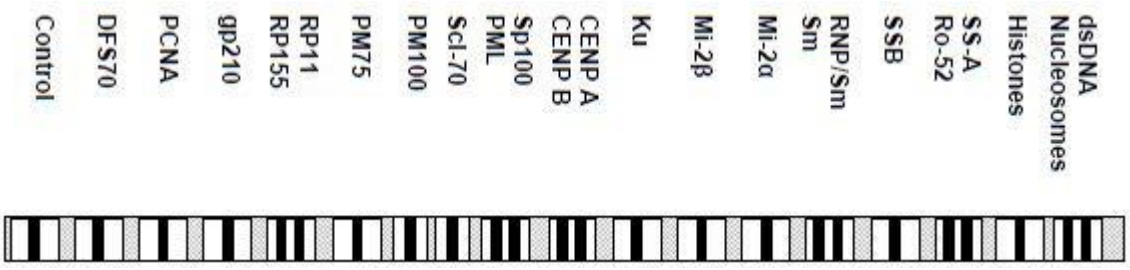

Figure 2-1 Schematic assembly of Euroline ANA profile (IgG) 23 (adapted from EUROIMMUN AG [33])
Poly-Immunoglobulin serves as incubation control on the left. The 23 purified ANA target antigens are coated on the strip. The black bands on the individual membrane indicate positive reaction.

Strips were washed again as described above and incubated with NBT/BCIP substrate solution for 10 minutes. Then, the substrate solution was discarded and the reaction was stopped by washing three times with 1 ml distilled water. The strips were placed on the evaluation protocol and analyzed using the software EUROLineScan (EUROIMMUN AG, Germany).

2.2.2 Indirect immunofluorescence assay (IFA)

IFA with HEp-2 cells is the gold standard for ANA screening [34]. The BIOCHIP slides were specially produced for research use by EUROIMMUN AG. Taken ANA research slide as example (Figure 2-2, B), each BIOCHIP Mosaic® consisted of three different substrates, HEp-2 cells (acetone fixed only), HEp-2 cells (standard product, EUROIMMUN AG) and monkey liver, respectively. There were 10 BIOCHIP Mosaic® (5 x 5 mm) on one slide. TITERPLANE™ Technique (Figure 2-2, A) developed by EUROIMMUN was applied.

35 µl diluted sera were spotted on each reaction field of the reagent tray (EUROIMMUN AG, Germany). 1:100, 1:1000 and 1:10000 dilutions were applied according to condition. The slide was covered over the reagent tray with BIOCHIPs facing down and each reaction field formed a “humidity chamber”. After 30 minutes incubation, the BIOCHIP slide was rinsed with PBS-Tween and incubated in a PBS-Tween filled cuvette for 5 minutes. FITC-labelled anti-human-IgG (goat) (ready-to-use) was then applied undiluted. Alternatively, Alexa Fluor® 488 AffiniPure Goat Anti-Human IgG was diluted 1:500 with PBS-Tween including 1:2000 diluted TO-PRO™-3 Iodide. A clean reagent tray was applied with 30 µl diluted secondary antibody on the reaction field. The slide was then incubated on the reagent tray for 30 minutes in dark. After that it was rinsed and incubated in the same way as above. Glycerol/PBS droplets were applied onto a cover glass. The slide was placed over the prepared cover glass with BIOCHIPs facing downwards. After that the samples were analyzed using fluorescence microscope EUROstar II. Images were captured using Europicture software (EUROIMMUN AG, Germany).

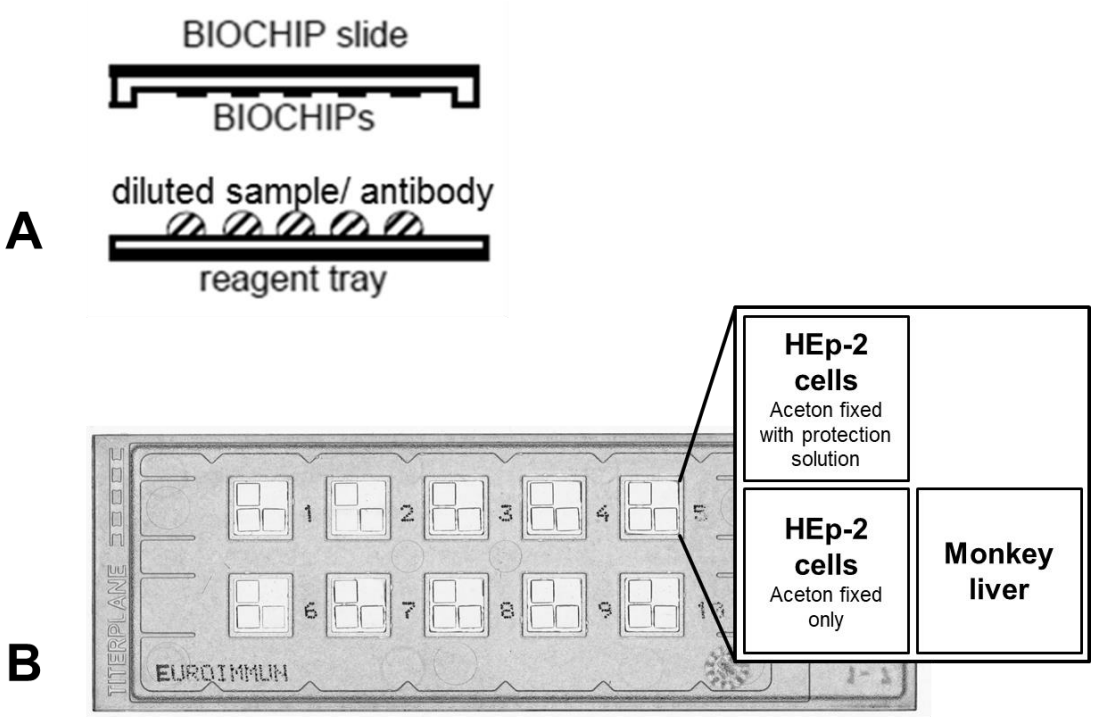

Figure 2-2 Schema of TITERPLANE™ technique (adapted from EUROIMMUN AG [34]) and ANA research BIOCHIP slide
A) Schema of TITERPLANE™ technique. Diluted serum sample or antibody was applied on reagent tray. BIOCHIP slide was covered over reagent tray with BIOCHIPs facing down and "humidity chamber" was formed for incubation. **B)** ANA research BIOCHIP slide. Each slide contains ten reaction fields and each field consists of three different biochips.

Alternatively, Confocal laser scanning microscope LSM700- Axio Imager M2 was used to analyze samples and ZEN 2000 software (Carl Zeiss Microscopy GmbH, Germany) was used to capture images.

2.2.3 Extractability test

In order to find a suitable extraction buffer for immune complexes, HEp-2 cells and liver cryosections were treated with different reagents prior to conjugate incubation. The method was similar to IFA described above. Additional steps were added before conjugate incubation.

Four ANA research slides were incubated with diluted serum samples. After washing with PBS-Tween, the slides were placed into compartments of a square tissue culture dish (quadriPERM® dish, Sarstedt AG &Co., Germany). Each compartment contained one slide with BIOCHIPs facing up. PBS buffer was applied as control buffer. The other three slides were incubated with RIPA lysis buffer, RIPA-2U buffer or RIPA-4U buffer for 30 minutes at RT on a lab shaker. The slides were then rinsed and incubated with PBS-Tween for 5 minutes. Conjugate incubation and slide preparation for microscopy were performed as described in section 2.2.2.

2.3 HEp-2 cell culture

The human epithelial cell line HEp-2 was cultivated for immunoprecipitation experiments. The HEp-2 cryo culture was obtained from cell culture department of EUROIMMUN AG: HEp-2 cells were cultured in 175-cm^2-flasks with 25 ml complete medium in a BBD 6220 CO_2 incubator at 37°C, 5% CO_2 and 95% humidity, or alternatively in HYPERFlask® M cell culture vessel surface area 1720 cm² (Corning Life Sciences B.V., The Netherlands) with 560 ml complete medium.

50 ml fetal bovine serum and 5 ml penicillin-streptomycin (10000 U/ml) were added to each 500 ml DMEM to make complete medium. Trypsin-EDTA (0.5%) stock solution was diluted with 0.9% sodium chloride injection solution to make 0.05% Trypsin-EDTA solution. All works were done under the sterile station Heraeus® HERAsafe® HS15. Centrifuge ROTANTA 460 R was used for cell culture centrifugation. The cell culture was checked every day under inverted microscope Axio Vert.A1 to exclude possible contamination with fungi and bacteria.

2.3.1 Cell seeding

Thawed HEp-2 cell suspension with 2 x 10^6 cells was gently mixed with 10 ml warm complete medium. It was centrifuged at 221 x g at RT for 5 minutes. The HEp-2 cell sediment was resuspended in 5 ml medium and pipetted into a 75-cm^2-flask with 10 ml complete medium. After incubation overnight, it was observed that cells grow well with less than 1% dead cell. On the following day, HEp-2 cells were splitted 1:4 in 175-cm^2-flasks.

2.3.2 Subculturing

When the degree of confluency of the HEp-2 cells reached about 90%, sub-culturing was necessary to prevent cell death.

After medium was discarded, cell culture was washed with 0.9% sodium chloride injection solution. Then it was trypsinized with 5 ml 0.05% Trypsin-EDTA for 5 minutes at 37°C. Detached cells were mixed with fresh complete medium to deactivate trypsin. Cells were sedimented at 221 x g for 5 minutes at RT and then resuspended in 10 ml warm complete medium. Cell suspension was split 1:5 or 1:10 as demanded in pre-labeled new 175-cm^2-flasks.

For subculturing from 175-cm^2-flasks in HYPERFlask®, two to three confluent 175-cm^2-flasks with HEp-2 cells were necessary. The cells were detached as described

above and then gently mixed together with 560 ml warm complete medium. After that, the 560 ml cell suspension was transferred into a pre-labeled HYPERFlask®.

2.3.3 Cell harvesting

HEp-2 cells were harvested in sucrose buffer for further experiments.

2.3.3.1 Cell harvesting from 175-cm^2-flasks

HEp-2 cell sediments were produced as mentioned in section 2.3.2. Cell sediments were then resuspended in 20 ml 0.9% sodium chloride injection solution. The cell number was determined on Assistent® counting chambers (Glaswarenfabrik Karl Hecht GmbH & Co KG, Germany). Cell suspension was spun down at 221 x g, RT for 5 minutes prior to adding sucrose buffer to the sediment as demanded. The final cell concentration was 25 x 10^6 cells/ml. The cell suspension was then aliquoted in 400 µl and 800 µl and stored at -80°C.

2.3.3.2 Cell harvesting from HYPERFlask®

After medium was discarded, 510 ml 0.9% sodium chloride solution supplemented with 50 ml 0.05% Trypsin-EDTA was added to the cell culture. It was then incubated for 5 minutes at 37°C to detach the cells. The cell suspension in diluted Trypsin-EDTA was filled in 500 ml centrifuge tubes. The cells were sedimented at 2500 x g for 5 minutes at RT and then resuspended in 20 ml 0.9% sodium chloride injection solution. The cell number was determined on Assistent® counting chambers. Cell suspension was spun down at 221 x g, RT for 5 minutes prior to adding sucrose buffer as demanded. The final cell concentration was 25 x 10^6 cells/ml. The cell suspension was then aliquoted in 400 µl and 800 µl and stored at -80°C.

2.3.4 Synchronization of HEp-2 cells with double thymidine block

HEp-2 cells were first arrested in G1/S-phase using double thymidine block [35]. In the second step the cells were released in complete medium supplemented with 24 µM deoxycytidine to generate G2-phase synchronized cells.

2.3.4.1 Time course experiment for analysis of cell synchronization

HEp-2 cells were prepared in ten 25 cm^2-flasks as described in section 2.3.2. After 40% confluence was reached, medium was discarded. Complete medium supplemented with 2 mM thymidine was added to HEp-2 cells. The cells were cultivated for 19 h to arrest them in G1/S-phase. The thymidine containing complete medium was then discarded and the cells were washed with 0.9% sodium chloride

solution. After that, the complete medium supplemented with 24 µM deoxycytidine was added in order to release the cells. After culturing for 9 h, the medium was discarded and the cells were cultivated in complete medium containing 2 mM thymidine for 16 to 19 hours. The cells were washed again with 0.9% sodium chloride solution prior to cultivation in complete medium supplemented with 24 µM deoxycytidine. After the cells were released from the second thymidine block, the cells from one 25 cm^2-flask were harvested and lysed in 200 µl 1x NuPAGE® LDS sample buffer at the following time points: 0.5, 1, 2, 3, 4, 4.5, 5, 6, 7 and 8 hours. The lysates were analyzed by Western blot (see section 2.4.2.2) using anti-cyclin B1 (1:1000) and anti-actin (1:1000) antibodies.

2.3.4.2 Preparation of G2-synchronized biomaterial

The cells were prepared in HYPERFlask® as described in section 2.3.2. The synchronization was implemented as mentioned above. The cells were harvested as mentioned in section 2.3.3.2 after releasing the cells from double thymidine block for 6 h. The final cell concentration was 25 x 10^6 cells/ml. The cell suspension was then aliquoted in 400 µl and 800 µl and stored at -80°C.

2.4 Antigen identification with immunoprecipitation (IP) and mass spectrometry

The recharacterized serum samples and the prepared HEp-2 cells were applied in order to identify the target antigens. An immunoprecipitation method with fractionated HEp-2 cells was applied in this work. All steps were carried out on ice. DynaMag™ (Thermo Fisher Scientific Inc., USA) was applied to attract and separate Dynabeads® Protein G.

2.4.1 Fractionated IP with cell homogenate

600 µl HEp-2 lysis buffer was added to each 400 µl frozen cell suspension in sucrose buffer to produce 10 x 10^6 cells/ml cell homogenate. 5 µl serum was incubated with 500 µl cell homogenate in HEp-2 lysis buffer overnight at 4°C on a rotator. After centrifugation 16000 x g for 10 minutes at 4°C, the supernatant was discarded. The sediment was washed with 500 µl HEp-2 lysis buffer and centrifuged again as described. Then, the sediment was resuspended in 500 µl RIPA lysis buffer and rotated for 1 h at 4°C. The suspension was spun down at 16000 x g for 20 minutes at 4°C. The supernatant was incubated with 50 µl Dynabeads® Protein G for 3 h.

Following this, the beads were washed three times with 1 ml RIPA lysis buffer. After the last wash, the beads were transferred into a new Eppendorf tube. For elution, 40 µl 1x NuPAGE® LDS sample buffer was added to the beads and mixed gently followed by incubation at 70°C, 900 rpm for 10 minutes. 25 mM DTT was included in 1x NuPAGE® LDS sample buffer to reduce the disulfide bonds. The eluate fraction was then mixed with 4 µl 650 mM Iodoacetamide (IAA) and incubated in the dark for 30 minutes. During this step, the thiol group of cysteine was bound covalently with IAA so that the proteins could not form disulfide bonds. The alkylation was essential for mass spectrometry. The samples were directly loaded on SDS-PAGE or stored at -20°C.

2.4.2 Sodium dodecyl sulfate polyacrylamide gel electrophoresis (SDS-PAGE) and Western blot (WB)

Immunoprecipitates were analyzed with SDS-PAGE and Western blot. Proteins were separated according to their size using NuPAGE™ Novex™ 4-12% Bis-Tris Protein Gels (8 cm x 8 cm x 1 mm, Thermo Fisher Scientific Inc., USA). 1x NuPAGE® MES SDS Running Buffer was filled in both lower and upper chamber of electrophoresis tank (XCell SureLock® Mini-Cell). Gels were run at 200 V (PowerPac™ Basic Power Supply) for about 45 minutes until the tracking dye reach the end of the gels. Then, as demanded gels were stained with blue silver coomassie stain or transferred onto a nitrocellulose membrane (0.22 µm, Sartorius Stedim Biotech GmbH, Germany).

2.4.2.1 Blue silver coomassie staining

Gels were incubated in blue silver- fixing solution for 1 h prior to staining overnight with blue silver- staining solution. On the second day, gels were destained with blue silver- destaining solution for 30 minutes. Afterwards gels were scanned with Canon 9000F Mark II Scanner and then stored at 4°C in distilled water.

2.4.2.2 Western blot

Nitrocellulose membrane, filter paper and foam sponges were presoaked with 1x NuPAGE® Transfer Buffer. Gels containing separated proteins were placed on nitrocellulose membrane and placed between filter paper and foam sponges (3 mm and 6 mm).

Proteins were electrotransferred using tank blotter (TE22 Mighty Small Transfer Tank) at 400 mA for 1 h supplied by PowerPac™ Basic Power Supply. The

membranes were stained with ponceau-S solution to confirm efficiency of transfer. Wet membranes were cut into suitable size and destained with 50 mM Tris-HCl. Membranes were blocked with 1x blot wash buffer plus for 15 minutes at RT before serum incubation was performed overnight. The sera were diluted 1:200 in 1x blot wash buffer plus. Next day, the membranes were washed three times for 5 minutes with 1x blot wash buffer. Membranes were incubated in 1x blot wash buffer plus containing 1:10 diluted anti-human-IgG-B/E-AP for 30 minutes at RT. After this procedure, membranes were washed again three times with 1x blot wash buffer, and NBT/BCIP was used to detect bound antibodies. The incubated membranes were scanned with Canon 9000F Mark II Scanner.

2.4.3 Matrix Assisted Laser Desorption/Ionization - Time of Flight Mass Spectrometry (MALDI-TOF-MS)

MALDI-TOF-MS was applied to identify the specific protein bands on blue silver gels. The experiment was carried out and analyzed by MS specialists from EUROIMMUN AG.

A small hole was stabbed with cannula at the bottom of each well of a 96-well, non-skirted PCR plate (0.3 ml, Thermo Fisher Scientific Inc., USA) which was placed in a 96-well deep well microplate (MASTERBLOCK®, 2 ml, Greiner Bio One International GmbH, Germany). Selected bands were cut out with a scalpel and transferred into wells. Each well contained one band. The band in each well was destained with 100 µl MALDI-Destaining solution 1 two times for 20 minutes, one time with 100 µl MALDI-Destaining solution 2 for 20 minutes and one time with 100 µl acetonitrile for 10 minutes. Solutions were discarded by centrifugation at 178 x g for 1 minute at RT between each destaining. After that, protein samples were digested in gel with 15 µl MALDI-trypsin stock solution for 3 h at 37°C in humid chamber. 10 µl MALDI-Extraction solution was then added to each well and extracted for 45 minutes at RT. A new 96-well, non-skirted PCR plate was placed under the old one with hole and the extracts which contained the digested peptides sample were collected by centrifugation at 178 x g for 1 minute at RT. 0.8 µl peptide extract of each sample was applied on a single spot of a MTP AnchorChip 384 Taget (Bruker Daltonik GmbH, Germany). After droplets were dried, 0.5 µl MALDI-Matrix solution was added to each sample on the target. 0.5 µl MALDI-Peptide calibration/Matrix was applied on calibration spots on the target.

The samples on the target were measured using Autoflex™ III Smartbeam MALDI-TOF/TOF200 (Bruker Daltonik GmbH, Germany) controlled by software flexControl™ 3.4 (Bruker Daltonik GmbH, Germany). Positive ion reflector mode with 6000 shots was applied. MS spectra were recorded in a mass range from 600 Da to 4000 Da. The spectra were processed by software flexAnalysis™ 3.4 (Bruker Daltonik GmbH, Germany) and analyzed by software BioTools™ 3.2 (Bruker Daltonik GmbH, Germany). Identification of proteins was performed in software Mascot Server 2.3 (Matrix Science Ltd, UK) by searching against NCBI protein database or SwissProt limited to Homo sapiens. Searching settings for peptide mass fingerprinting (PMF) were: 80 ppm mass tolerance, one missed cleavage accepted, fixed modification of carbamidomethylation of cysteine residues, variable modification of oxidation of methionine residues and significance threshold $p < 0.05$.

WARP mechanism of BioTools™ was applied for tandem mass spectrometry (MS/MS) measurements in order to confirm PMF measurements. Two peptides of each identified protein were selected. 1000 shots of parent mass and 1000 shots of fragment mass were recorded. Procession and analyzation of spectra were same as above with a fragment mass tolerance of 0.7 Da.

2.5 Preparation of recombinant antigens

All antigens were designed with His-tag for purification and/or detection. The coding region of recombinant antigens was amplified from cDNA clones (Source BioScience, United Kingdom) by standard techniques (Sambrook et al., 1989). Plasmids applied for *E. coli* expression system were derived from pET24d (Merck KGaA, Germany). And plasmids employed for expression in Human Embryonic Kidney 293 (HEK293) cells were derived from pTriEx™-1.1 vector (Merck KGaA, Germany). The recombinant antigens were purified for the following experiments and the recombinant cells were applied in cell-based assay as well.

2.5.1 Cloning, expression and purification of recombinant antigens in *E. coli*

Small antigens (< 100 kDa) were subcloned for expression in *E. coli*. Cloning and expression of recombinant antigens were performed by the recombinant synthesis department of EUROIMMUN AG. Purified recombinant antigens were obtained from the immunobiochemical research department of EUROIMMUN AG. Table 2-2 shows a list of all recombinant antigens expressed in *E. coli*.

Protein name	Uniprot accession number	His-tag	Protein concentration mg/ml	Buffer
NVL	O15381	c-terminal	0.32	PBS1000(U)
CD2BP2	O95400	n-terminal	0.30	TN600
TFAP2A	P05549	n-terminal	4.45	PBS1000(U)
TDP43	Q13148	n-terminal	1.61	PBS1000(U)
PSME3	P61289	n-terminal	0.76	PBS1000(U)
TJP1 aa1-575	fragments of Q07157	n-terminal	0.81	PBS1000(U)
TJP1 aa561-1103		c-terminal	Not purified	-
TJP1 aa1089-1668		n-terminal	Not purified	-
POLR2A aa1475-1970	fragments of P24928	c-terminal	0.25	TNI-300
POLR2A aa1-488		c-terminal	Not purified	-
POLR2A aa489-951		c-terminal	Not purified	-
POLR2A aa952-1474		c-terminal	Not purified	-

Table 2-2 List of recombinant antigens expressed in *E. coli*
TN600: 20 mM Tris-HCl pH 8.5, 600 mM NaCl; TNI-300: 5 mM Tris-HCl pH 8.0, 300 mM NaCl, 300 mM Imidazol; PBS1000(U): 1x PBS pH 7.4, 1 M NaCl, 8 M Urea.

2.5.2 Cloning and expression of recombinant proteins in HEK293 cells

Molecular cloning and recombinant expression of candidate antigens in HEK293 cells were implemented by the recombinant synthesis department of EUROIMMUN AG. All recombinant proteins were designed with N-terminal His-tag. Transfected HEK293 cells were used as substrates for IFA or recombinant antigens were purified for subsequent experiments. A list of all recombinant antigens expressed in HEK293 cells is shown in Table 2-3.

Protein name	Uniprot accession number	Application in
PSME3	P61289	IFA
TFAP2A	P05549	IFA
TDP43	Q13148	IFA
DHX9	Q08211	IFA and purification
POLR2A	P24928	IFA
RPA1	P27694	IFA
RPA2	P15927	IFA
RPA3	P35244	IFA
RuvBL1	Q9Y265	IFA
RuvBL2	Q9Y230	IFA
SMCHD1	A6NHR9	IFA and purification
PELP1	Q8IZL8	IFA
SENP3	Q9H4L4	IFA
NVL	O15381	IFA
XRN2	Q9H0D6	IFA
MATR3	P43243	Purification
TJP1	Q07157	IFA
CD2BP2	O95400	IFA
KIF11	P52732	IFA

Table 2-3 List of recombinant antigens expressed in HEK293 cells
All recombinant proteins were designed with N-terminal His-tag.

2.5.3 Purification of recombinant antigens from HEK293 cells

The purification strategy was adapted for each individual recombinant antigen. In Figure 2-3, the workflow of the purification is shown. Under native condition, recombinant antigens were purified though ammonium sulfate precipitation followed by serial chromatography. Under denatured condition, recombinant antigens were prepared direct using chromatography. The result of each purification step was analyzed by Western blot (described in section 2.4.2.2) using anti-His-tag antibody (1:8000 diluted anti-His-tag-AP or 1:2000 diluted anti-His-tag prior to 1:2000 diluted anti-mouse-IgG-AP).

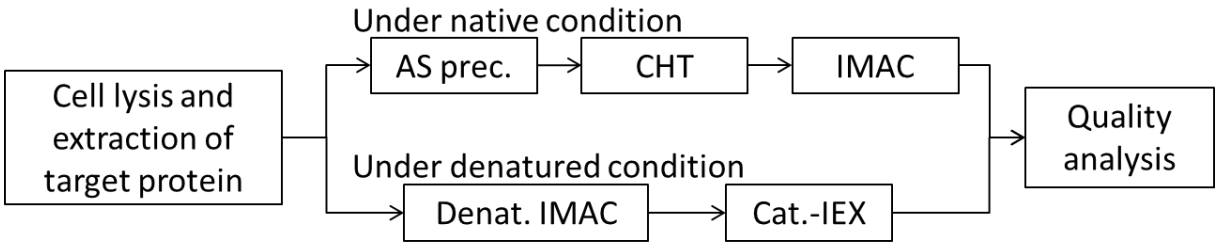

Figure 2-3 Purification strategy for native and denatured condition.
AS prec.: ammonium sulfate precipitation; CHT: CHT™ ceramic hydroxyapatite chromatography; IMAC: immobilized metal affinity chromatography; Denat.: denatured; Cat.-IEX: denatured cation exchange chromatography.

2.5.3.1 Lysis of HEK293 cells and extraction of target protein

10 ml HEK293 cells sediment (~50 x 10^6 cells/ml) was resuspended in 90 ml HEK293 lysis buffer supplemented with 200 U Benzonase® to digest DNA and RNA. The cells were then homogenized with Dounce tissue grinder, 10 strokes of large pestle prior to 10 strokes of small pestle. Cell homogenate was supplemented with 1-2 mM DTT to minimize the influence of disulfide bonds and incubated on ice for 30 minutes. After that, it was sedimented with 21200 x g for 20 minutes at 4°C. The supernatant (S1) was transferred into a clean bottle. The sediment (P1) was resuspended in 50 ml HEK293 lysis buffer supplemented 1% Triton-X-100 and incubated for 1 h. The supernatant (S2) was collected as described above. The sediment (P2) was successively washed with 10 ml isopropanol, 8 ml acetone and 10 ml isopropanol prior to be further solubilized in 20 ml TNUDI-20 buffer. The supernatant (S3) was collected as described. The sediment (P3) was resuspended in 5 ml TNUDI-20 buffer. Equal volumes of each fraction were analyzed by Western blot. The supernatant containing most of the target antigen was further processed.

2.5.3.2 Protein precipitation with ammonium sulfate

Serial ammonium sulfate (AS) precipitation was implemented. Therefore, 14.4 g AS was added slowly under stirring to 100 ml 0% saturation supernatant (S1 or S2 from section 2.5.3.1) to achieve 25% saturation. It was incubated at 4°C for at least 1 h and then centrifuged at 37800 x g for 30 min at 4°C. The sediment (P_{AS25}) was resuspended in 20 ml TNTMDI buffer and the supernatant (S_{AS25}) was applied for next AS precipitation, where 6.5 g AS was added. The precipitation process was repeated until the 100% saturation was reached. The amount of AS that was added at each step is listed in Table 2-4.

% Saturation AS in 100 ml supernatant	0	25	35	45	60	100
AS added after last step /g	0	14.4	6.5	6.8	11.3	27.2

Table 2-4 Amount of ammonium sulfate to reach 100% saturation

The sediment of each step (P_{AS25}, P_{AS35}, P_{AS45}, P_{AS60}, P_{AS100}) in TNTMDI buffer and the final supernatant were analyzed by SDS-PAGE and Western blot. The fraction(s) with the highest amount of target antigen was dialyzed in dialysis tube (Spectrum™ Spectra/Por™ 1 dialysis membrane, MWCO 6 - 8 kD, Spectrum Chemical Mfg. Corp., USA) twice against 30x volume of TNTMDI buffer to remove the exceeded AS. The dialysate was subjected to the following chromatography.

2.5.3.3 Chromatography under native condition

The dialysate was first loaded on the CHT™ Ceramic Hydroxyapatite, Type II (CHT) resin to reduce the lipid compartments, DNA and RNA. IMAC was the second chromatography step, which enriched the target antigen via its His-tag.

CHT™ Ceramic Hydroxyapatite chromatography

Bio-scale Mini CHT-II, 40 µm, 5 ml prepacked column was employed and combined with manual batch process. The following chromatographic process was implemented and fractions of one column volume (CV) were collected in 8 ml tubes. Elution steps were tested for the first purification to determine the suitable phosphate concentration for washing and elution. The stepwise elution buffer was produced by mixing TNTDI-20 and TNTDI-20Pi250.

Column preparation	3 CV destilled water	
	3 CV 1 M NaOH	
Column equilibration	3 CV destilled water	
	3 CV TNTDI-20Pi250	
	4 CV TNTMDI	
Sample application	flow through collected in one fraction	
Column wash	4 CV TNTDI-20	fraction collected
Column elution	5 CV TNTDI-20Pi50	fraction collected
	5 CV TNTDI-20Pi100	fraction collected
	5 CV TNTDI-20Pi150	fraction collected
	5 CV TNTDI-20Pi200	fraction collected
	5 CV TNTDI-20Pi250	fraction collected

The second fraction of each elution step was examined by SDS-PAGE and Western blot. The elution fractions that contained most of the target protein were pooled and prepared for IMAC.

Immobilized metal affinity chromatography (IMAC)

NICKEL RAPID RUN™ was packed on column with 0.45 µl filter (CHROMABOND® polypropylene columns, MACHEREY-NAGEL GmbH & Co. KG, Germany) and manual batch method was applied. The following program was applied for IMAC and fractions of 1 CV were collected in 8 ml tubes.

Column preparation	2 CV destilled water	
	2 CV TI500-Eq	
Column equilibration	2 CV destilled water	
	2 CV TNTDI-150	
	4 CV TNTDI-20	
Sample application	flow through collected in one fraction	
Column wash	4 CV TNTDI-20	fraction collected
Column elution	5 CV TNTDI-150	fraction collected

The fractions were analyzed by SDS-PAGE and Western blot and the fractions with the highest amount of the target protein were pooled. The pooled fractions were concentrated with Vivaspin® 20 Centrifugal Concentrator (100 kDa cut-off, Sartorius Stedim Biotech GmbH, Germany) according to manufacturer's instruction. If buffer exchange was necessary for the subsequent experiment, the pooled fractions were exchanged five times in end buffer.

2.5.3.4 Chromatography under denatured condition

The soluble denatured recombinant antigens in supernatant (S3) from section 2.5.3.1 were directly subjected to chromatography. Two chromatography techniques were applied in series, IMAC and cation exchange chromatography (cat.-IEX). The packing materials were packed in column with a 0.45 µl filter.

Denatured IMAC

The procedure of denatured IMAC was the same as described above with different buffer system. The column was equilibrated with TNUDI-150 followed by TNUDI-20. After the sample application, the column was washed with TNUDI-20 and the target antigen was eluted with TNUDI-150. After analysis with SDS-PAGE and Western blot, the elution fractions that contained most of the target protein were pooled and prepared for cat.-IEX.

Denatured cation exchange chromatography (cat.-IEX)

The pooled eluate from denatured IMAC was dialyzed in a dialysis tube against A50 buffer overnight and then the dialysate was supplemented with urea to reach the final

concentration of 8 M prior to being applied on the column. SP-Sepharose Fast Flow was packed in column with a 0.45 µl filter. The following steps were applied for denatured Cat.-IEX and fractions of 1 CV were collected in 8 ml tubes manually.

Column preparation	2 CV destilled water	
	2 CV PBS1000(U)	
Column equilibration	2 CV destilled water	
	4 CV AU	
Sample application	flow through collected in one fraction	
Column wash	4 CV AU	fraction collected
Column elution	5 CV PBS1000(U)	fraction collected

The fractions were then treated as described in 2.5.3.3.

2.5.3.5 Quality analysis of purified antigens

The quality of the final preparations was analyzed with different methods.

Determination of protein concentration

The protein concentration of the preparation was determined by the advanced protein assay. The measurement and result was controlled and documented by software Magellan 7.1 SP1 at 570 nm with TECAN Reader Sunrise.

Advanced protein assay was carried out according to manufacturer's instruction. In short, the calibration curve was generated with the serial dilution of BSA from 750 µg/ml to 0 µg/ml in 0.9% sodium chloride injection solution. The diluted preparation samples were prepared as above. 10 µl of calibrators or samples were mixed with 300 µl 1:5 diluted advanced protein assay reagent in the well of microplate. The mixture was then directly measured. Each calibrator or sample was tested twice.

SDS-PAGE and MALDI-TOF-MS

The procedure was the same as described in section 2.4.2 and 2.4.3. 1 µg of recombinant protein was loaded on NuPAGE™ Novex™ 4-12% Bis-Tris Protein Gel under reduced and unreduced condition. The protein bands were visualized using blue silver coomassie stain and the detectable bands were further analyzed with MALDI-TOF-MS. Thus, the identity and the purity of the preparation could be determined.

The satisfactory preparations were portioned in 0.1 to 2 ml Aliquots and stored at -80°C for subsequent experiment.

2.6 Verification of candidate antigens and development of immunoassays

Candidate antigens were verified by different methods: (1) neutralization test with purified recombinant antigens; (2) colocalization test with a commercial antibody; (3) Western blot with purified recombinant antigens or unpurified recombinant *E. coli* or HEK293 cell lysates; and (4) IFA with recombinant HEK293 cells. Based on the verification, the development of an immunoassay was carried out subsequently.

2.6.1 Neutralization test

The purified antigens were applied in this experiment. Diluted serum samples (1:100 and 1:1000) were preincubated for 1 hour with diluted purified antigen to neutralize the reactivity of the specific antinuclear autoantibody before they were incubated on ANA research slides. As control, the respective buffer without antigen was used. The subsequent steps were as described in section 2.2.2. The samples were visualized using confocal laser scanning microscope LSM700- Axio Imager M2 and the images could be captured by ZEN 2000 software. The neutralization effect was assessed by comparing the fluorescence signal of neutralized samples and control.

2.6.2 Colocalization analysis of TJP1

A parallel staining of HEp-2 cells, transfected HEK293 cells with serum and anti-TJP1 antibody was used to compare the expression patterns. Therefore, 1:10 or 1:100 diluted UNA25 was mixed with 1:50 diluted anti-TJP1 in PBS-Tween. Incubation and washing steps were as described in section 2.2.2. The detection of primary antibodies was enabled by incubation with anti-human-IgG-alexa488 (1:500) and anti-mouse-IgG-Cy3 (1:200). Confocal laser scanning microscope LSM700- Axio Imager M2 was used to analyze samples and ZEN 2000 software was used to capture images.

2.6.3 Western blot

10 µl unpurified *E. coli* or HEK293 cell lysates or 2 µg purified recombinant antigens were applied in SDS-PAGE and Western blot as described in section 2.4.2. The cut membranes were incubated with index sera and/or healthy control sera (n=15). A two-step incubation for the detection of the His-tag was implemented as described in 2.5.3.

2.6.3.1 Prototype lineblot profile

After the candidate antigens were tested in Western blot, dot blot was performed in order to select the suitable antigen dilution. The blot incubation and evaluation procedure were the same as described in section 2.2.1.

Dot blot

Precut (3 mm x 5 mm) empty Biodyne™ B membranes (Biodyne™ B Nylon Membrane, 0.45 µm, Thermo Fisher Scientific Inc., USA) were fixed on strips by the blot department of EUROIMMUN AG. The antigen was serial diluted in the respective buffer. On each field, 1 µl undiluted or diluted antigen solution (1:3.2, 1:10, 1:32, 1:100, 1:320, 1:1000 and 1:3200) was applied and dried for 20 minutes at RT. The strips were then packed in aluminum foil bag and stored at 4°C. The incubation of the antigen coated on dot blot strips was performed on the second day.

The optimum dilution, with which index serum samples showed a reaction and healthy control sera (n=10) did not, was selected and used for the production of research lineblots by the Blot department of EUROIMMUN AG.

Stability test

The research lineblots were stored at 4°C and 37°C, respectively. They were incubated with anti-His-tag, index sera and ten healthy control sera on day 0, day 7 and day 14. The results were evaluated with the software EUROLineScan.

Research lineblot: UFO-ANA profile 1

The antigens that passed the stability test were further assembled on one strip to produce the research lineblot, UFO-ANA profile 1 (Figure 2-4). Eight purified recombinant antigens were combianed on this strip: SMCHD1, CD2BP2, NVL, TFAP2A, fragment aa1-575 of TJP1, fragment aa1475-1970 of POLR2A and PSME3 It was incubated with anti-His-tag, index sera and healthy control sera (n=50) followed by clinically characterized patient sera (SARD cohort).

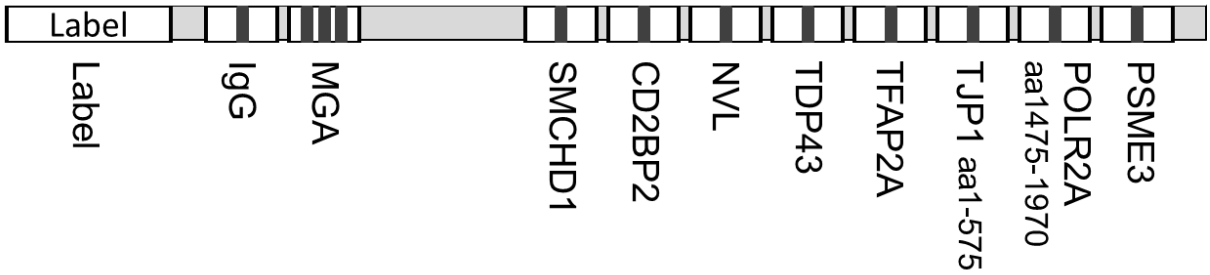

Figure 2-4 A schematic picture of the research lineblot, UFO-ANA profile 1
Each black line indicates the individual positive reaction. Eight antigens could be tested with this strip.

An experimental cut-off for the research lineblot was applied as follows: TJP1 aa1-575, TFAP2A, NVL and CD2BP2 with cut-off=20; PSME3, POLR2A aa1475-1970, TDP43 and SMCHD1 with cut-off=10.

2.6.4 IFA with transfected HEK293 cells

Recombinant HEK293 cells expressing different target antigens were cultured on cover glasses for two days and fixed with acetone by the recombinant synthesis department of EUROIMMUN AG. Cover glasses with fixed cells were then cut into suitable pieces and applied for the production of BIOCHIP Mosaic[@] research slides for verification. Transfected HEK293 cells expressing individual candidate antigens were incubated with anti-His-tag antibody (1:200), index serum samples (1:100) and 50 healthy control sera (1:100). HEK293 cells transfected with empty plasmid and HEp-2 cells were applied as controls in each Mosaic[@]. The incubation and evaluation procedure were the same as described in section 2.2.2

2.6.4.1 Composition of two research slides for recombinant HEK293 cells based IFA (RC-IFA)

Eleven antigens were selected for RC-IFA with HEK293 cells and arranged in two research slides for studying the clinical association, namely UFO-ANA clinical association 1 and 2 (Figure 2-5). Besides of HEK293 cells transfected with empty plasmid and HEp-2 cells as controls on each slide, the first slide contained transfected HEK293 cells expressing the seven candidate antigens, PSME3, TFAP2A, TDP43, DHX9, POLR2A, RPA, and RuvBL. The second slide incorporated transfected HEK293 cells expressing the four antigens: SMCHD1, PELP1+SENP3, NVL and XRN2. Three subunits of RPA (RPA1, RPA2 and RPA3), two homologs for RuvBL (RuvBL1 and RuvBL2), and the two interaction partners (PELP1 and SENP3) were co-expressed respectively.

The research slides were employed for screening a SARD cohort with index sera as positive controls and healthy control sera as negative controls. Incubation procedure was the same as mentioned above with anti-human-IgG-FITC (ready-to-use) in secondary incubation.

Evaluation of the result was implemented using a level system. Level 0, 0.5 and 1 to 5 was defined as negative, borderline and the weak positive to the strongest positive reaction, respectively.

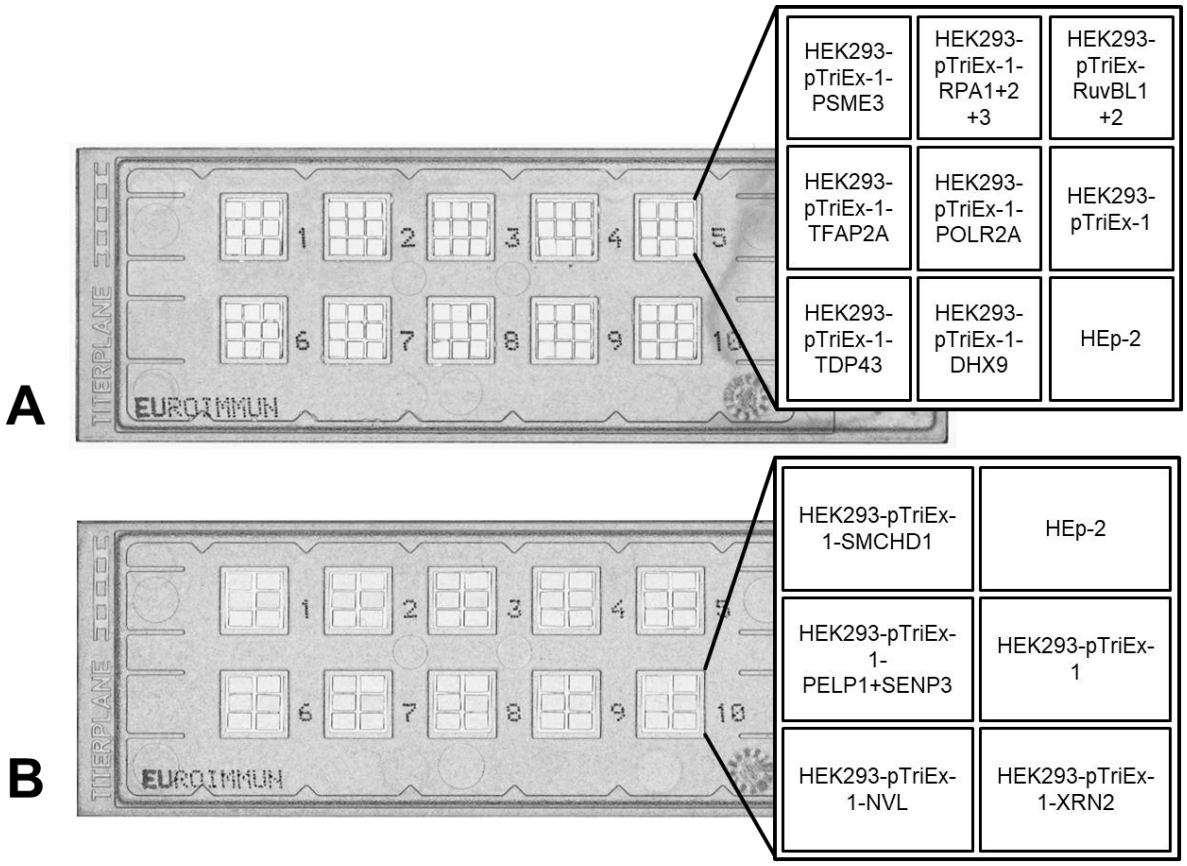

Figure 2-5 Schema of two research BIOCHIP slides for studying clinical association
A) UFO-ANA clinical association 1. This slide consisted of HEp-2 cells, HEK293 cells individually transfected with plasmids coding for PSME3, TFAP2A, TDP43, DHX9, POLR2A, and empty vector, HEK293 cells concurrent transfected with RPA1, RPA2, RPA3 and HEK293 cells transfected concurrent transfected with RuvBL1 and RuvBL2. **B)** UFO-ANA clinical association 2. This slide consisted of HEp-2 cells, HEK293 cells individually transfected with plasmids coding for SMCHD1, NVL, XRN2 and empty vector, HEK293 cells concurrent transfected with PELP1 and SENP3. All cells were fixed with acetone.

2.7 Statistics

In this exploratory study, descriptive statistics were used for statistical analysis. Microsoft® Office Excel 2010 was employed for processing raw data and generations of diagrams.

3 Results

This work intended to identify novel ANA autoantigens and study their clinical relevance. Therefore, immunoassays with recombinant antigens were developed. The results of this project include two parts: a) antigen identification with UNA samples and b) antigen identification with clinically characterized serum samples with novel patterns. The relevant results are presented in this chapter. The supplement data can be found in the appendix.

Part a: Antigen identification with UNA samples

3.1 Characterization of serum samples

In total, 190 HEp-2 ANA positive serum samples, which showed negative results in the requested monospecific analyses, were collected from the Clinical Immunological Laboratory of Prof. Dr. med. Winfried Stöcker. All the sera were re-characterized with IFA using ANA research slides and the Euroline ANA profile 23 (IgG) (Figure 2-1). The observed nuclear pattern and estimated titers were documented and compared with the original results from the Clinical Immunological Laboratory. Serum samples were not considered for antigen identification experiments, if at least one of the following conditions was met: 1) convincing reaction against an established ANA antigen was detected (51/190 samples), 2) volume less than 0.4 ml (59/190 samples). The remaining 80 samples defined the UNA cohort (Figure 3-1).

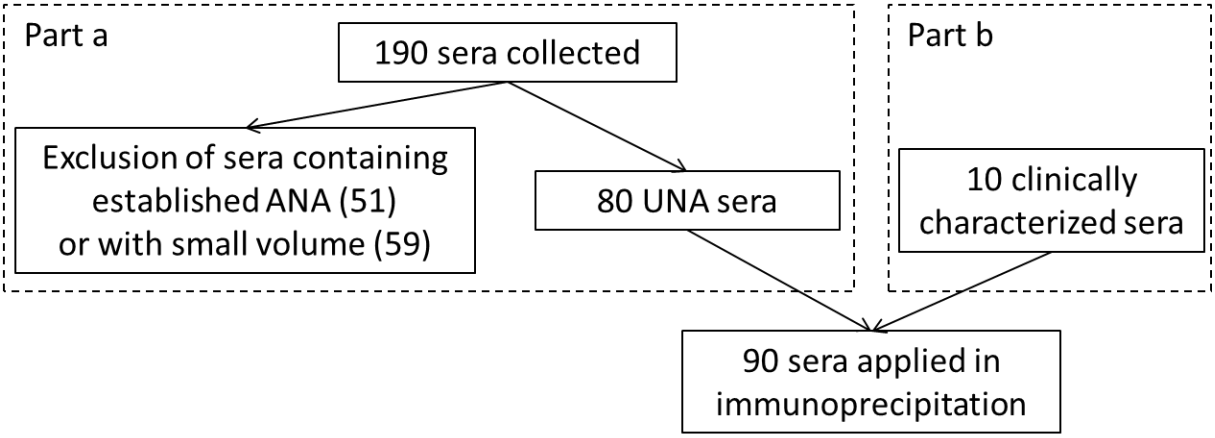

Figure 3-1 Serum samples for immunoprecipitation
ANA: antinuclear autoantibody; UNA: unknown nuclear antigen

Autoantibodies against established antigens were most frequently directed against DFS70 (26 samples, Figure 3-2, A), followed by anti-SSA (6 samples), anti-Ro52 (4 samples), anti-Mi-2a/b (3 samples), anti-RNA polymerase III (3 samples), anti-

fibrillarin (2 samples), anti-NOR90 (2 samples), anti-dsDNA (1 sample), anti-RNP/Sm (1 sample), anti-PM75/100 (1 samples), anti-centromere (1 sample) and anti-gp210 (1 sample). All in all, 80 UNA samples were further processed.

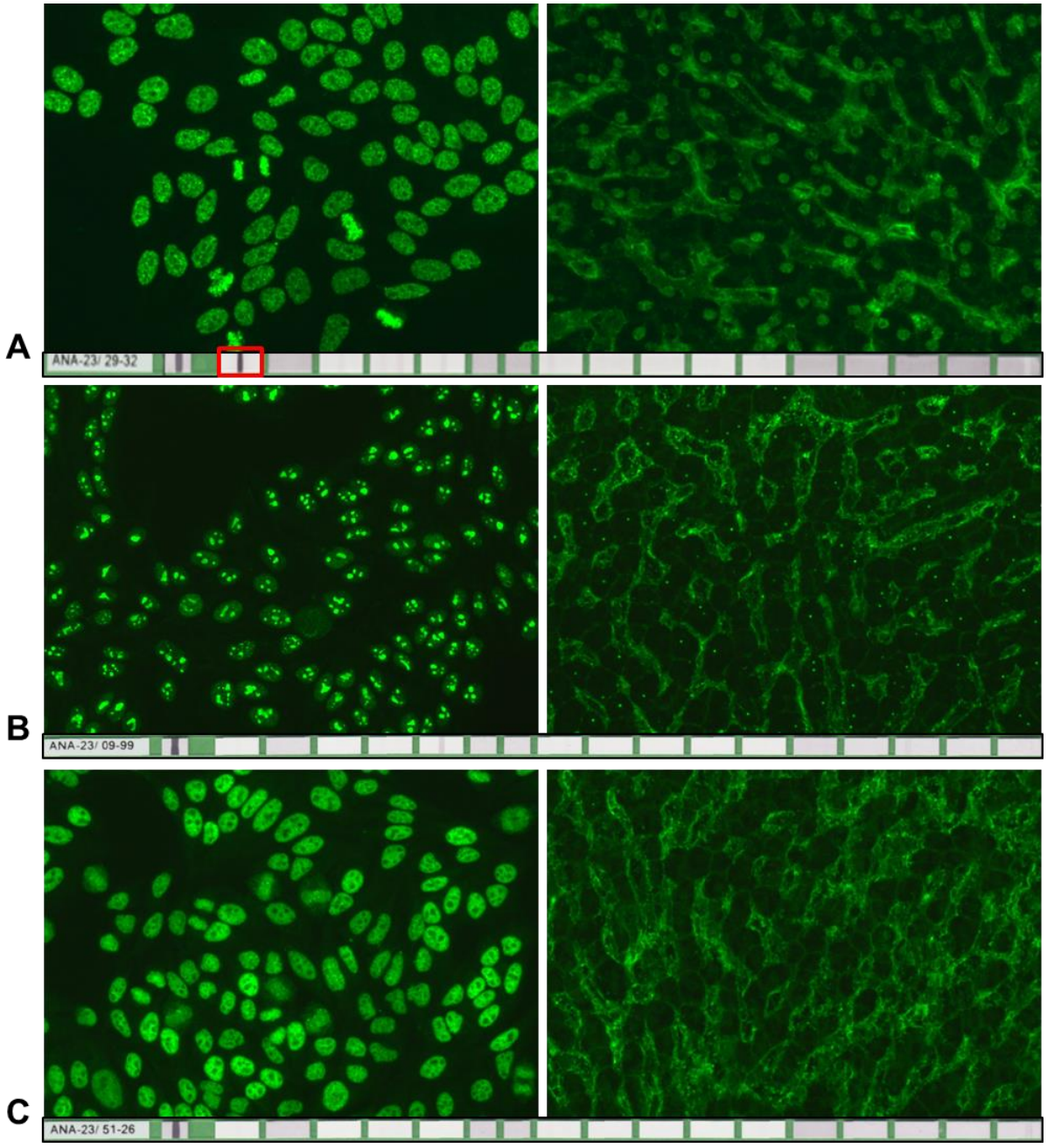

Figure 3-2 Characterization of UNA sera with IFA and EUROLINE
Sera (1:100) were analyzed in IFA with HEp-2 cells (left) and monkey liver (right). Anti-Human-IgG-Alexa488 (1:500) was applied as secondary antibody. Sera (1:101) were tested with Euroline ANA profile 23 (bottom). Anti-human-IgG-B/E-AP (1:10) was employed in secondary incubation. **A)** "false" UNA sera: UNA59 shows a dense fine speckled pattern. A positive reaction against DFS70 is indicated with the red square. **B)** "true" UNA sera: UNA74 shows a nucleolar pattern. A borderline anti-PM-Scl75 reactivity was detected. **C)** "true" UNA sera: UNA96 shows a pseudo-dense fine speckled pattern. (IFA magnification 200x)

Two representative UNA samples are displayed in Figure 3-2, B and C. UNA74 showed nucleolar pattern and UNA96 showed granular pattern with positive

chromosome stain in mitotic cells. Both samples were negative in Euroline ANA profile 23.

In Table 3-1, these samples are gathered in different groups according to the ANA patterns, namely nucleolar, granular, homogeneous, pseudo-dense fine speckled (DFS), few nuclear dots, pleomorphic/granular (partly stronger) and nuclear envelope. Because the different patterns could overlap, one sample may be in several groups. The sample number and example pictures of IFA with HEp-2 cells are listed.

ANA pattern Group	Example picture of IFA with HEp-2 cells	Total number of samples with pattern	Belonging UNA samples (UNA No.)
Nucleolar (UNA74)	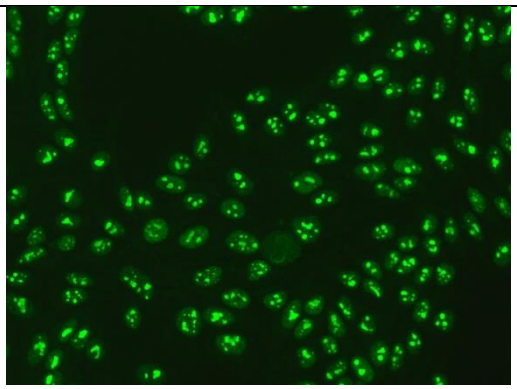	20	2, 17, 26, 29, 74, 75, 81, 87, 102, 125, 128, 129, 132, 134, 170, 176, 177, 178, 200, 202
Pseudo-dense fine speckled (DFS) (UNA96)	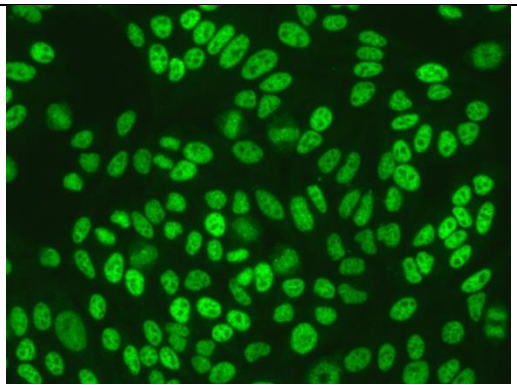	16	1, 16, 36, 49, 53, 62, 96, 119, 162, 163, 168, 169, 172, 190, 209, 219
Granular (UNA71)	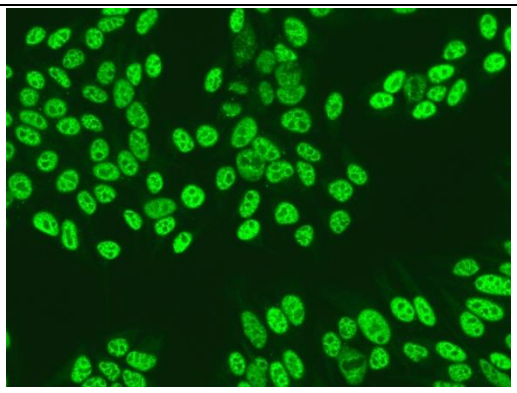	38	2, 3, 6, 17, 23, 26, 32, 33, 34, 35, 38, 41, 43, 44, 54, 61, 63, 65, 70, 71, 86, 92, 102, 103, 108, 123, 125, 133, 134, 177, 179, 180, 189, 194, 202, 206, 211, 218

Homo -geneous (UNA105)	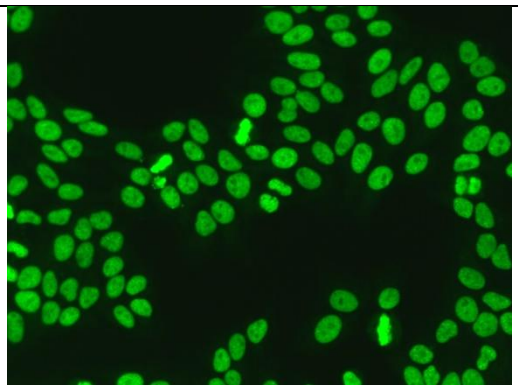	10	25, 72, 105, 127, 131, 132, 173, 174, 198, 216
Few nuclear dots (UNA112)	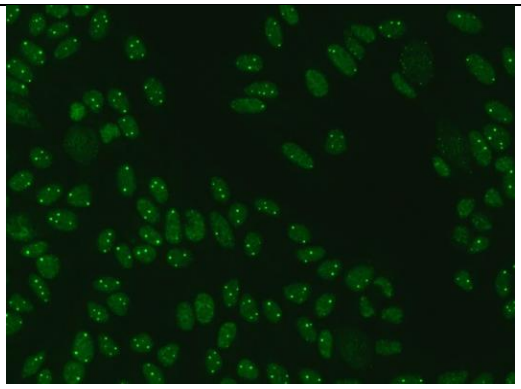	5	3, 108, 112, 194, 195
Pleomor- phic/ granular (partly stronger) (UNA111)	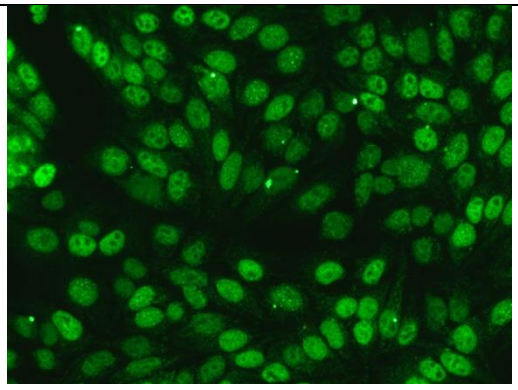	2	111, 220
Nuclear envelope (UNA123)	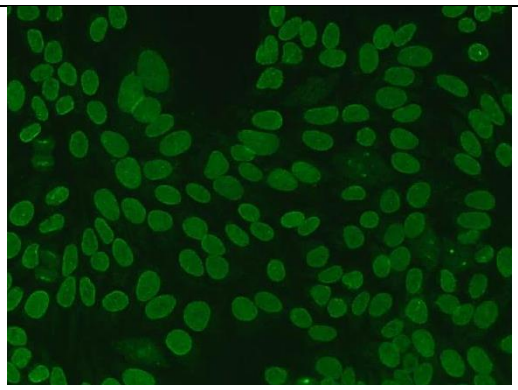	3	29, 105, 123,

Table 3-1 Groups of UNA samples and example IFA pictures
IFA with HEp-2 cells with 1:100 dilution, magnification 200x

3.2 Candidate antigens

In order to identify the target antigens, 80 UNA sera were subjected to fractionated IP (FIP) with HEp-2 cell homogenate as described in 2.4. Immunoprecipated proteins were resolved by SDS-PAGE and stained with blue silver coomassie stain. Additionally, Western blots with autologous serum samples were performed to detect immunoreactive proteins. A representative image of a coomassie stained gel and the corresponding Western blot is shown in Figure 3-3. UNA74, UNA92 and UNA96 showed Western blot reactivity against immunoprecipitated antigens at approximately 100 kDa, 100 kDa and 50 kDa respectively; while UNA75 and UNA87 did not. The selected bands (Figure 3-3, arrowhead) were sent to immunobiochemical research department of EUROIMMUN AG for MALDI-TOF-MS analysis and to identify the target antigens. All successful antigen identification experiments were repeated at least once to confirm the results.

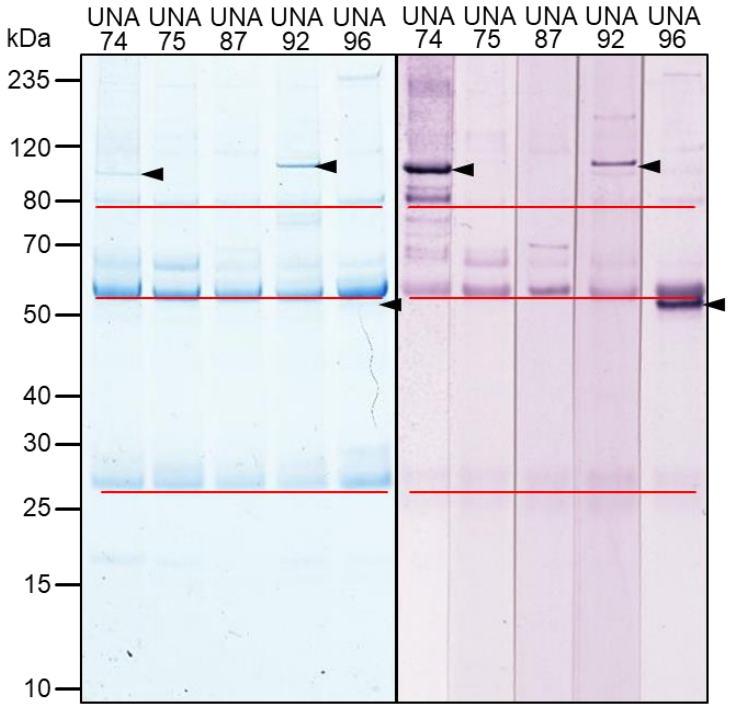

Figure 3-3 Fractionated immunoprecipitation (FIP) with UNA sera.
UNA74 (granular and nucleolar), UNA75 (nucleolar), UNA87 (nucleolar), UNA92 (granular) and UNA96 (pseudo-dense fine speckled) were analyzed using FIP. Immunoprecipitated proteins were separated by SDS-PAGE. Gels were stained with coomassie (left) or analyzed by Western blot (right) incubated with autologous serum samples (1:200) followed by anti-human-IgG-B/E-AP (1:10) incubation. The arrowhead marked bands were selected according to the Western blot reaction. The red lines indicate bands of IgG fragments.

3.2.1 Four candidate antigens identified with sera of the nucleolar group

Four novel candidate antigens were identified with 5 of 20 nucleolar samples. Nuclear valosin-containing protein-like (NVL) was identified as target antigen of UNA74, UNA81 and UNA170. The result of IP-Western blot analysis with UNA74 is shown as an example in Figure 3-4, A. After FIP, a band at approximately 100 kDa was detected in the eluate in coomassie stained gel and in Western blot incubated with autologous serum. The marked band 1 was analyzed by mass spectrometry and identified as different isoforms of NVL. The results of MALDI-TOF-MS are shown in Table 3-2.

In the IP eluate of UNA177 a strong band (band 2) at approximately 100 kDa was found in the coomassie stained gel (Figure 3-4, B1). In a corresponding Western blot, a band at the same size showed strong reactivity. 5'-3' exoribonuclease 2 (XRN2) was identified as target antigen of UNA177 in PMF and MS/MS measurements (Table 3-2). UNA177 showed a granular and nucleolar pattern on both HEp-2 cells and monkey liver (Figure 3-4, B2 and B3).

In a Western blot with the UNA26 IP eluate and autologous serum, two bands with high intensity were detected at around 120 kDa and 70 kDa. The corresponding bands were marked as band 3 and band 4 in the coomassie gel (Figure 3-4, C1). With MALDI-TOF-MS, proline-, glutamic acid- and leucine-rich protein 1 (PELP1) (band 3) and sentrin-specific protease 3 (SENP3) (band 4) were identified (Table 3-2). The ANA pattern of UNA26 was very similar to the pattern of UNA177. It presented also a granular and nucleolar staining (Figure 3-4, C2 and C3).

In the remaining 15 UNA samples of the nucleolar group, the target antigen could not be identified using FIP. No specific band was observed in coomassie stained gels, neither a Western blot reaction was detected.

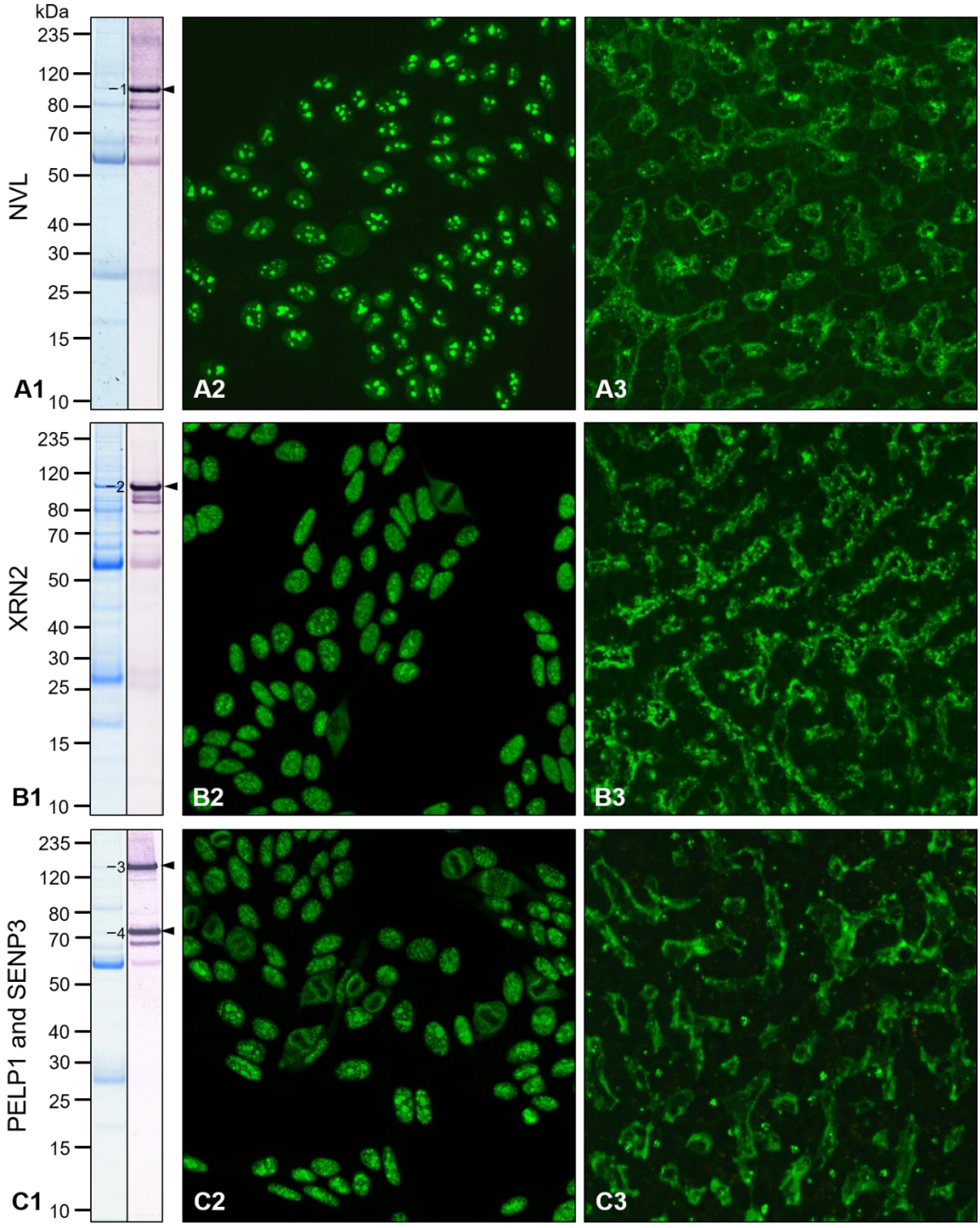

Figure 3-4 Identification of candidate antigens with sera of the nucleolar group.
1) FIP of UNA sera with nucleolar pattern. Immunoprecipitates were analyzed with coomassie stained gel (left) or Western blot with autologous sera (right). According to Western blot reaction (arrowhead), protein bands were selected for MALDI-TOF-MS. **2)** IFA with HEp-2 cells and **3)** monkey liver with UNA sera (1:1000) and anti-Human-IgG-Alexa488 (1:500) as secondary antibody. **A)** Nuclear valosin containing protein-like (NVL) was identified as target antigen of UNA74, which showed nucleolar pattern on both substrates. **B)** 5'-3' exoribonuclease 2 (XRN2) was identified as target antigen of UNA177. ANA pattern of UNA177 was granular and nucleolar. **C)** Proline-, glutamic acid- and leucine-rich protein 1 (PELP1) and sentrin-specific protease 3 (SENP3) were identified as target antigens of UNA26. UNA26 showed granular and nucleolar ANA pattern, which was similar to the pattern of UNA177. (magnification 200x)

Band	Annotation	Cut off	Score	Seq. cov.	Pep-tides	Mass /Da	Database
1	Nuclear valosin-containing protein-like OS=Homo sapiens GN=NVL PE=1 SV=1	59	164	33	21	96017	SwissProt_Homo_sapiens
1	Nuclear valosin-containing protein-like OS=Homo sapiens GN=NVL PE=1 SV=1 (Score under Cut Off)	32	4	1	1	96017	SwissProt_Homo_sapiens
2	5'-3' exoribonuclease 2 OS=Homo sapiens OX=9606 GN=XRN2 PE=1 SV=1	59	270	50	47	109426	SwissProt_Homo_sapiens
2	5'-3' exoribonuclease 2 OS=Homo sapiens OX=9606 GN=XRN2 PE=1 SV=1	32	32	2	2	109426	SwissProt_Homo_sapiens
3	Proline-, glutamic acid- and leucine-rich protein 1 OS=Homo sapiens GN=PELP1 PE=1 SV=2	56	161	32	26	120879	SwissProt_Homo_sapiens
3	Proline-, glutamic acid- and leucine-rich protein 1 OS=Homo sapiens GN=PELP1 PE=1 SV=2	27	50	3	2	120879	SwissProt_Homo_sapiens
4	Sentrin-specific protease 3 OS=Homo sapiens GN=SENP3 PE=1 SV=2	56	103	32	16	65596	SwissProt_Homo_sapiens
4	Not identified						SwissProt_Homo_sapiens

Table 3-2 Mass spectrometry analysis of three UNA samples with nucleolar pattern.
Peptide-mass-fingerprinting results are in black and tandem mass spectrometry results are in blue.

3.2.2 Two candidate antigens identified with sera of the pseudo-DFS group

In the pseudo-DFS group, two candidate antigens were found. The results are shown in Figure 3-5.

Using UNA219 in FIP and Western blot, a band slightly beneath 50 kDa was detected with moderate intensity (Figure 3-5, A1). CD2 antigen cytoplasmic tail-binding protein 2 (CD2BP2) was identified with the help of MALDI-TOF-MS (Table 3-3). UNA219 showed pseudo-DFS pattern on both Hep-2 cells and monkey liver (Figure 3-5, A2 and A3).

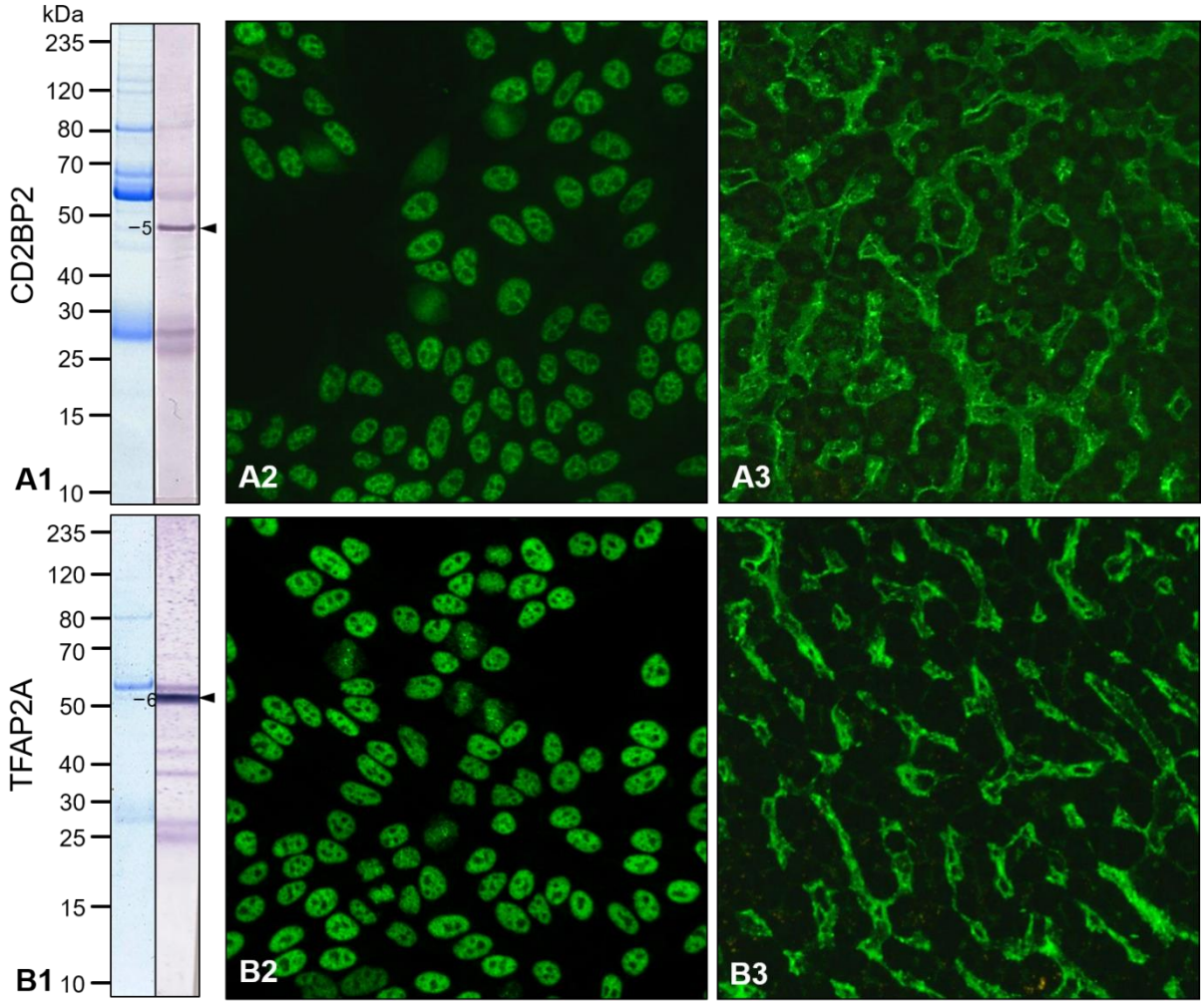

Figure 3-5 Identificaiton of candidate antigens with sera of the pseudo-DFS group.
1) FIP of UNA sera with nucleolar pattern. Immunoprecipitates were analyzed with coomassie stained gel (left) or Western blot with autologous sera (right). According to Western blot reaction (arrowhead), protein bands were selected for MALDI-TOF-MS. **2)** IFA with HEp-2 cells and **3)** monkey liver with 1:100 diluted UNA sera and anti-Human-IgG-Alexa488 (1:500) as secondary antibody. **A)** CD2 antigen cytoplasmic tail-binding protein 2 (CD2BP2) was identified as target antigen of UNA219. IFA showed pseudo-dense fine speckled pattern on HEp-2 cells and monkey liver. **B)** Transcription factor AP-2-alpha (TFAP2A) was identified as target antigen of UNA96. In IFA, it showed a pseudo-DFS pattern on HEp-2 cells while monkey liver remained negative. (magnification 200x)

Transcription factor AP-2-alpha (TFAP2A) was identified as candidate antigen of UNA53 and UNA96. The IP-Western blot analysis of UNA96 is shown in Figure 3-5, B as an example. A strong Western blot reaction of UNA96 with the corresponding IP eluate (Figure 3-5, arrowhead) indicated that the target antigen is approximately 50 kDa. The corresponding band detected in the coomassie stained gel was marked as band 6 and identified as TFAP2A with MALDI-TOF-MS (Table 3-3). UNA96 showed a pseudo-dense fine specked pattern on HEp-2 cells, but monkey liver remained negative.

No conspicuous bands were observed in IP eluates of the other 13/16 UNA samples of the pseudo-DFS group.

Band	Annotation	Cut off	Score	Seq. cov.	Pep-tides	Mass /Da	Database
5	CD2 antigen cytoplasmic tail-binding protein 2 OS=Homo sapiens GN=CD2BP2 E=1 SV=1	59	100	36	10	37737	SwissProt _Homo _sapiens
5	Not identified						SwissProt _Homo _sapiens
6	Transcription factor AP-2-alpha OS=Homo sapiens GN=TFAP2A PE=1 SV=1	59	126	38	15	48432	SwissProt _Homo _sapiens
6	Transcription factor AP-2-alpha OS=Homo sapiens GN=TFAP2A PE=1 SV=1	30	37	4	1	48432	SwissProt _Homo _sapiens

Table 3-3 Mass spectrometry analysis of two UNA samples with pseudo-DFS pattern.
Peptide-mass-fingerprinting results are in black and tandem mass spectrometry results are in blue.

3.2.3 Eight candidate antigens identified with sera of the granular group

Among 37 UNA samples with granular pattern, eight candidate antigens were identified with 13/37 sera. Four of them were previously described in the master thesis [32]. They are listed in the summary of candidate antigens in Table 3-6. Four newly identified antigens are present below.

Matrin-3 (MATR3) was identified as the target antigen of UNA92. A specific band at approximately 100 kDa was found in the coomassie stained gel of UNA92 IP eluate, which showed Western blot reactivity with the autologous serum sample (Figure 3-6, A1). This band was marked as band 7 and according to PMF measurements MATR3 was detected (Table 3-4). As it is shown in Figure 3-6, A2 and A3, the ANA pattern of UNA92 was granular on both HEp-2 cells and monkey liver.

UNA3 was tested in FIP. The coomassie stained gel and the Western blot are shown in Figure 3-6, B1. A band at about 50 kDa with specific Western blot reaction was selected for MALDI-TOF-MS analysis. The PMF result and MS/MS result supported that TAR DNA-binding protein 43 (TDP43) was the target antigen of UNA3 (Table 3-4). It was observed that UNA3 showed a mix pattern of granular and few nuclear dots on HEp-2 cells and monkey liver in IFA (Figure 3-6, B2 and B3).

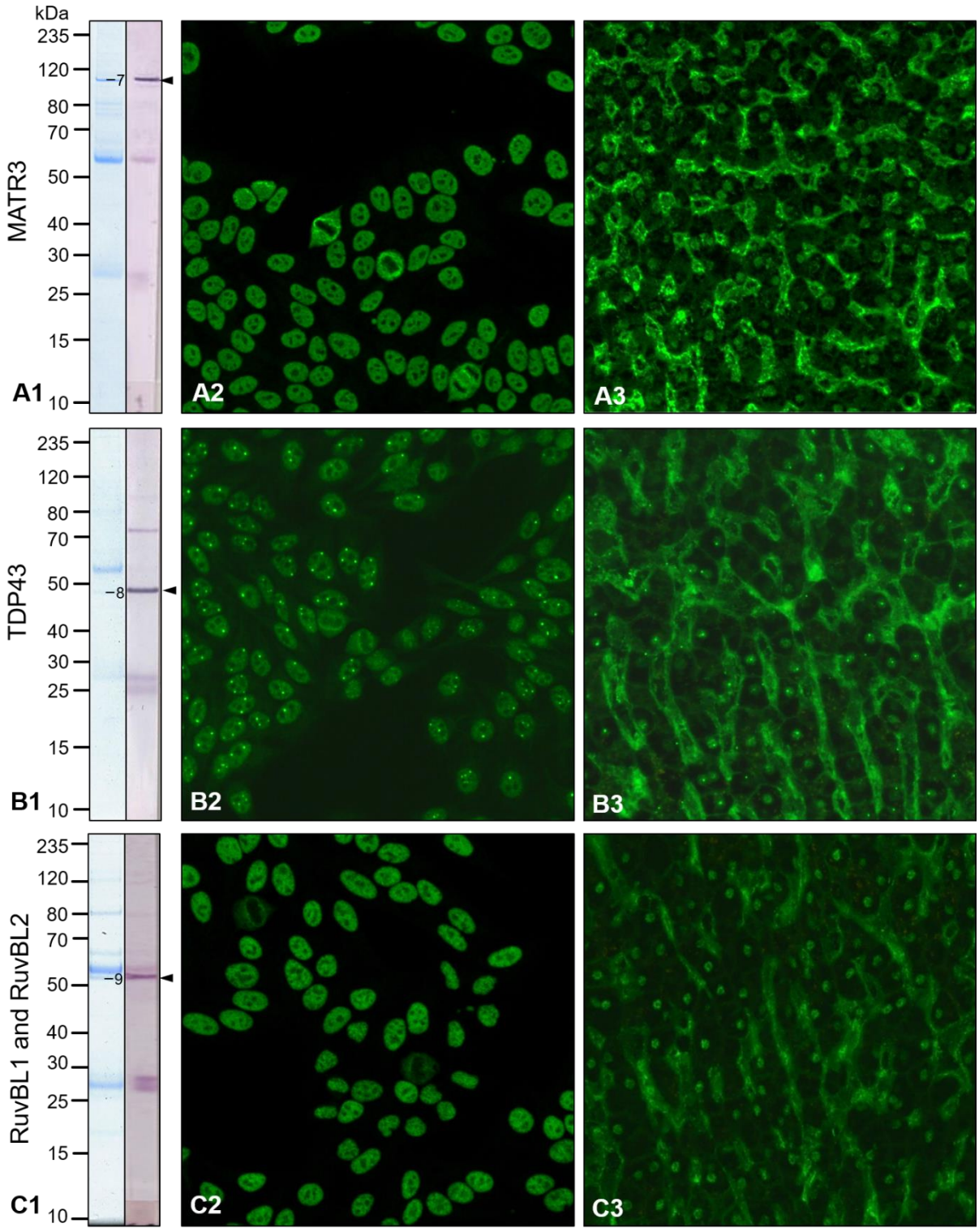

Figure 3-6 Identificaiton of candidate antigens with sera of the granular group.
1) FIP of UNA sera with nucleolar pattern. Immunoprecipitates were analyzed with coomassie stained gel (left) or Western blot with autologous sera (right). According to Western blot reaction (arrowhead), protein bands were selected for MALDI-TOF-MS. **2)** IFA with HEp-2 cells and **3)** monkey liver with UNA sera (UNA92 and UNA96 1:1000, UNA3 1:100) and anti-Human-IgG-Alexa488 (1:500) as secondary antibody. **A)** Matrin-3 (MATR3) was identified as target antigen of UNA92. IFA showed granular pattern on HEp-2 cells and monkey liver. **B)** TAR DNA-binding protein 43 (TDP43) was identified as target antigen of UNA3. Besides of granular pattern, few nuclear dots pattern was observed in IFA. **C)** RuvB-like 1 (RuvBL1) and RuvB-like 2 (RuvBL2) were identified as target antigens of UNA65. In addition to classic granular pattern, chromosome area in mitotic cells was stained occasionally. (magnification 200x)

Two homolog proteins, RuvB-like 1 (RuvBL1) and RuvB-like 2 (RuvBL2), were identified using UNA65 in FIP. A specific band around 50 kDa was detected in the coomassie stained gel and in Western blot as well (Figure 3-6, C1). Band 9 was analyzed with MALDI-TOF-MS (Table 3-4). The ANA pattern of UNA65 was granular on both HEp-2 cells and monkey liver (Figure 3-6, C2 and C3). In IFA with HEp-2 cells it was observed that in mitotic cells the condensed chromosome area was stained occasionally.

The identification of the target antigens of UNA26 and UNA177 was already described above in the nucleolar group (section 3.2.1). With the remaining 22/37 UNA samples with granular pattern, no candidate antigen was identified. Either no specific band was observed (19/22) or results were not reproducible (3/22).

Band	Annotation	Cut off	Score	Seq. cov.	Pep-tides	Mass /Da	Database
7	Matrin-3 OS=Homo sapiens GN=MATR3 PE=1 SV=2	59	189	28	19	95078	SwissProt _Homo _sapiens
7	Not identified						SwissProt _Homo _sapiens
8	TAR DNA-binding protein 43 [Homo sapiens] (Score under Cutoff)	68	55	31	8	45053	NCBInr_ sub_Homo _sapiens
8	TAR DNA-binding protein 43 [Homo sapiens]	37	43	4	1	45053	NCBInr_ sub_Homo _sapiens
9	RuvB-like 2 isoform 1 [Homo sapiens]	68	114	33	14	51296	NCBInr _sub_Homo _sapiens
9	PREDICTED: RuvB-like 1 isoform X1 [Homo sapiens]	68	76	28	9	51812	NCBInr_ sub_Homo _sapiens
9	PREDICTED: RuvB-like 1 isoform X1 [Homo sapiens] (Score unter Cutoff)	38	37	3	1	51812	NCBInr_ sub_Homo _sapiens

Table 3-4 Mass spectrometry analysis of three UNA samples with granular pattern.
Peptide-mass-fingerprinting results are in black and tandem mass spectrometry results are in blue.

3.2.4 Candidate antigens identified with one sera of the pleomorphic group

Two UNA samples were oriented in the pleomorphic group. One of them, UNA 111, was able to pull down replication protein A (RPA) using FIP. The IP eluate showed three specific bands at around 70 kDa, 35 kDa and 13 kDa in the coomassie stained gel (Figure 3-7, A, band 10, 11 and 12). The corresponding bands of band 10 and

band 12 in Western blot with UNA111 showed moderate to weak reactions, while the corresponding Western blot of band 11 showed a strong positive reaction. These three bands were analyzed with MALDI-TOF-MS and RPA 70 kDa subunit (RPA1), RPA 32 kDa subunit (RPA2) and RPA 14 kDa subunit (RPA3) were identified in band 10, band 11 and band 12 respectively (Table 3-5). UNA111 showed a pleomorphic pattern in HEp-2 cells and monkey liver (Figure 3-7, B and C).

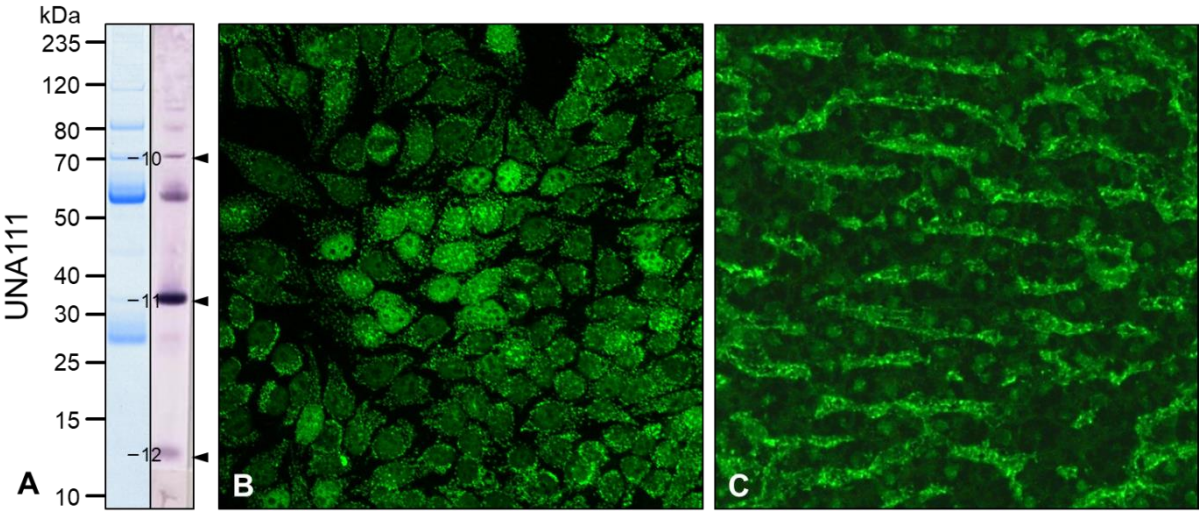

Figure 3-7 Identification of candidate antigen with sera of the pleomorphic group.
A) UNA111 was subjected to fractionated immunoprecipitation. The coomassie stained gel and the Western blot with the IP eluate and UNA111 are presented. Arrowheads indicate three specific reactions. With the help of MALDI-TOF-MS, RPA was identified and the marked bands represent three subunits of RPA. Band 10 was 70 kDa subunit (RPA1), band 11 was 32 kDa subunit (RPA2) and band 12 was 14 kDa subunit (RPA3). **B)** IFA with HEp-2 cells and **C)** monkey liver with 1:100 diluted UNA111 and anti-Human-IgG-Alexa488 (1:500) as secondary antibody. It showed pleomorphic ANA pattern with granular nuclear and granular cytoplasmic stain with different intensity on HEp-2 cells. A granular pattern was observed on monkey liver. (magnification 200x)

Band	Annotation	Cut off	Score	Seq. cov.	Pep-tides	Mass /Da	Database
10	Replication protein A 70 kDa DNA-binding subunit [Homo sapiens]	68	227	39	22	68723	NCBInr_ sub_Homo_s apiens
10	Replication protein A 70 kDa DNA-binding subunit [Homo sapiens]	38	64	2	1	68723	NCBInr_ sub_Homo_s apiens
11	Replication protein A 32 kDa subunit isoform 1 [Homo sapiens] (Score under Cutoff)	68	50	25	4	38342	NCBInr_ sub_Homo_s apiens
11	Replication protein A 32 kDa subunit isoform 1 [Homo sapiens] (Score under Cutoff)	38	33	13	1	38342	NCBInr_ sub_Homo_s apiens
12	Replication protein A 14 kDa subunit [Homo sapiens] (Score unter Cutoff)	68	62	71	5	13674	NCBInr_ sub_Homo_s apiens
12	Replication protein A 14 kDa subunit [Homo sapiens]	37	47	29	1	13674	NCBInr_ sub_Homo_s apiens

Table 3-5 Mass spectrometry analysis of a UNA samples with pleomorphic pattern.
Peptide-mass-fingerprinting results are in black and tandem mass spectrometry results are in blue.

3.2.5 Brief summary of candidate antigens

The identified candidate antigens are briefly summarized in Table 3-6. Besides of the nine candidate antigens/antigen complexes identified in this work, five antigens reported in the previous master project [32] are included as they were subsequently processed in this work. This includes to verify these antigens (section 3.4), to develop corresponding immunoassays (section 3.5) and to study their clinical relevance (section 3.6). All in all, the identification approach led to candidate antigens with 23/80 UNA samples. In FIP eluates of 54/80 UNA sera, no specific protein bands were observed. The results were not reproducible with 3/80 UNA samples.

Candidate antigen	Mass /kDa	ANA pattern	UNA No.	Estimated titer
Nuclear valosin-containing protein-like (**NVL**)	86	Nucleolar	74	1:3200
			81	1:1000
			170	1:10000
5'-3' exoribonuclease 2 (**XRN2**)	109	Nucleolar and granular	177	1:10000
Proline-, glutamic acid- and leucine-rich protein 1 (**PELP1**) and sentrin-specific protease 3 (**SENP3**)	120 and 65	Nucleolar and granular	26	1:3200
CD2 antigen cytoplasmic tail-binding protein 2 (**CD2BP2**)	37	Pseudo-dense fine speckled	219	1:320
Transcription factor AP-2 alpha (**TFAP2A**)	48	Pseudo-dense fine speckled	53	1:3200
			96	1:1000
Matrin-3 (**MATR3**)	95	Granular	92	1:3200
TAR DNA-binding protein 43 (**TDP43**)	45	Granular	3	1:1000
RuvB-like 1 and RuvB-like 2 (**RuvBL1**, **RuvBL2**)	50 and 51	Granular	65	1:3200
Structural maintenance of chromosomes flexible hinge domain-containing protein 1 **(SMCHD1)**	226	Granular	43	1:1000
			70	1:3200
ATP-dependent RNA helicase A **(DHX9)**	140	Granular	41	1:3200
			180	1:3200
			189	1:3200
DNA-directed RNA polymerase II subunit RPB1 **(POLR2A)**	217	Granular	6	1:320
			61	1:3200
			63	1:3200
Proteasome activator complex subunit 3 **(PSME3)**	30	Granular	38	1:10000
			71	1:1000
Replication protein A subunits (**RPA1, RPA2, RPA3**)	68, 29 and 14	Pleomorphic	111	1:1000
Tight junction protein ZO-1 **(TJP1)**	195	Homogeneous	25	1:10000

Table 3-6 List of candidate antigens
In total, 14 antigens/ antigen complexes were identified using FIP with HEp-2 cells and MALDI-TOF-MS. The five antigens already reported in the previous master project [32] are in grey.

3.3 Purification of recombinant proteins from HEK293 cells

Purification of three recombinant antigens was implemented in this work in order to use the purified antigens for the development of lineblot immunoassays. The strategy was adjusted individually to purify the recombinant target antigen from the HEK293 expression system. Biomaterials were delivered by the recombinant synthesis department of EUROIMMUN AG.

3.3.1 Recombinant SMCHD1-His

Recombinant SMCHD1-His was prepared sufficiently by applying the following procedure: cell lysis followed by ammonium sulfate (AS) precipitation and chromatography under native conditions as mentioned in section 2.5.3. Western blot

analysis of fractions of the different purification steps are presented in Figure 3-8, A-C and recombinant SMCHD1-His was detected at around 235 kDa. After cells lysis with HEK293 lysis buffer, the majority (>~70%) of the recombinant protein was found in the supernatant (S1). With AS precipitation of S1, recombinant SMCHD1-His was further enriched in the sediment fraction P_{AS35}. Resolubilized P_{AS35} was applied in CHT chromatography. A complex protein mixture with approximately 40% of recombinant SMCHD1-His was eluted with TNTDI-20Pi50 (E_{50}) and the rest of ~60% recombinant SMCHD1-His was eluted with TNTDI-20Pi100 (E_{100}) with clearly less impurities. E_{100} fractions were selected for further purification by IMAC. With 4 ml NICKEL RAPID RUN™ material, His-tag containing SMCHD1 was enriched. After removal of irrelevant proteins, the target protein was eluted with TNTDI-150. Eluted fractions 2 to 4 were pooled and concentrated to a volume of 2 ml. This concentrate was applied as final preparation and the concentration of 0.05 mg/ml was determined by advanced protein assay, resulting in a final yield of 0.1 mg. The coomassie stained gel in Figure 3-8, D a thick band is observed near 235 kDa under reducing condition, which shows that the final preparation of recombinant SMCHD1-His was clean and it was confirmed by MALDI-TOF-MS analysis. In an SDS-PAGE under non-reducing conditions SMCHD1-His migrated with a higher molecular wight indicating that most of SMCHD1 in the preparation formed homooligomers (Figure 3-8, D).

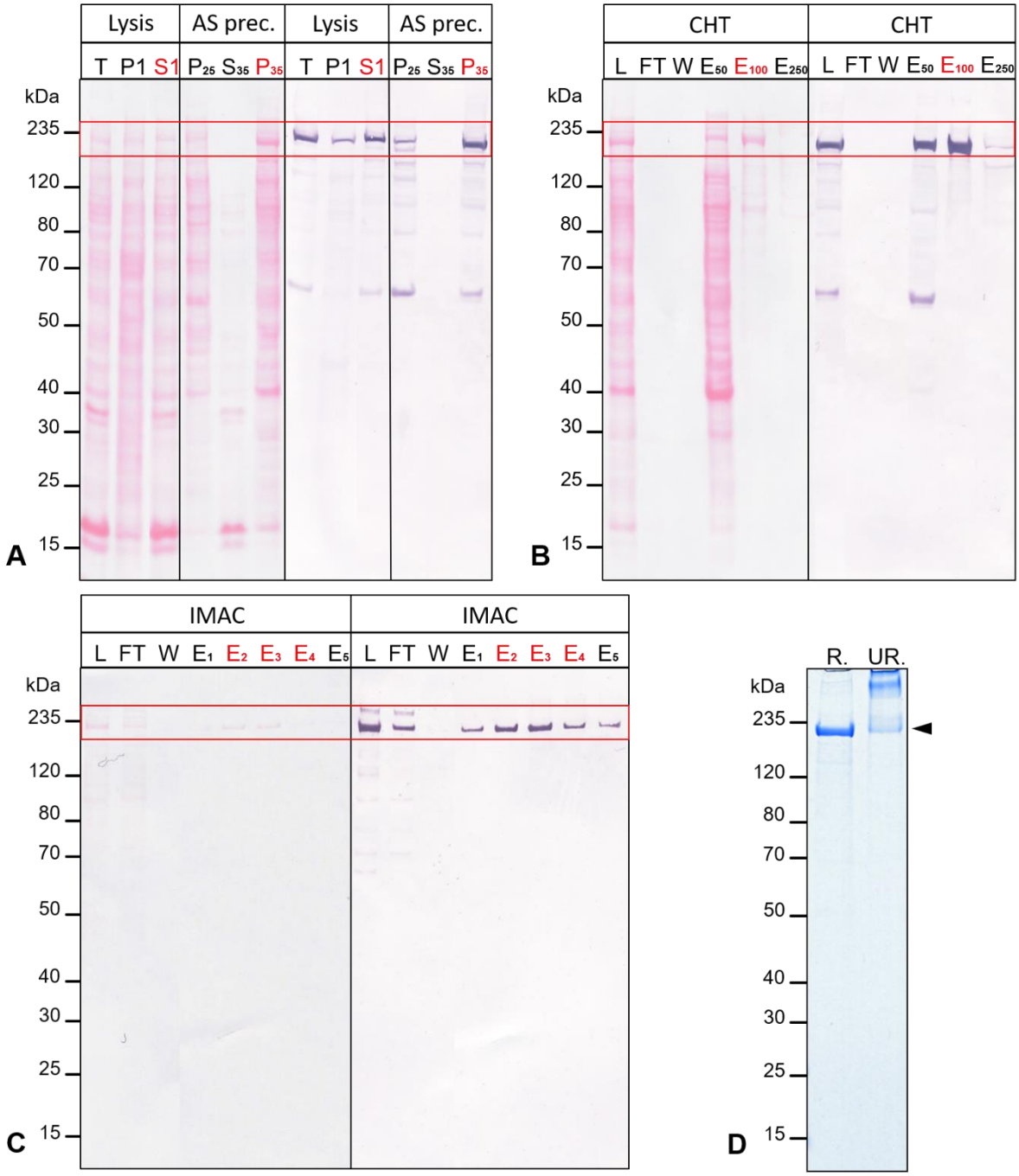

Figure 3-8 Purification of recombinant SMCHD1-His from HEK293 cells
A)-C) Western blot of the different fractions from the purification of SMCHD1-His from HEK293 cells. Left side of each picture: ponceau protein staining; right side of each picture: detection of the recombinant protein with anti-His-tag antibody (1:2000). Fractions in red color were selected for the next step. Red boxes indicate recombinant SMCHD1-His. **A)** Cell lysis and ammonium sulfate precipitation (AS prec.). T: total lysate in HEK293 lysis buffer, P1 and S1: sediment and supernatant of T, P_{25}: Sediment from 25% AS precipitation, S_{35}: supernatant from 35% AS precipitation, P_{35}: sediment from 35% AS precipitation. **B)** CHT^{TM} Ceramic Hydroxyapatite chromatography. L: load, FT: flow through, W: wash, E_{50}: elution with 50 mM phosphate (Pi), E_{100}: elution with 100 mM Pi, E_{250}: elution with 250 mM Pi. **C)** Immobilized metal affinity chromatography. L: load, FT: flow through, W: wash, E_1-E_5: eluted fractions. **D)** Coomassie stained gel of the final preparation. 1 µg recombinant SMCHD1 was loaded under reducing (R) or non-reducing (UR.) conditions. Visible bands were analyzed by mass spectrometry and identified as recombinant SMCHD1. Black arrow points at band of recombinant SMCHD1.

3.3.2 Recombinant DHX9-His

The strategy for the purification of recombinant DHX9-His was similar as for the purification of recombinant SMCHD1-His. The detailed parameters were adapted in each step. The purification process is shown in Figure 3-9, A and recombinant DHX9-His was detected at around 120 kDa. Approximately 90% of recombinant DHX9-His was found in the supernatant (S1) after cell lysis with HEK293 lysis buffer. AS precipitation result revealed that a large portion of recombinant DHX9-His was precipitated in P_{AS25}. Additionally, P_{AS35} contained most of the remaining DHX9-His. Therefore, P_{AS25} and P_{AS35} were selected for CHT chromatography. Here, the main portion of recombinant DHX9-His was detected after elution with TNTDI-20Pi50 (E_{50}). The TNTDI-20Pi50 fractions were applied for 4 ml IMAC.

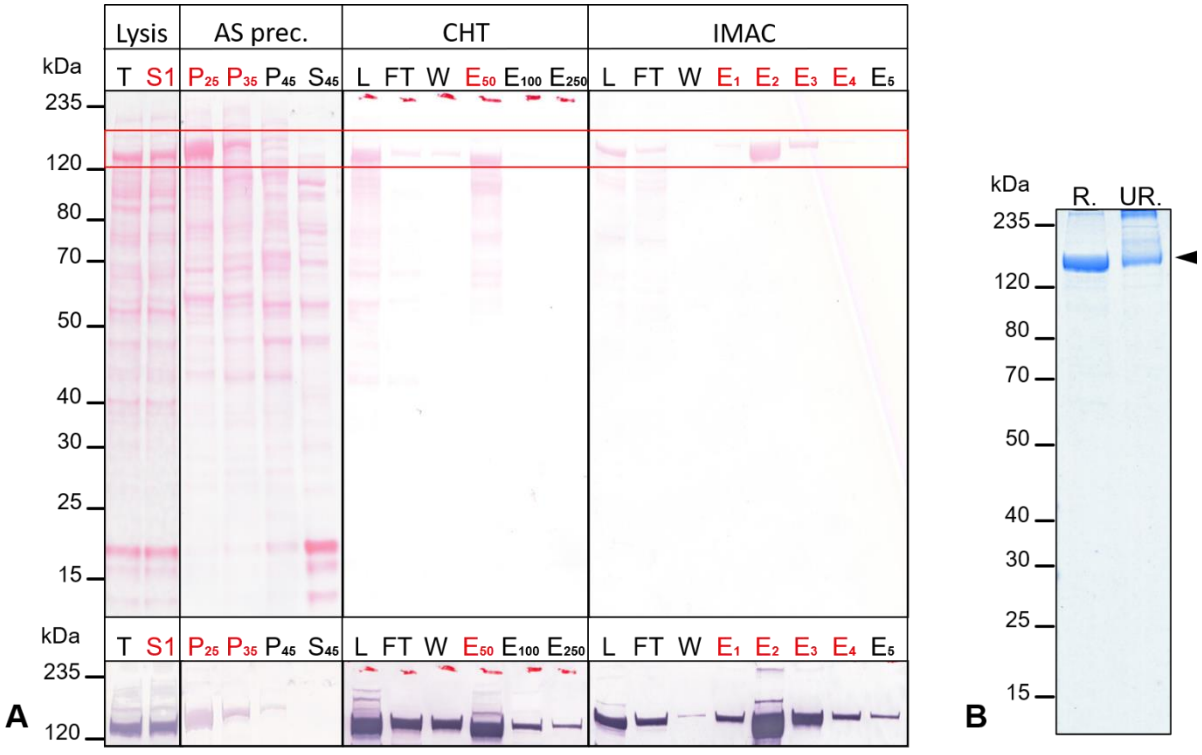

Figure 3-9 Purification of recombinant DHX9-His from HEK293 cells
A) Western blot of the different fractions from the purification of DHX9-His from recombinant HEK293 cells. Upper panel shows ponceau protein staining; lower panel shows detection of the recombinant protein with anti-His-tag antibody (1:2000). Red box indicates the bands of recombinant DHX9-His and fractions in red were applied for next step. T: total lysate in HEK293 lysis buffer, S1: supernatant of T, P_{25}-P_{45}: sediments from 25%, 35% and 45% ammonium sulfate precipitation (AS prec.), S_{45}: supernatant of 45% AS prec., CHT: ceramic hydroxyapatite chromatography, IMAC: immobilized metal affinity chromatography, L: load, FT: flow through, W: wash, E_{50}, E_{100}, E_{250}: eluted fractions of CHT in 50 mM phosphate (Pi), 100 mM Pi and 250 mM Pi, E_1-E_5: eluted fractions of IMAC in 150 mM imidazole. **B)** Coomassie stained gel of the final preparation. 1 µg recombinant DHX9 was loaded under reducing (R) or non-reducing (UR.) conditions. Visible bands were analyzed by mass spectrometry and identified as recombinant DHX9-His (arrowhead).

As Figure 3-9, A shows, irrelevant proteins were effectively removed by IMAC and the target antigen was enriched in fraction E1 to E4. These fractions were pooled and concentrated prior to be analyzed by advanced protein assay. The final preparation contained 0.11 mg/ml protein in 4 ml TNTDI-150 and the yield was 0.44 mg. The coomassie stained gel in Figure 3-9, B shows a thick band around 120 kDa under reducing condition, which proofed that the preparation was pure and mass spectrometry confirmed that the visible band was recombinant DHX9-His. Analyzing the preparation under non-reducing conditions revealed a band near 120 kDa and a band near 235 kDa, which implied that approximately half of recombinant DHX9 formed homodimers in the preparation.

3.3.3 Recombinant MATR3-His

Recombinant MATR3-His was prepared under denaturing conditions. As it is shown in Figure 3-10, A, recombinant MATR3-his was detected at approximately 120 kDa and most of recombinant MATR3-His was not soluble in buffer with or without detergent. After treatment with 8 M urea-containing buffer TNUDI-20, recombinant MATR3-His was denatured and solubilized in supernatant (S3), which was applied in 4 ml denatured IMAC and 2.5 ml cation exchange chromatography (cat.-IEX) in series. Fractions from serial chromatography were analyzed by SDS-PAGE and coomassie staining as shown in Figure 3-10, B. After the first sample application to denatured IMAC, about half of target antigen was found in flow through (FT_1). FT_1 was loaded again on the column after first sample application and approximately one fourth was found in the second flow through (FT_2). This implied that recombinant MATR3 required longer retention time to bind sufficiently on the Ni-NTA column. In the subsequent washing step, impurities were removed efficiently and eluted fractions E_1 to E_3 were pooled and subjected to cat.-IEX. After elution, fractions E_5 and E_6 contained most of the recombinant MATR3-His with high purity. Therefore, the finial preparation was the pool of E_5 and E_6 with a concentration of 0.09 mg/ml in 5 ml PBS1000(U) and the yield was 0.45 mg. Visible bands near 120 kDa and 100 kDa in the coomassie stained gel (Figure 3-10, C) were analyzed by mass spectrometry and identified as full-length recombinant MATR3-His (arrowhead) and its fragments. The denatured recombinant MATR3 remained monomeric in preparation.

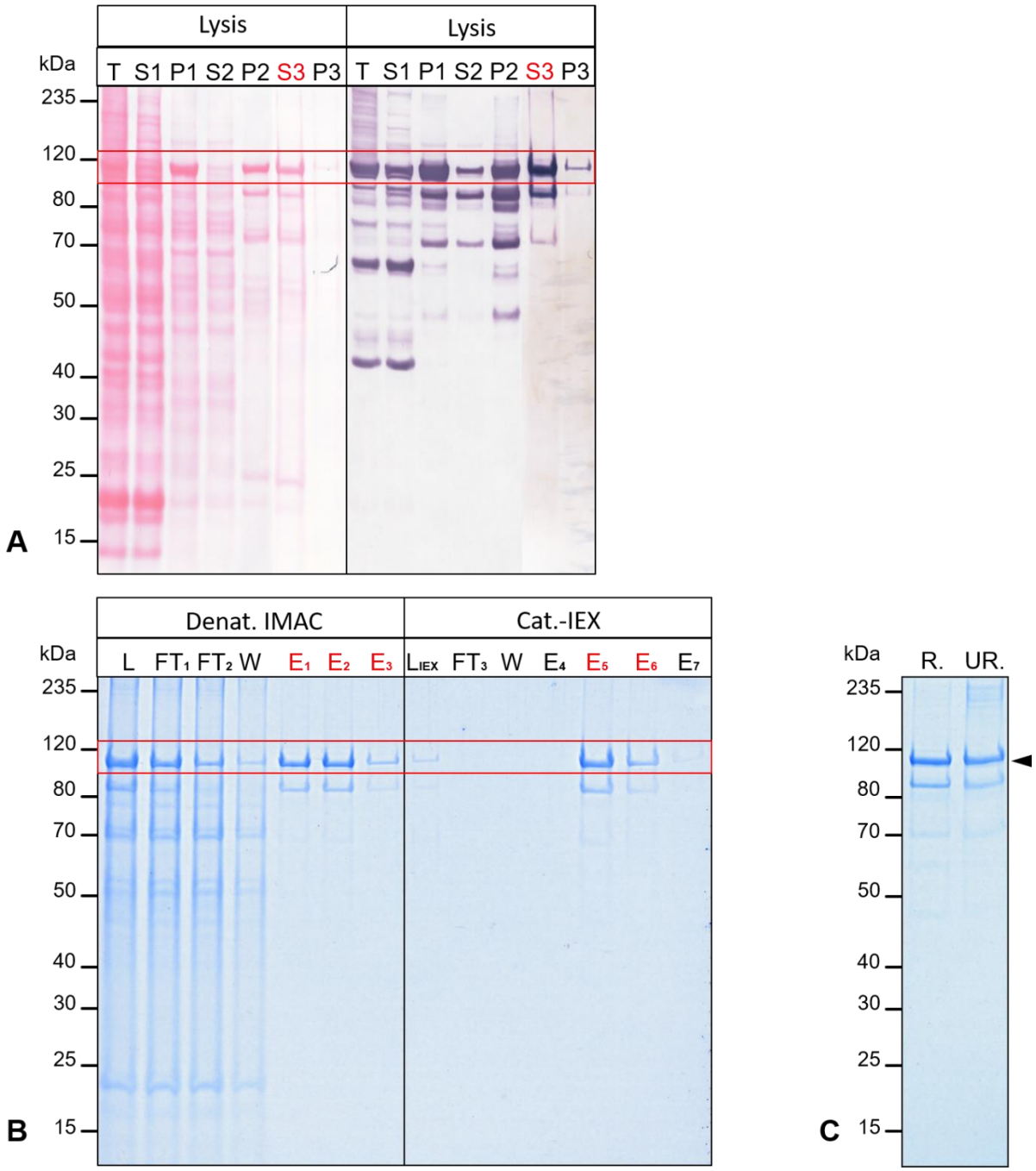

Figure 3-10 Purification of recombinant MATR3 from HEK239 cells
A) Western blot of the different fractions from the extraction of MATR3-His from HEK293 cells. Left side shows ponceau protein staining; and right side shows detection of the recombinant protein with anti-His-tag-AP antibody (1:8000). Red box indicates the bands of recombinant MATR3-His and fraction in red were applied for next step. T: total lysate in HEK293 lysis buffer, S1; supernatant of T, P1: sediment of T, S2: supernatant of lysed P1 in HEK293 lysis buffer supplemented 1% Triton-X-100, P2: sediment of lysed P1, S3: supernatant of lysed P2 in TNUDI-20, P3: sediment of lysed P2. **B)** Coomassie stained gel with fractions from denatured (denat.) IMAC and cation exchange chromoatography (cat.-IEX). L: load of IMAC, FT_1: and FT_2: serial flow through of IMAC, W: wash, E_1-E_3: eluted fractions of IMAC, L_{IEX}: load of cat.-IEX, FT_3: flow through of cat.-IEX, E_4-E_7: eluted fractions of cat.-IEX. **C)** Coomassie stained gel of final preparation. 1 µg recombinant MATR3 was loaded under reducing (R) or unreducing (UR.) conditions. Visible bands were analyzed by mass spectrometry and identified as recombinant MATR3-His (arrowhead) or its fragments.

3.4 Verification of candidate antigens

The 14 identified antigens were verified by Western blot with recombinant proteins, IFA with transfected HEK293 cells, IFA based neutralization test and IFA colocalization analysis. Based on the observed results, a prototype lineblot and two recombinant IFA research slides were developed.

3.4.1 Western blot using unpurified lysates of recombinant cells (HEK293 cells and *E. coli*)

Two candidate antigens (around 200 kDa), TJP1 and POLR2A, were selected to analyze the epitopes and to apply fragments instead of full-length proteins in subsequent test, because the preparation of the full-length proteins were more complicated than fragments. Different fragments of the two candidate antigens were recombinantly expressed in *E. coli* and the full-length antigens in HEK293 cells in addition. Unpurified lysate was obtained from the recombinant synthesis department of EUROIMMUN AG. Western blot with fragments and full-length antigens was performed to verify the antigen-antibody reaction.

As it is shown in Figure 3-11, UNA25 (anti-TJP1 index serum), PC6 (anti-DFS70 positive serum) and anti-His-tag antibody (positive control) were tested against TJP1 fragments of aa1-575 (#1), aa561-1130 (#2), aa1089-1668 (#3) and full-length TJP1 (#4). The anti-His-tag incubation indicated that expression of TJP1 aa1-575 and TJP1 aa561-1130 was abundant while expression of the full-length protein was lower. In addition, the expression of TJP1 aa1089-1668 was not detected. UNA25 showed a strong reaction with full-length TJP1 and TJP1 aa1-575, but no reaction with TJP1 aa561-1130. PC6 was applied as negative control and showed no reaction against TJP1 or its fragments. Therefore, it was verified that TJP1 is the target antigen of UNA25 and TJP1 aa1-575 showed a similar reactivity as the full-length protein.

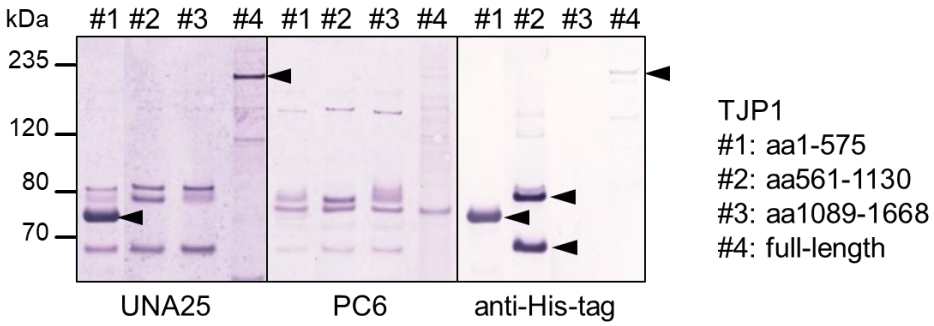

Figure 3-11 Verification of TJP1 using recombinant TJP1 and its fragments
Full-length TJP1 (lysate from transfected HEK293 cells) and its fragments (lysates from recombinant *E. coli*) were analyzed by Western blot with UNA25 (index, 1:200), PC6 (anti-DFS70 positive, 1:200) and anti-His-tag antibody (1:2000). Arrowheads indicate positive reactions of specific bands.

Four fragments of POLR2A, aa1-488, aa489-951, aa951-1474 and aa1475-1970, and the full-length protein were tested with UNA61 (anti-POLR2A index serum). The same control serum and positive control were applied as for TJP1. Figure 3-12 showed the Western blot results. With anti-His-tag incubation, it was detected that the full-length protein (#1), POLR2A aa489-951 (#3), POLR2A aa952-1474(#4) and POLR2A aa1475-1970 (#5) were sufficiently expressed while POLR2A aa1-488 (#2) was not. No reaction against any POLR2A variant was detected after incubation with PC6. UNA61 showed a very strong reaction against the full-length POLR2A and POLR2A aa1475-1970 as well. At the same time, aa489-951 and aa952-1474 were not reactive in Western blot. This confirmed that UNA61 targeted at POLR2A and aa1475-1970 displayed a similar reactivity as the full-length protein.

Thus, the N-terminal fragment of TJP1, aa1-575, and the C-terminal fragment of POLR2A, aa1475-1970, were selected to be purified and applied for following experiments.

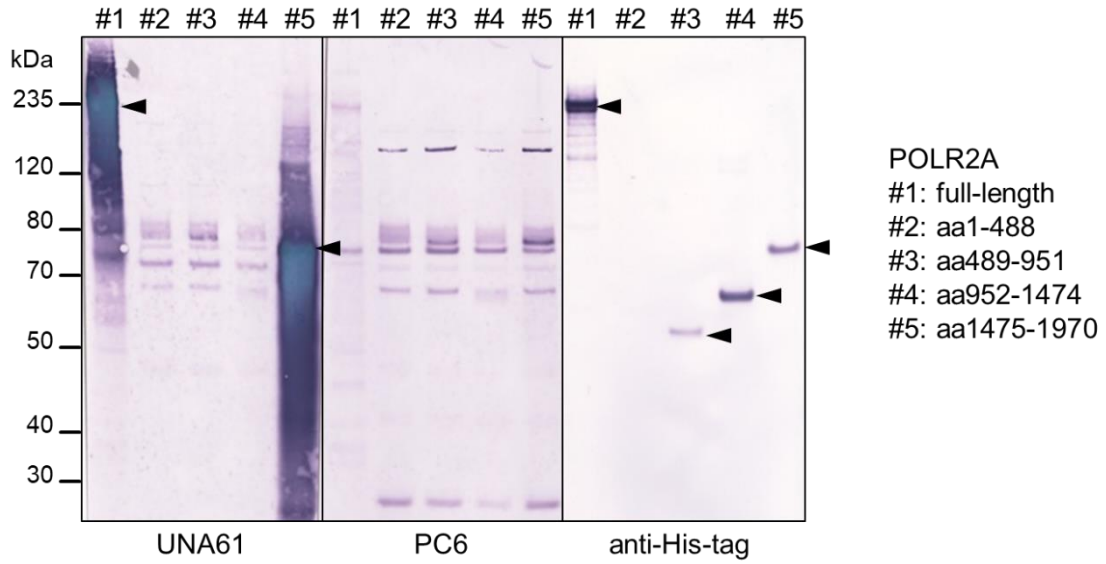

Figure 3-12 Verification of POLR2A with recombinant POLR2A and its fragments
Full-length POLR2A (lysate from transfected HEK293 cells) and its fragments (lysates from recombinant *E. coli*) were tested with UNA61 (index, 1:200), PC6 (anti-DFS70 positive, 1:200) and anti-His-tag (1:2000). Arrowheads indicate positive reactions of specific bands.

3.4.2 Western blot using purified antigens

Totally, ten recombinant antigens were purified in cooperation with the team from recombinant synthesis department as listed in 2.5.1 or prepared as described in 3.3. Four candidate antigens/ complexes, XRN2, PELP1/SENP3, RuvBL1/2 and RPA1/2/3, were not purified, thus not included in this section. In order to verify the candidate antigens, the purified recombinant antigens were applied in Western blot and tested with an anti-His-tag antibody, the individual index serum sample and healthy control sera (n=15). As it is shown in Figure 3-13, the anti-His-tag antibody (blue arrow) and index samples (red arrow) showed positive reactions. Meanwhile, fifteen healthy control sera showed no or very weak reactions when compared to the index sera. Taken Figure 3-13, D as example, one healthy control serum showed a very weak band while the index serum, UNA92 revealed a much stronger reaction. Occasional weak reactions were observed for DHX9 and TJP1 aa1-575. In summary, the specific antigen-antibody reaction was confirmed for NVL (UNA74), CD2BP2 (UNA219), TFAP2A (UNA96), MATR3 (UNA92), TDP43 (UNA3), SMCHD1 (UNA70), DHX9 (UNA41), POLR2A aa1475-1970 (UNA61), TJP1 aa1-575 (UNA25) and PSME3 (UNA38). In other words, all ten antigens were successfully verified using Western blot.

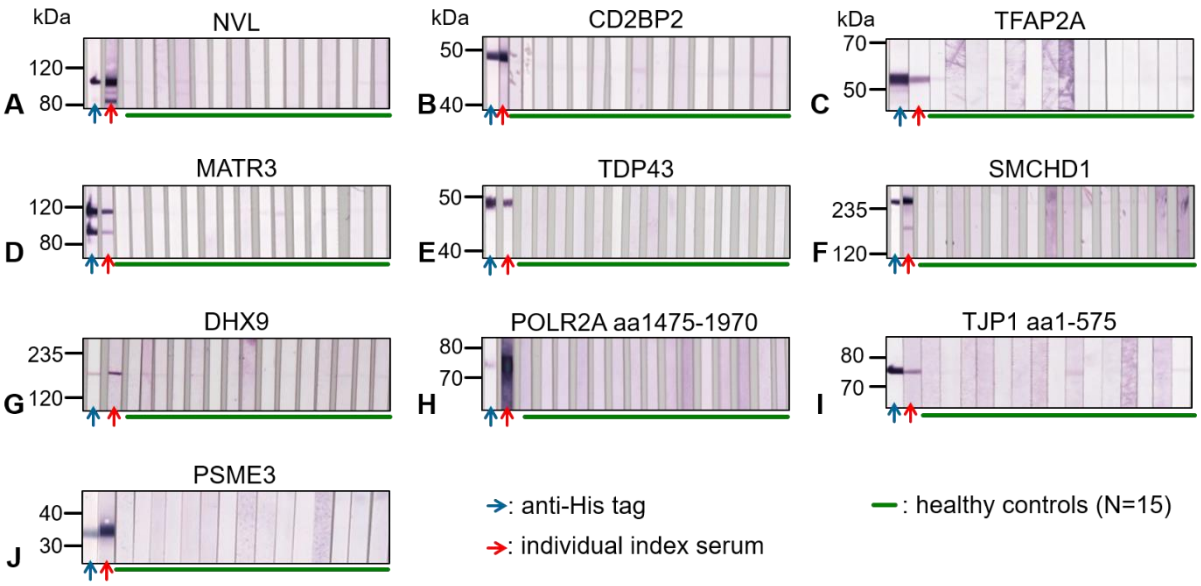

Figure 3-13 Verification of ten candidate antigens using purified recombinant antigens in Western blot.
A-J) Purified recombinant antigens were applied in SDS-PAGE with a 2D-gel (2 µg/ gel) and transferred on a nitrocellulose membrane. The membrane was then cut into suitable pieces and incubated with anti-His-tag (1:2000), individual index sample (1:200) and healthy control sera (1:200). Anti-mouse-IgG-AP (1:2000) and anti-human-IgG-B/E-AP (1:10) were used in secondary incubation. **A)** NVL and UNA74, **B)** CD2BP2 and UNA219, **C)** TFAP2A and UNA96, **D)** MATR3 and UNA92, **E)** TDP43 and UNA3, **F)** SMCHD1 and UNA70, **G)** DHX9 and UNA41, **H)** POLR2A aa1475-1970 and UNA61, **I)** TJP1 aa1-575 and UNA25, **J)** PSME3 and UNA38.

3.4.3 Neutralization test

Besides of Western blot, the ten purified antigens were further applied in neutralization test to examine their ability to abolish the ANA pattern of the respective index sera in IFA. The experiment was implemented with the same index sera as mention in section 3.4.2. Index sera were incubated with the individual antigens prior to standard IFA on HEp-2 cells (Figure 3-14, A-J, left side). In parallel, an incubation of the index sera with the respective control buffer was performed (Figure 3-14, A-J, right side). The result in Figure 3-14 indicated that a preincubation with NVL (A), TFAP2A (C), MATR3 (D), SMCHD1 (F), DHX9 (G), POLR2A aa1475-1970 (H) and PSME3 (J) was able to completely abolish the specific ANA pattern of the respective index serum. Additionally, it was observed that the preincubation of the index sera with CD2BP2 (Figure 3-14, B) and TDP43 (Figure 3-14, E) led to a partial reduction of the IFA signal on HEp-2 cells.

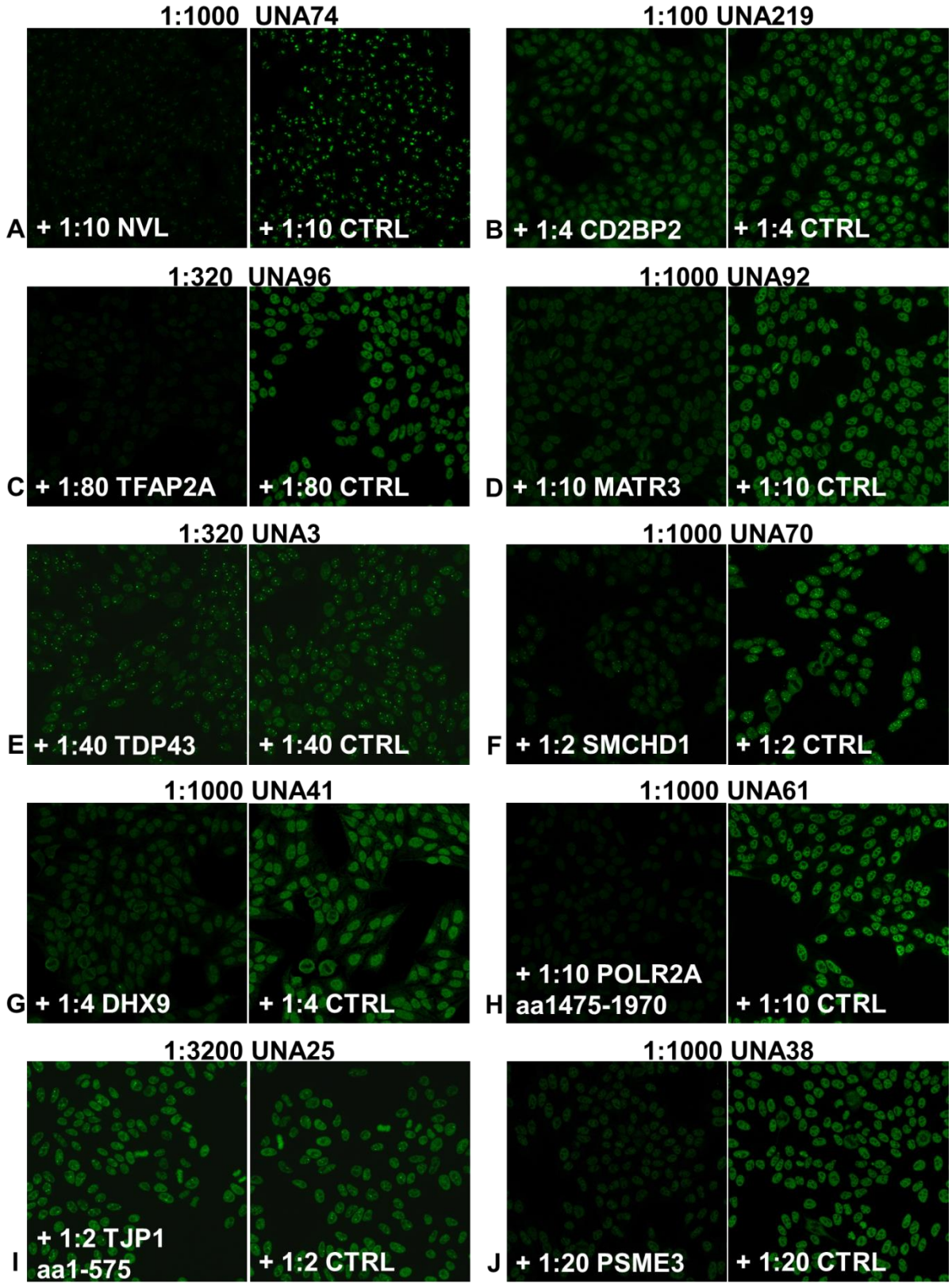

Figure 3-14 Application of ten purified recombinant antigens in IFA based neutralization test
Individual diluted index serum was incubated with diluted purified recombinant antigens and control buffer prior to be applied in IFA with HEp-2 cells. Anti-Human-IgG-Alexa488 (1:500) was applied as secondary antibody. **A)** NVL and UNA74, **B)** CD2BP2 and UNA219, **C)** TFAP2A and UNA96, **D)** MATR3 and UNA92, **E)** TDP43 and UNA3, **F)** SMCHD1 and UNA70, **G)** DHX9 and UNA41, **H)** POLR2A aa1475-1970 and UNA61, **I)** TJP1 aa1-575 and UNA25, **J)** PSME3 and UNA38. (magnification 200x)

These results confirmed that the respective ANA pattern of UNA74, UNA219, UNA96, UNA92, UNA3, UNA70, UNA41, UNA61, UNA25 and UNA38 in IFA with HEp-2 cells were indeed caused by an autoantibody targeting the identified antigens. On the other hand, after incubation of UNA25 with purified TJP1 aa1-575 the same fluorescence signal was observed compared to the control incubation (Figure 3-14, I).

3.4.4 IFA with transfected HEK293 cells

To further verify the antigen-antibody reaction, IFA was performed with transfected HEK293 cells expressing the individual recombinant antigens (Figure 3-15) or antigen complexes (Figure 3-16).

Figure 3-15 shows IFA with transfected HEK293 cells individually expressing either of eleven candidate antigens. Each index serum was incubated with the corresponding antigen and empty plasmid transfected HEK293 cells. Taken NVL as an example (Figure 3-15, A): it was observed that after incubated with 1:100 diluted UNA74, HEK-NVL substrate showed a specific staining pattern, which was not detected with HEK-control cells. Transfected HEK293 cells overexpressing recombinant NVL are marked by red arrows. The same effect was observed using HEK-TFAP2A and UNA96 (C), HEK-TDP43 and UNA3 (E), HEK-SMCHD1 and UNA70 (F), HEK-DHX9 and UNA41 (G), HEK-POLR2A and UNA61 (H), HEK-PSME3 and UNA38 (J) and HEK-XRN2 and UNA177 (K).

However, UNA219 (1:100) showed no positive reaction with HEK-CD2BP2 cells, indicating that recombinant IFA was not feasible for anti-CD2BP2 autoantibody detection (Figure 3-15, B). In Figure 3-15, D the reaction of UNA92 (1:100) with the HEK-MATR3 substrate was difficult to distinguish from the spherical stain of the HEK-control substrate. Therefore, IFA with HEK-MATR3 was also not suitable for the detection of anti-MATR3 autoantibodies. Interestingly, in Figure 3-15, I, HEK-TJP1 cells showed a specific staining pattern (red arrow) only with the 1:10 diluted but not with a 1:100 or higher diluted UNA25 serum.

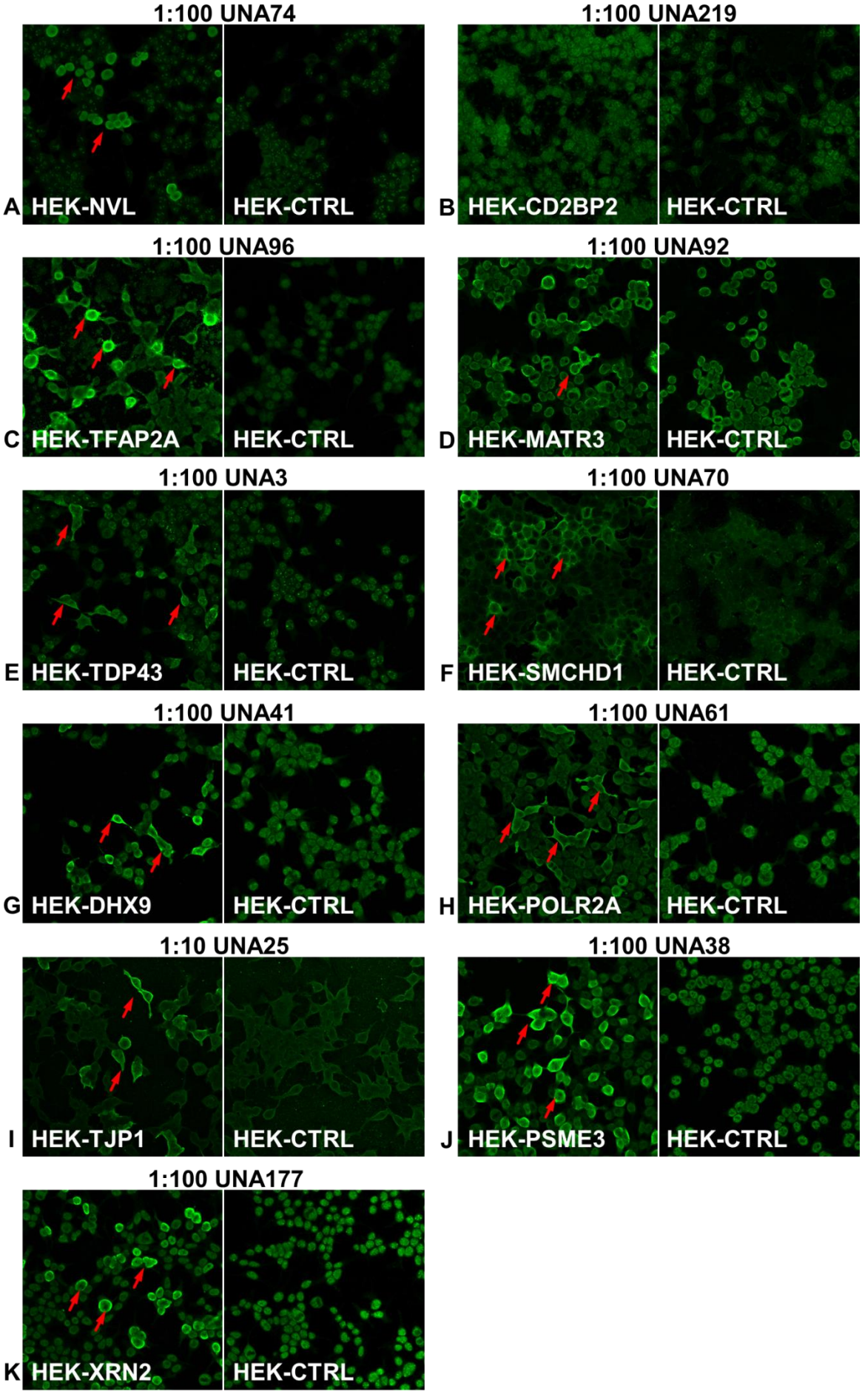
1:100 UNA74
A HEK-NVL
HEK-CTRL
1:100 UNA219
B HEK-CD2BP2
HEK-CTRL
1:100 UNA96
C HEK-TFAP2A
HEK-CTRL
1:100 UNA92
D HEK-MATR3
HEK-CTRL
1:100 UNA3
E HEK-TDP43
HEK-CTRL
1:100 UNA70
F HEK-SMCHD1
HEK-CTRL
1:100 UNA41
G HEK-DHX9
HEK-CTRL
1:100 UNA61
H HEK-POLR2A
HEK-CTRL
1:10 UNA25
I HEK-TJP1
HEK-CTRL
1:100 UNA38
J HEK-PSME3
HEK-CTRL
1:100 UNA177
K HEK-XRN2
HEK-CTRL

Figure 3-15 IFA with transfected HEK293 cells expressing eleven candidate antigens individually.
Each index serum was incubated with HEK293 cells and control HEK293 cells transfected with the corresponding antigen or an empty control plasmid. All serum samples were 1:100 diluted, only UNA25 was diluted 1:10. Anti-human-IgG-Alexa488 (1:500) was applied as secondary antibody. Red arrows indicate the specific fluorescence signal. **A)** NVL and UNA74, **B)** CD2BP2 and UNA219, **C)** TFAP2A and UNA96, **D)** MATR3 and UNA92, **E)** TDP43 and UNA3, **F)** SMCHD1 and UNA70, **G)** DHX9 and UNA41, **H)** POLR2A and UNA61, **I)** TJP1 and UNA25, **J)** PSME3 and UNA38, **K)** XRN2 and UNA177. (magnification 200x)

Secondly, to verify the antigen complexes that were identified using one serum sample, the co-expression of corresponding recombinant antigens in HEK293 cells was examined with IFA as well. Three kinds of co-expression HEK293 cells were prepared: RPA subunits (RPA1, RPA2, RPA3), RuvBL homologs (RuvBL1, RuvBL2) and the interaction partner PELP1 and SENP3.

Figure 3-16 shows an IFA with recombinant HEK-substrates with the single candidates or the co-expressions. Figure 3-16, A shows HEK-PELP1, HEK-SENP3, HEK-PELP1+SENP3 and HEK-control after incubated with 1:100 diluted UNA26 in IFA. UNA26 showed an enhanced staining of the nucleus of PELP1 expressing HEK293 cells (red arrow) compared to control cells, while HEK293 cells expressing SENP3 showed a slightly increased fluorescence intensity in a few nucleoli (Figure 3-16, A). When comparing HEK-PELP1+SENP3 to the individual antigen expressing substrates, it was obvious that the specific fluorescence signal was much stronger. This meant that antibodies in UNA26 recognized a complex of PELP1.

As it is displayed in Figure 3-16, B, when the homologs of RuvBL were separately expressed in HEK293 cells, the incubation with UNA65 revealed unsatisfying results. HEK-RuvBL1 cells showed a specific immunoreaction, but the morphology of the cells was altered and made it difficult for evaluation. In contrast, the morphology of HEK-RuvBL2 cells was normal but no specific reaction was observed. However, a co-expression of RuvBL1 and RuvBL2 revealed clearly positive cells with a normal cell morphology.

UNA111 (1:100) showed a positive immunoreaction with HEK-RPA1 and HEK-RPA2 but not with HEK-RPA3 or HEK-control cells (Figure 3-16, C). Meanwhile, HEK-RPA1+2+3 showed slightly reduced intensity of specific fluorescence signal.

All the recombinant HEK-substrates and the HEK-control cells were also analyzed with 50 healthy control sera under the same conditions. The specific reaction described above with index sera was not observed with the healthy control sera.

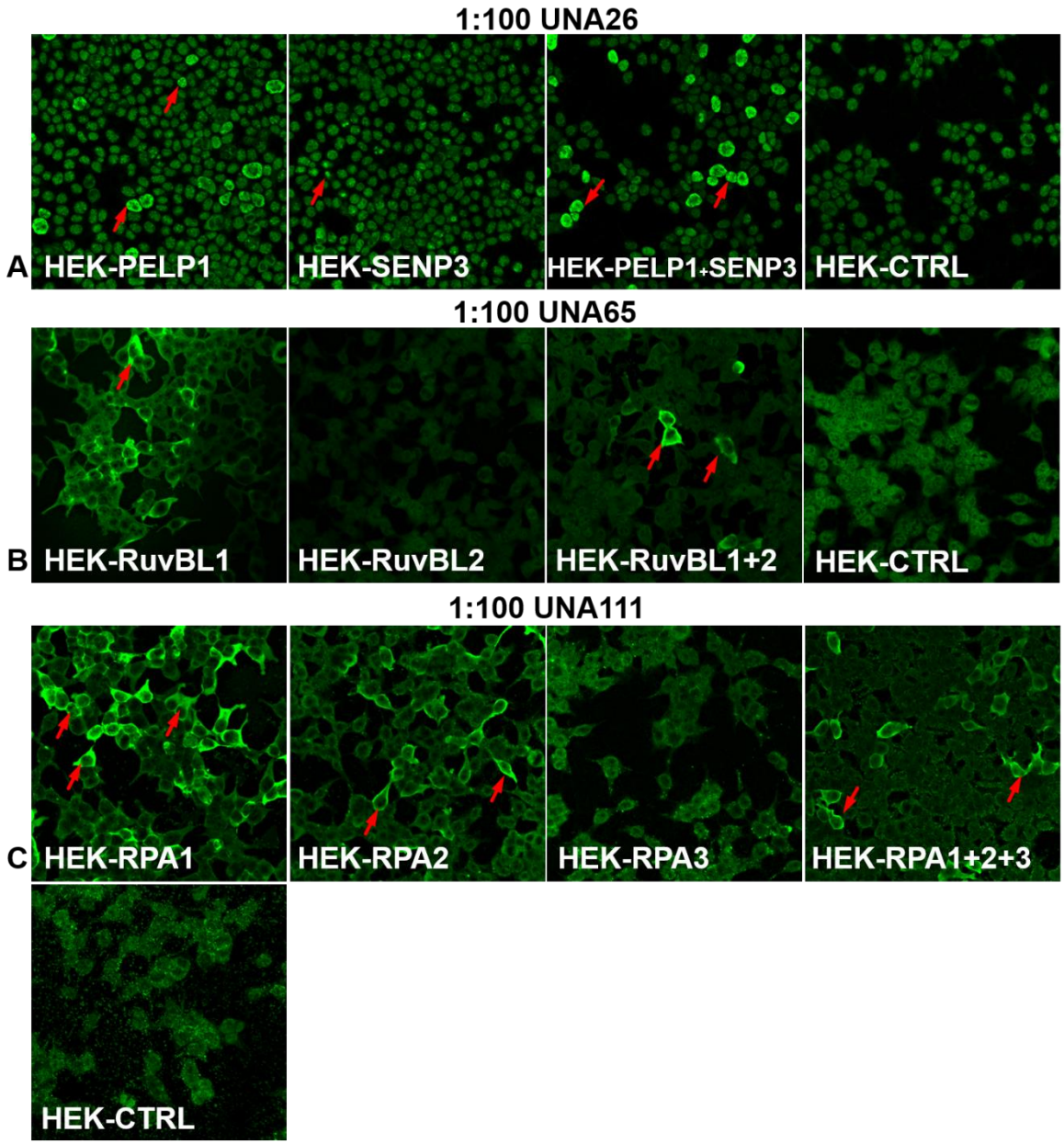

Figure 3-16 IFA with transfected HEK293 cells expressing individual candidate antigens or antigen complexes
Each index serum sample (1:100) was incubated with HEK293 cells transfected with the corresponding antigen, antigen complexes or empty control plasmid. Anti-human-IgG-Alexa488 (1:500) was applied as secondary antibody. Red arrow indicates the specific fluorescence signal. **A)** PELP1, SENP3 and UNA26, **B)** RuvBL1, RuvBL2 and UNA65, **C)** RPA1, RPA2, RPA3 and UNA111 (magnification 200x)

Shortly summarized, except CD2BP2 and MATR3, all of the other twelve candidate antigens were verified using IFA with transfected HEK293 cells.

3.4.4.1 Development of recombinant cells-based assay

Thirteen recombinant HEK-substrates showed a positive reaction with index sera (section 3.4.4). However, HEK-MATR3 and HEK-TJP1 were not included in the recombinant HEK293 cell-based IFA (RC-IFA) because the specific pattern observed

using HEK-MATR3 was difficult to distinguish from the control cells; and for the HEK-TJP1 RC-IFA a different serum dilution compared to the other substrates was required. Therefore, eleven HEK-substrates were applied for RC-IFA. For this purpose, two slides were assembled as shown in section 2.6.4.1, UFO-ANA clinical association 1 and 2. Both slides were first examined with the corresponding index sera and 50 healthy control sera. The cut-off of standard IFA for ANA using HEp-2 was applied as serum dilution (1:100). Evaluation of the result was implemented using a level system. Level 0 was defined as negative, 0.5 as borderline and 1 to 5 as weak positive to very strong positive reaction, respectively.

The intensity levels of the index sera measured in the RC-IFA are listed in Table 3-7 and Table 3-8. Each index serum showed a positive reaction against the corresponding substrate. After both slides were verified with index sera, they were analyzed with 50 healthy control sera in order to confirm the specificity of the HEK-substrates. All healthy controls showed negative results with both slides.

	HEK-PSME3	HEK-TFAP2A	HEK-TDP43	HEK-DHX9	HEK-POLR2A	HEK-RPA1+2+3	HEK-RuvBL1+2	HEK-control
UNA38	**4**	0	0	0	0	0	0	0
UNA96	0	**3**	0	0	0	0	0	0
UNA3	0	0	**3**	0	0	0	0	0
UNA41	0	0	0	**3**	0	0	0	0
UNA61	0	0	0	0	**3**	0	0	0
UNA111	0	0	0	0	0	**3**	0	0
UNA65	0	0	0	0	0	0	**3**	0

Table 3-7 Intensities of index sera in IFA with UFO-ANA clinical association 1
The serum samples were diluted 1:100 and anti-human-IgG-FITC (ready-to-use) was applied as secondary antibody. The intensity levels indicate negative (0), borderline (0.5) and weak to very strong positive reaction (1-5).

	HEK-SMCHD1	HEK-PELP1 +SENP3	HEK-NVL	HEK-XRN2	HEK-control
UNA70	**3**	0	0	0	0
UNA26	0	**3**	0	0	0
UNA74	0	0	**3**	0	0
UNA177	0	0	0	**2**	0

Table 3-8 Intensities of index sera in IFA with UFO-ANA clinical association 2
The serum samples were diluted 1:100 and anti-human-IgG-FITC (ready-to-use) was applied as secondary antibody. The intensity levels indicate negative (0), borderline (0.5) and weak to very strong positive reaction (1-5).

3.4.5 Colocalization analysis with anti-TJP1 antibody

A colocalization analysis with a commercial anti-TJP1 antibody and UNA25 was implemented to further confirm that anti-TJP1 autoantibodies were present in UNA25 but not lead to a defined ANA pattern. UNA25 and a commercial anti-TJP1 antibody were incubated with HEp-2 cells, recombinant HEK-TJP1 cells and HEK-control cells. As Figure 3-17, A illustrates the commercial anti-TJP1 antibody showed a diffused cytoplasmic stain in HEp-2 cells, which was also observed in IFA with UNA25. The homogenous ANA pattern observed in IFA with UNA25 was therefore probably not caused by anti-TJP1 autoantibodies.

In Figure 3-17, B, the commercial anti-TJP1 antibody showed the same specific immunoreaction against transfected HEK293 cells expressing TJP1 as UNA25. The merged picture supported that UNA25 was targeting recombinant TJP1. Furthermore, this particular pattern was not observed in HEK-control cells (Figure 3-17, C). Interestingly, the commercial anti-TJP1 showed a specific reaction at junctions between HEK-control cells. The magnification of the selected area (grey square) shows that antibodies from UNA25 also localized in the area of intercellular contacts indicating that UNA25 recognizes endogenous TJP1 at cell junctions.

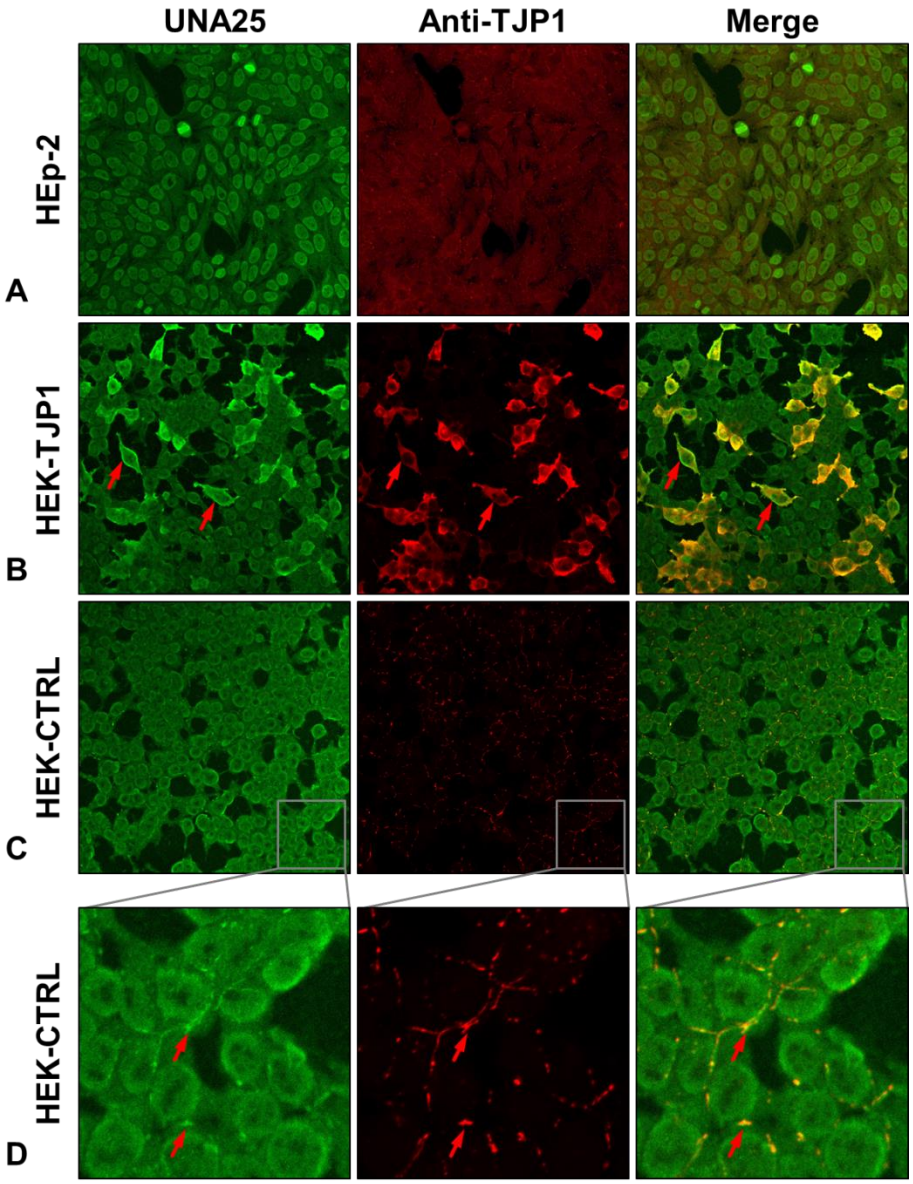

Figure 3-17 Colocalization analysis with anti-TJP1 antibody in HEp-2, HEK-TJP1 and HEK-control cells
A mixture of UNA25 (1:10) and anti-TJP1 (1:50) was applied in IFA. Anti-human-IgG-alexa488 (1:500, green) and anti-mouse-IgG-Cy3 (1:200, red) were employed as secondary antibodies. Individual signals from UNA25 (left) and anti-TJP1 (middle) are presented and merged pictures are shown on the right. **A)** HEp-2 cells. **B)** transfected HEK293 cells overexpressing TJP1. Red arrows indicate two example cells that showed specific immunoreaction. **C)** control HEK293 cells transfected with empty vector. (magnification 200x) **D)** control HEK293 cells transfected with empty vector. Red arrows point at two example junctions. (magnification 3200x)

3.4.6 Brief summary of verification

All fourteen candidate antigens were verified with at least one method (Table 3-9). 10/14 candidate antigens were analyzed in Western blot experiments and IFA neutralization test. With a neutralization test, 9/10 candidate antigens were confirmed to cause the observed ANA pattern. All candidate antigens were analyzed using IFA with transfected HEK293 cells. Autoantibodies targeting 12/14 candidate antigens showed specific fluorescence pattern with the corresponding transfected HEK293

cells. Additionally, colocalization analysis of TJP1 using commercial anti-TJP1 antibody and UNA25 confirmed the results of the TJP1 Western blot and neutralization test, which proofed that anti-TJP1 autoantibodies were present in UNA25. The homogenous ANA pattern observed using UNA25 was not caused by anti-TJP1 autoantibodies.

Candidate antigen	Verified with		
	Western blot	Neutralization test	IFA with transfected HEK293 cells
NVL	Yes	Yes	Yes
XRN2	Not tested	Not tested	Yes
PELP1 and SENP3	Not tested	Not tested	Yes
CD2BP2	Yes	Yes	No
TFAP2A	Yes	Yes	Yes
MATR3	Yes	Yes	No
TDP43	Yes	Yes	Yes
RuvBL1 and RuvBL2	Not tested	Not tested	Yes
SMCHD1	Yes	Yes	Yes
DHX9	Yes	Yes	Yes
POLR2A	Yes	Yes	Yes
PSME3	Yes	Yes	Yes
RPA1, RPA2 and RPA3	Not tested	Not tested	Yes
TJP1	Yes	No	Yes

Table 3-9 Summary of candidate antigen verification results

3.5 Development of lineblot

Based on the results shown in section 3.4.2, the antigens were used in a lineblot was developed and validated with index sera and healthy control sera (n=50). The results of NVL are presented in this section as an example of the development.

3.5.1 Determination of antigen dilution

Firstly, dot blot was performed to select the optimum antigen dilution. NVL is shown as an example in Figure 3-18. Undiluted, 1:3.2, 1:10, 1:32, 1:100, 1:320, and 1:1000 diluted antigen was spotted on the membrane and was incubated with the respective index serum UNA74. The anti-His-tag-AP antibody confirmed the presence of recombinant antigens. Ten healthy control sera (HC1-10) were tested as negative controls. The index serum showed a strong reaction against purified recombinant NVL. With a high concentration of the antigen, healthy control sera showed occasionally weak reactions as well. As the optimal antigen amount, the antigen

dilution was selected, which still showed a weak reaction with some of the healthy controls. The optimum dilution was around 1:10.

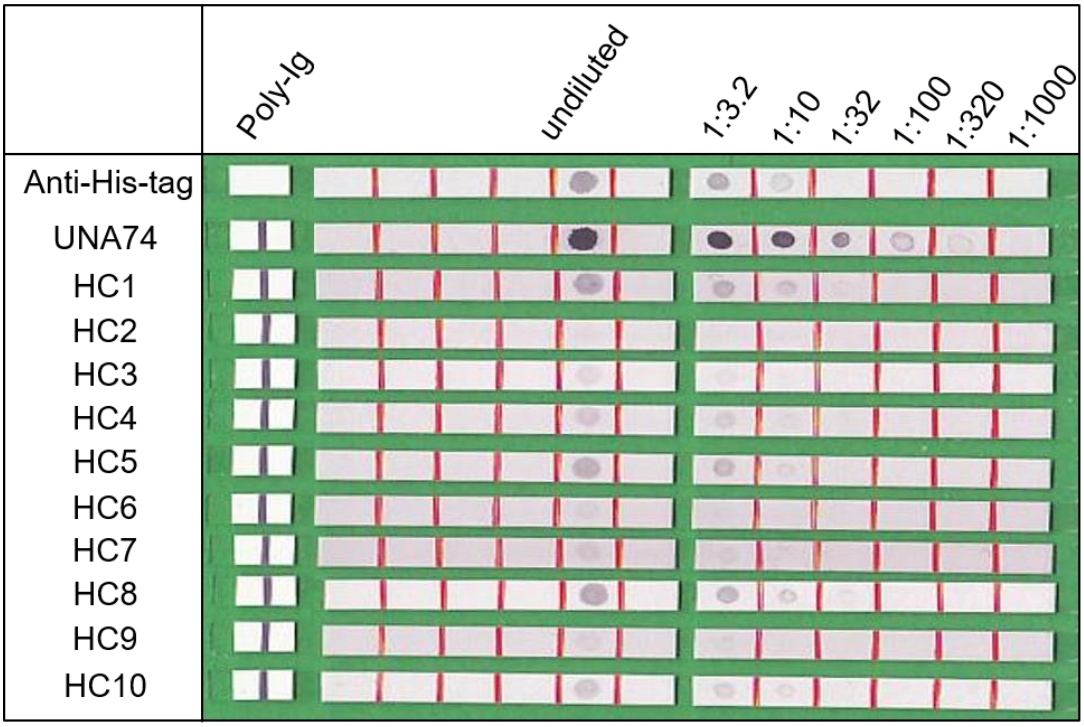

Figure 3-18 NVL dot blot with anti-His-tag index serum and healthy control sera
Purified recombinant NVL was serial diluted and applied on empty dot blot strips. Poly-Ig was the incubation control. Anti-His-tag-AP (1:8000) was used as positive control. UNA74 was anti-NVL positive. Ten healthy control sera (HC1-10) were applied as negative controls. Serum samples were diluted 1:101. Anti-Human-IgG-B/E-AP (1:10) was the secondary antibody.

3.5.2 Stability test

Three dilutions, 1:6, 1:11 and 1:21, were selected for NVL. The test strips with diluted NVL were produced in cooperation with the Blot department of EUROIMMUN AG. They were subsequently stored at 4°C or 37°C for 0, 7 or 14 days and analyzed in a stability test with anti-His-tag-AP, UNA74 and ten healthy control sera. An example blot result of day 0 is shown in Fiugre 3-19. It was observed that with different antigen dilutions, the index sample showed a strong intensity and all healthy controls remained negative. Representative results of the measured intensities after incubation with anti-His-tag-AP and UNA74 are presented in Table 3-10. The intensities on day 0, day 7 and day 14 were relative consistent regardless of different storage conditions. It was concluded that the NVL lineblot was stable under different storage conditions. As a second result, it was observed that the 1:6 diluted antigen showed the strongest reaction. Therefore, this dilution was selected for the NVL prototype lineblot.

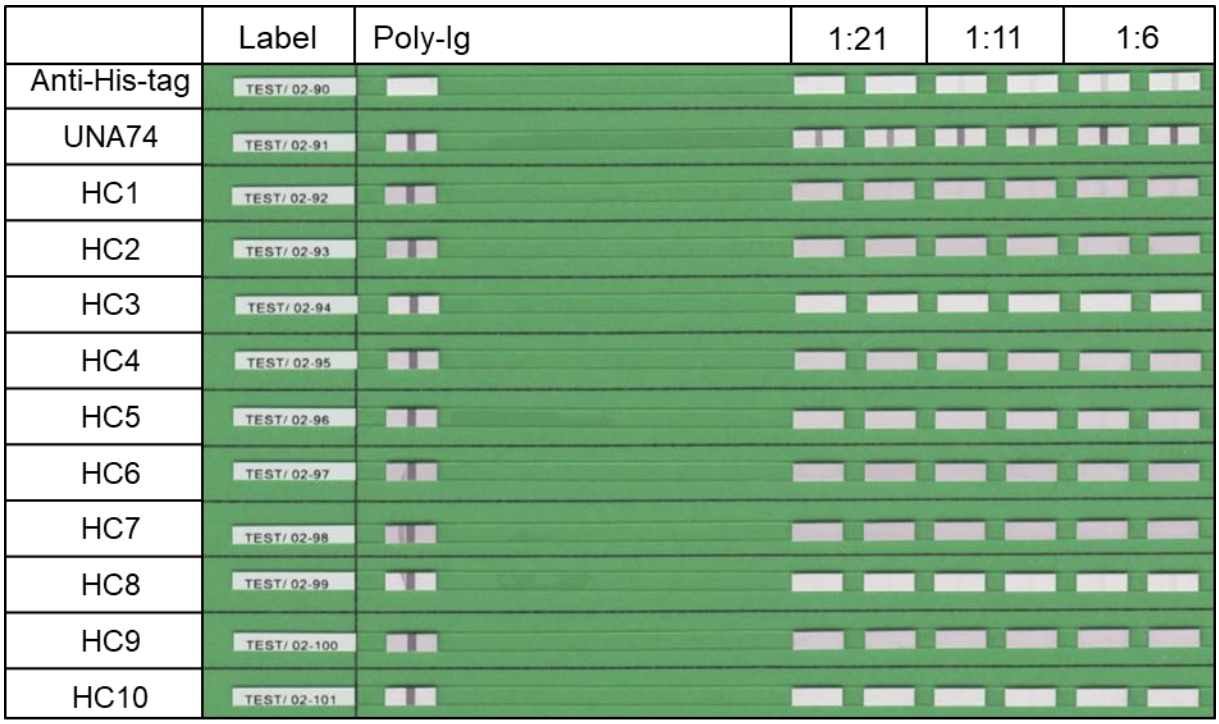

Figure 3-19 NVL stability test on day 0.
Diluted NVL was coated on a lineblot for stability test. Poly-Ig was the incubation control. Each dilution was coated twice on the strip. Anti-His-tag-AP (1:8000) was applied for His-tag detection. UNA74 was the index serum and positive control. HC1-10 were healthy control sera. Serum samples were diluted 1:101. Anti-Human-IgG-B/E-AP (1:10) was the secondary antibody.

Storage		Sample	Poly-Ig control	Antigen dilution					
Temp /°C	Days			1:21		1:11		1:6	
				Line 2	Line 1	Line 2	Line 1	Line 2	Line 1
-	0	anti-His-tag-AP (1:8000)	0	2	2	7	8	23	21
4	7		0	3	2	9	7	22	23
	14		0	1	1	9	8	25	24
37	7		1	2	1	6	6	16	14
	14		0	2	3	6	7	19	14
-	0	UNA74 (1:101)	94	62	64	84	86	**102**	**99**
4	7		84	64	67	90	87	**104**	**103**
	14		88	68	68	92	89	**104**	**107**
37	7		92	74	74	94	93	**106**	**107**
	14		88	70	75	95	92	**104**	**104**

Table 3-10 NVL stability test: list of intensities

The other nine purified recombinant antigens were proceeded in dot blot and stability test as mentioned for NVL as well. Seven out of nine antigens were suitable for a storable lineblot and the optimum dilution was listed in Table 3-11. MATR3 and DHX9 were not further applied in lineblot because the antigen concentration was not sufficient for a dot blot, and thus stability tests were not performed.

Candidate antigen	SMCHD1	CD2BP2	NVL	TDP43	TFAPA2A	TJP1 aa1-575	POLR2A aa1475-1970	PSME3
Selected dilution	1:2	1:6	1:6	1:11	1:11	1:6	1:4.2	1:33
Final antigen concentration µg/ml	25	50	53	146	405	135	60	23

Table 3-11 List of selected dilution for prototype lineblot

3.5.3 Lineblot validation

With the selected dilutions, a lineblot with eight antigens, UFO-ANA profile 1, was produced in cooperation with the Blot department of EUROIMMUN AG. The lineblot was first validated with anti-His-tag-AP, eight index sera and three healthy control sera. Figure 3-20 displays that all index samples showed positive reactions against the corresponding antigens, whereas three healthy control sera did not. Due to the very low concentration of POLR2A aa1475-1970, no band was detected for POLR2A aa1475-1970 after anti-His-tag incubation. In Table 3-12, the intensity of each band is given. UFO-ANA profile 1 was further analysed with 47 healthy control sera to adjust the experimental cut-off. For SMCHD1, TDP43, POLR2A and PSME3, the band intensity was under 10 for all healthy controls, while for CD2BP2, NVL, TFAP2A and TJP1 aa1-575, the intensity was not exceeding 20 for all healthy controls (Appendix 2). According to this, the experimental cut-off for each antigen was selected (Table 3-12).

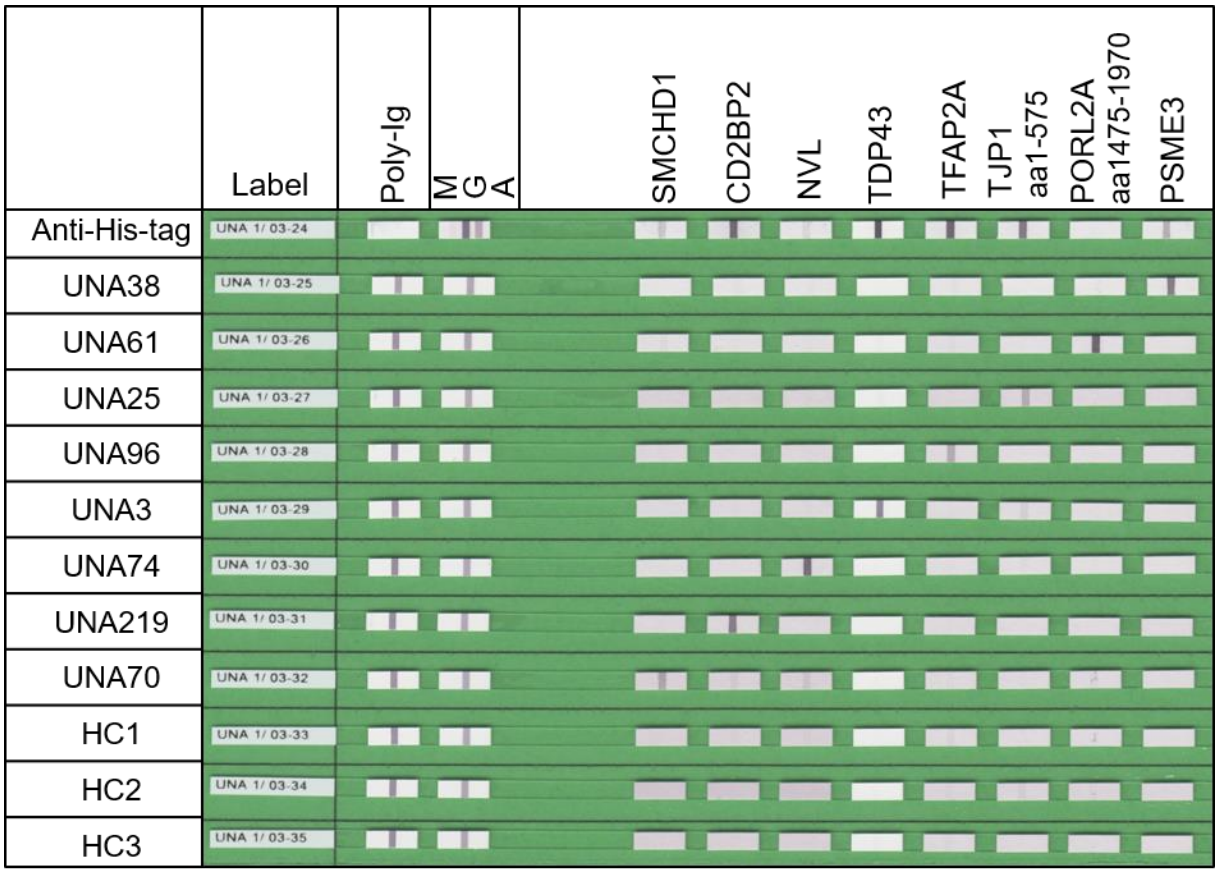

Figure 3-20 Prototype lineblot (UFO-ANA profile 1) with anti-His-tag, index sera and healthy control sera

Poly-Ig was the incubation control. Anti-His-tag-AP (1:8000) was applied for His-tag detection. Individual index serum was positive control. HC1-3 were healthy control sera. Serum samples were diluted 1:101. Anti-Human-IgG-B/E-AP (1:10) was the secondary antibody.

UFO-ANA profile 1	Poly-Ig control	M	G	A	SMCHD1	CD2BP2	NVL	TDP43	TFAPA2A	TJP1 aa1-575	POLR2A aa1475-1970	PSME3
anti-His-tag	0	6	100	48	**30**	**111**	**15**	**139**	**115**	**101**	**2**	**50**
UNA38	68	0	58	0	0	3	3	0	3	0	2	**99**
UNA61	81	0	60	0	5	1	1	3	3	0	**115**	0
UNA25	85	0	55	0	1	1	3	3	1	**41**	2	2
UNA96	86	0	58	0	1	0	2	0	**43**	0	1	0
UNA3	83	0	58	0	0	2	3	**89**	2	12	2	1
UNA74	86	0	59	0	1	2	**107**	0	2	3	1	0
UNA219	85	0	57	0	2	**86**	1	1	2	1	1	1
UNA70	79	0	57	0	**43**	10	14	1	2	2	8	1
BS1	82	0	58	0	1	4	4	2	6	1	9	1
BS2	83	0	59	0	1	2	0	1	4	9	3	0
BS3	84	0	59	0	2	2	1	3	3	0	1	1
Cut-off	-	-	-	-	10	20	20	10	20	20	10	10

Table 3-12 UFO-ANA profile 1: intensity of bands of Figure 3-20 and experimental cut-off of each antigen

3.6 Assessment of clinical association

529 sera from 488 patients in systemic rheumatic disease cohort (SARD) cohort were screened for autoantibodies against the thirteen candidate antigens with the developed immunoassays: RC-IFA (UFO-ANA clinical association 1 and 2) and lineblot (UNA-ANA profile 1). MATR3 was not analyzed as no suitable immunoassay was available. All positive cases are listed in Appendix 3 and are briefly summarized inTable 3-13. Six candidate antigens, NVL, TFAP2A, TDP43, SMCHD1, POLR2A and PSME3, were able to be tested with both RC-IFA and lineblot, while the other six, XRN2, PELP1/SENP3, CD2BP2, RuvBL1/2, RPA1/2/3 and TJP1, were analysed with RC-IFA or lineblot only due to limitations of the individual test systems as described before. Among the first group, NVL and PSME3 showed that both test assays agreed to high extent with each other. Meanwhile, for the other antigens discrepancy between lineblot and RC-IFA were observed. A complete discrepancy between both test methods was observed for TDP43, SMCHD1 and POLR2A.

Candidate antigen	Number of positive sera		
	RC-IFA	Lineblot	Discrepancy
NVL	8	6	2
XRN2	0	n.a.	-
PELP1 and SENP3	1	n.a.	-
CD2BP2	n.a.	11	-
TFAP2A	2	35	33
TDP43	0	6	6
RuvBL1 and RuvBL2	2	n.a.	-
SMCHD1	1	1	2
DHX9	4	n.a.	-
POLR2A	6	4	10
PSME3	7	8	3
RPA1, RPA2 and RPA3	3	n.a.	-
TJP1	n.a.	16	-

Table 3-13 Analysis of the systemic autoimmune rheumatic disease (SARD) cohort with the developed immunoassays
Sera were diluted 1:100 and anti-human-IgG-FITC (ready-to-use) was applied as secondary antibody for RC-IFA. The positive RC-IFA results were confirmed with a second analysis. 1:101 diluted sera were applied for lineblots and anti-human-IgG-B/E-AP (1:10) was used as secondary antibody. n.a.= not analysed

In order to evaluate the results, four candidate antigens, NVL, CD2BP2, PSME3 and TJP1, were selected, which showed a relatively high number of positive cases (n>5) and a relative low discrepancy. Positive sera against these four candidate antigens were then further analysed with Western blot using purified antigen (Figure 3-21).

3.6.1 NVL

Eight sera from six patients were anti-NVL positive according to the RC-IFA result. Meanwhile, the lineblot showed that the intensities of six sera out of eight were over the experimental cut-off. The two exceptions were SARD230 and SARD309. The Western blot with purified NVL confirmed that all eight sera were anti-NVL positive, including SARD230 and SARD309, which showed weak reactions (Figure 3-21, A). Five of six positive patients were diagnosed with SSc and one suffered on myositis.

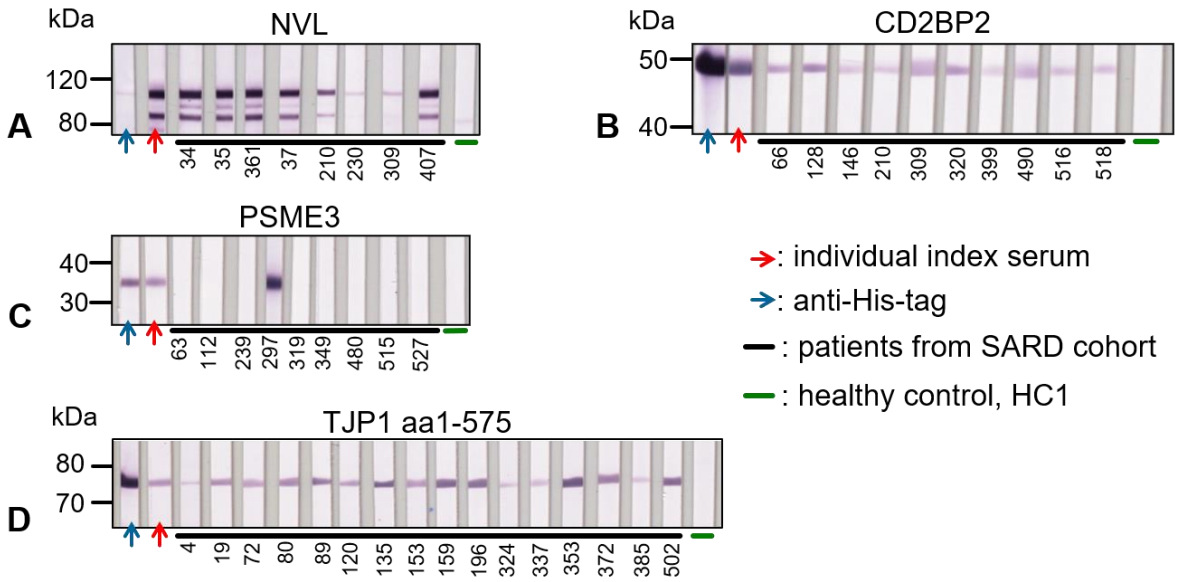

Figure 3-21 Western blot analysis of selected positive sera from the systemic rheumatic disease (SARD) cohort with purified candidate antigens
Purified recombinant antigens were applied on 2D-gels (2 µg/ gel) and transferred on a nitrocellulose membrane. It was cut into suitable pieces and incubated with anti-His-tag-AP (1:8000), individual index sample (1:200), positive sera from the SARD cohort (1:200) and healthy control sera (1:200). Anti-human-IgG-B/E-AP (1:10) was used in secondary incubation. **A)** Eight anti-NVL positive sera in NVL Western blot. **B)** Ten anti-CD2BP2 positive sera in CD2BP2 Western blot. **C)** Nine anti-PSME3 positive sera in PSME3 Western blot. **D)** Sixteen anti-TJP1 positive sera in TJP1 aa1-575 Western blot.

3.6.2 CD2BP2

Eleven sera from ten patients reacted positive against CD2BP2 in lineblot. Western blot with purified CD2BP2 confirmed that sera from these ten patients were all positive (Figure 3-21, B). Eight patients had SSc, one had MCTD and one had myositis.

3.6.3 PSME3

Totally, nine sera from nine patients were anti-PSME3 positive in at least one test assay. Seven sera were anti-PSME3 positive using RC-IFA and eight sera were lineblot positive. SARD319 and SARD515 were lineblot negative and SARD239 was RC-IFA negative. Nine sera were further analysed in Western blot with purified antigen. However, only SARD293 showed a positive reaction (Figure 3-21, C). The nine positive samples consisted of five patients with SSc, three with SLE and one with myositis.

3.6.4 TJP1

Sixteen sera from sixteen patients were positive using lineblot. All positive reactions were confirmed by Western blot with the purified antigen (Figure 3-21, D). Fifteen patients were diagnosed with SSc and one had UCTD.

Part b: Antigen identification with clinically characterized serum samples with two novel patterns

In this part, the established strategy was applied to identify the candidate antigen of clinically characterized sera. The received serum samples were added to UNA cohort (Figure 3-1). The methods were optimized and slightly differed from part a, as these sera showed different characters.

3.7 Characterization of serum samples

Ten serum samples (UNA336-UNA345) were received from the group of L.E.C Andrade, the Fleury Medicine and Health Laboratories in Brazil. These sera showed two novel immunofluorescence patterns on HEp-2 cells, which were a cell-circle dependent nucleolar pattern (Figure 3-22, A, UNA336-340) and a peculiar pattern with positive mitotic spindles and a cell-circle dependent cytoplasmic fine speckled staining (Figure 3-22, B, UNA341-345). The titers of UNA336-345 are listed in Appendix 1. Monkey liver showed no specific reaction.

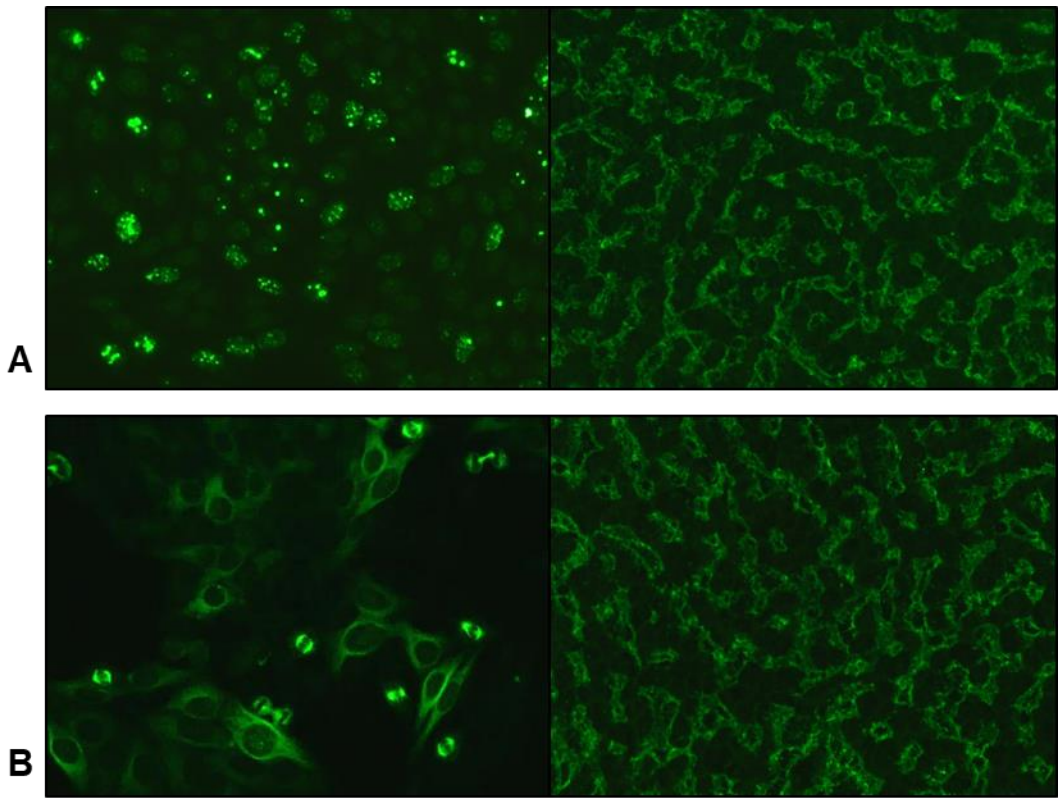

Figure 3-22 Characterization of G2-phase specific serum samples in IFA.
Sera (1:100) were analyzed in IFA with HEp-2 cells (left) and monkey lifer (right). Anti-Human-IgG-Alexa488 (1:500) was applied as secondary antibody. **A)** UNA340 showed a G2-phase specific nucleolar pattern on HEp-2 cells and monkey liver was negative. **B)** UNA345 showed a G2-phase specific fine speckled cytoplasm pattern with a positive reacted spindle apparatus in mitotic cells. Monkey liver showed no specific reaction. (magnification 200x)

The preliminary results from L.E.C Andrade's group indicated that these serum samples showed no consistent Western blot reaction and that the antigen targets of the sera were expressed only in the G2-Phase of the cell cycle. UNA336 was not further analyzed as it contained in addition to the cell-circle dependent nucleolar pattern a granular pattern.

3.7.1 Extractability test

The extractability test (see section 2.2.3) was performed to determine the suitable buffer for immunoprecipitation experiments with the serum samples. In Figure 3-23, UNA340 (A-D) and UNA345 (E-H) are presented as examples. A G2-phase specific nucleolar pattern of UNA340 was not detectable, when the immunocomplexes were extracted with RIPA buffer. However, UNA345 showed rigidity to RIPA buffer and 2 M urea containing RIPA-2U buffer. The G2-phase specific cytoplasmic pattern (UNA345) was only extractable using 4 M urea containing RIPA-4U buffer. Therefore, RIPA buffer was selected for immunoprecipitation experiments with serum samples with clear G2-phase specific nucleolar patterns. RIPA-4U buffer was applied for UNA341 to UNA345 with G2-phase specific cytoplasmic pattern.

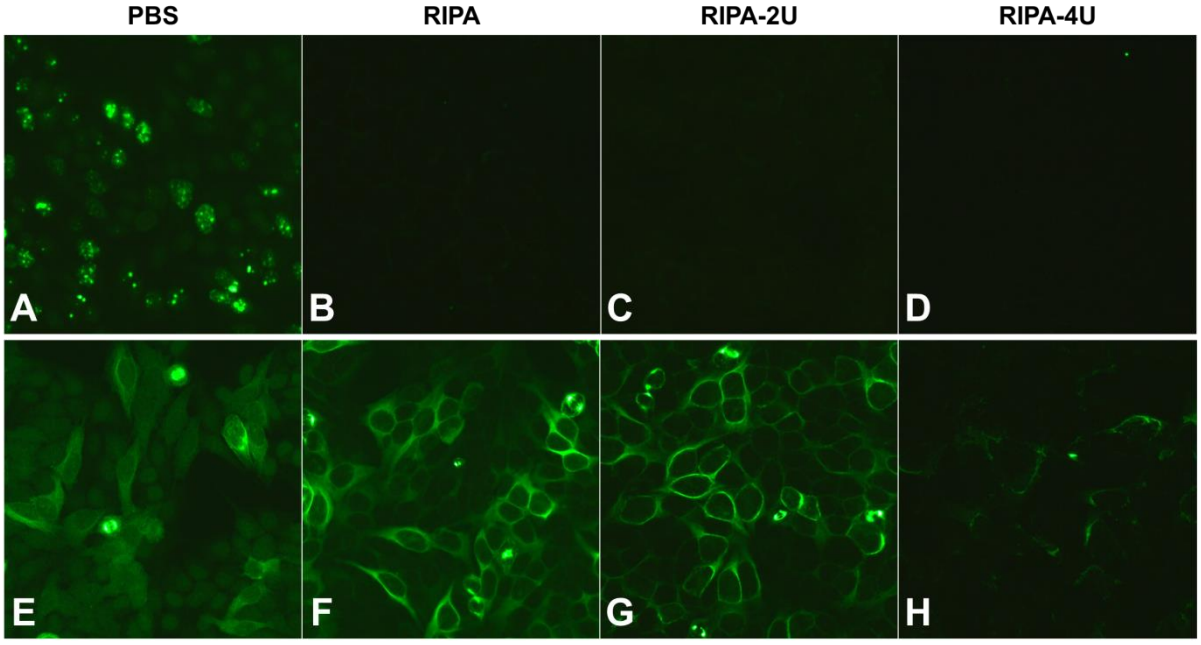

Figure 3-23 Extractability test with G2-phase specific serum samples
A)-D) UNA340, **E)-H)** UNA345. Following the principle of indirect immunofluorescence assay, after serum incubation, the slides were incubated with different extraction buffers, PBS **(A, E)**, RIPA **(B, F)**, RIPA-2U **(C, G)** or RIPA-4U **(D, H)**, prior to anti-human-IgG-Alexa488 (1:500) antibody incubation (serum dilution 1:100, magnification 200x)

3.8 Synchronization of HEp-2 cells

In order to enrich the target antigens of G2-phase specific serum samples, HEp-2 cells were arrested in G1/S-boundary of the cell cycle by a double thymidine block as described in 2.3.4. By removal of thymidine the cells were released and samples of different time points after the release were analyzed in Western blot (Figure 3-24) and IFA (Figure 3-25).

Figure 3-24, A shows a Western blot of lysates from different time points incubated with anti-cyclin B1 and anti-actin prior to anti-mouse-IgG-AP incubation. The intensity of the bands was quantified with Image J and the relative intensity of the cyclin B1 bands was normalized by dividing through the intensity of actin bands (Figure 3-24, B). It was found that the concentration of cyclin B1 started to increase 4 hours after removal of thymidine and reached the maximum around 7 hours; while the expression of actin did not change.

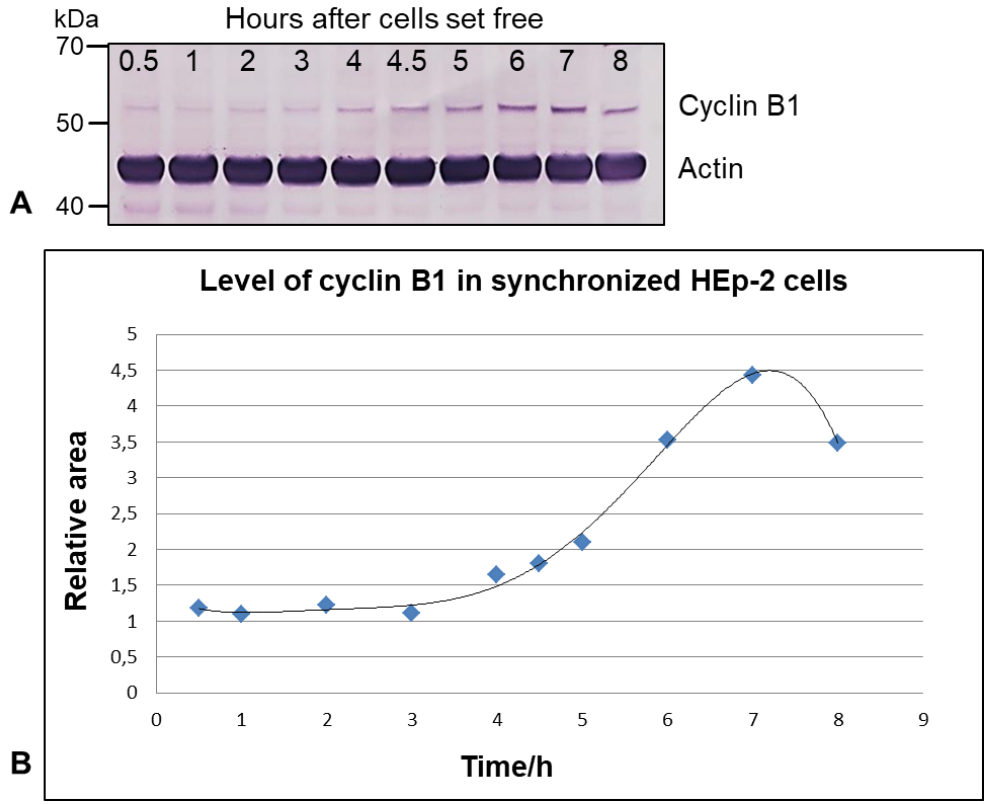

Figure 3-24 Western blot analysis of synchronized HEp-2 cells.
A) HEp2 cells were synchronized in G1/S phase using double thymidine block. The cells were released and further cultivated for eight hours and ten samples were collected from different time point: 0.5, 1, 2, 3, 4, 4.5, 5 h, 6, 7 and 8 hours. The samples were analyzed in Western blot with anti-cyclin B1 (1:1000) and anti-actin (1:1000) as primary antibodies and anti-mouse-IgG-AP (1:2000) as secondary antibody. **B)** The intensities of the bands in Western blot were analyzed with Image J. The relative area was calculated by dividing the area of cyclin B1 by the area of actin multiplied with 10000. The curve simulates the level of cyclin B1 in synchronized cells from G1/S phase to G2/M phase.

Cyclin B1 increases at the beginning of G2-phase and reaches a maximum in prometaphase [36]. Therefore, it was determined that starting from the G1/S block the cells were 4 hours after the release at the S/G2 boundary and reached the G2/M boundary 6 hours after the release. G1/S, S/G2 and G2/M cells were tested as substrate in IFA with G2-specific serum samples. IFA pictures of UNA340 and UNA345 are shown in Figure 3-25 as examples. G1/S cells showed no specific fluorescence signal (Figure 3-25, A and D); while in S/G2 cells, the fluorescence signal was slightly enhanced (Figure 3-25, B and E). The specific nucleolar pattern (UNA340) and cytoplasmic stain in interphase cells with spindle apparatus in mitotic cells (UNA345), were clearly observed in G2/M cells (Figure 3-25, C and F). These results show that the target antigens were enriched in G2/M cells. Thus, the G2/M cells were applied in following experiment to identify the target of G2-phase specific serum samples.

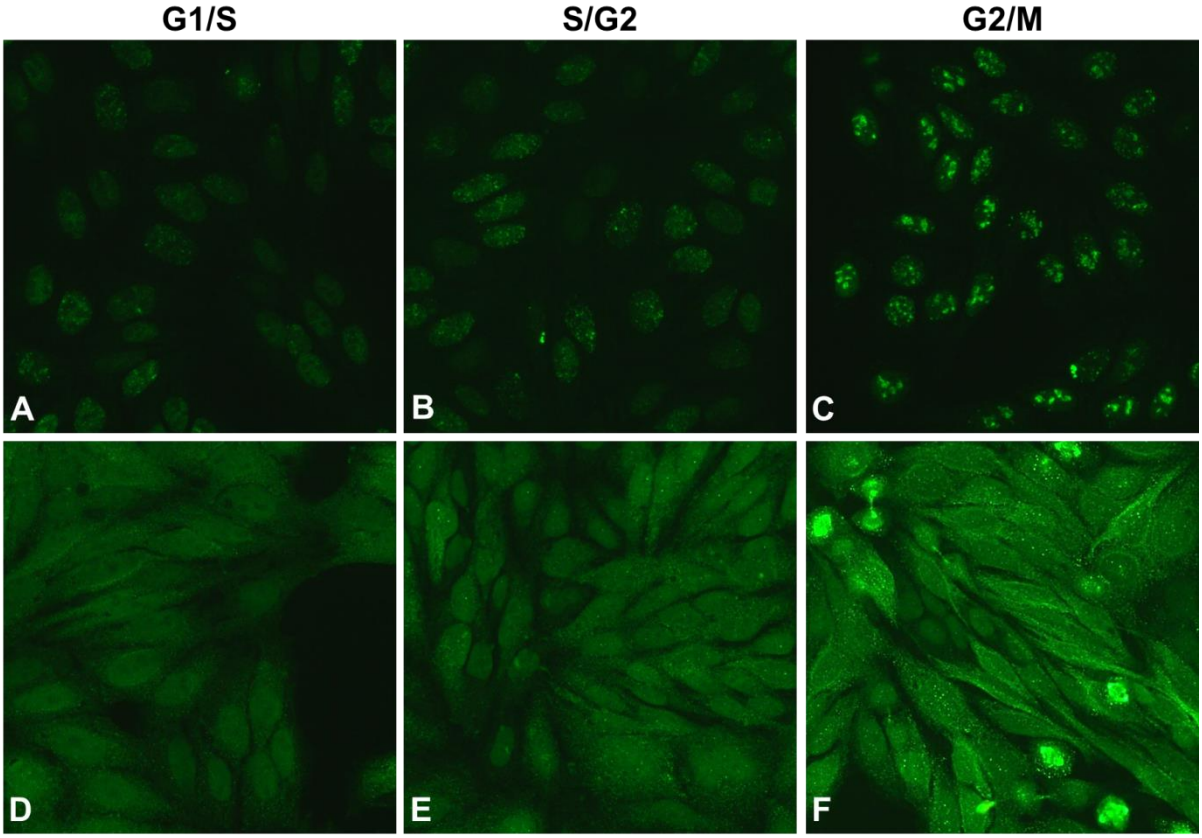

Figure 3-25 IFA with synchronized cells and G2-phase specific serum samples.
UNA340 **(A-C)** and UNA345 **(D-F)** were tested in IFA using synchronized HEp-2 cells as substrate. Anti-human-IgG-Alexa488 (1:500) was applied as secondary antibody. **A) and D)** Cells at G1/S boundary. **B) and E)** Cells at S/G2 boundary. **C) and F)** Cells at G2/M boundary. (serum dilution 1:100, magnification 200x)

3.9 Identification of kinesin-like protein KIF11 (KIF11) with modified fractionated IP

A fractionated IP with RIPA buffer and synchronized HEp-2 cells as substrate was implemented. Figure 3-26, A shows a coomassie stained gel of the IP eluates of UNA337 to UNA340 and a Western blot with the respective serum.

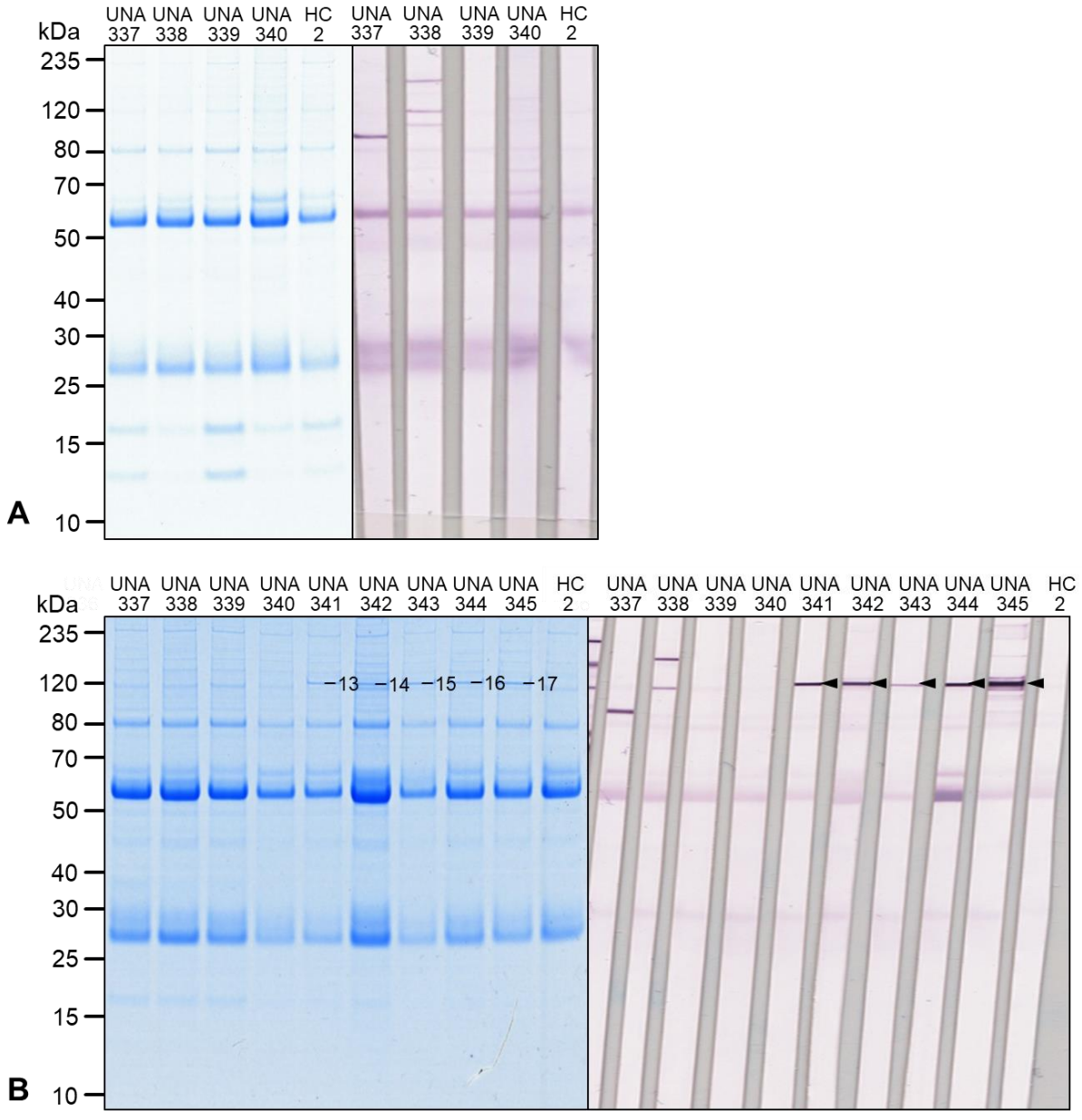

Figure 3-26 FIP with synchronized HEp-2 cells and G2-phase specific serum samples
A) FIP with UNA337 to UNA340, which showed a G2-phase specific nucleolar pattern, and HC2 as negative control with G2-synchronized HEp-2 cells and RIPA buffer. IP eluates were separated by SDS-PAGE and gels were analyzed by coomassie staining (left) and Western blot incubated with autologous serum samples (right). The bands corresponding to Western blot reaction in UNA337 and UNA338 was analyzed in MALDI-TOF-MS, but no protein was identified. **B)** FIP with UNA337 to UNA345 with RIPA-4U and G2-synchronized cells. HC2 was the negative control. In coomassie stained gel, consistent specific bands (band 13 to band 17) were selected according to the Western blot reaction.

HC2 was used as negative control. No specific bands were observed in the coomassie gel and only a mild reaction of UNA337 around 80 kDa and weak reactions of UNA338 around 120 and 180 kDa were observed in Western blot. However, no protein could be identified in the corresponding bands in MALDI-TOF-MS.

Subsequently, FIP with RIPA-4U buffer and synchronized HEp-2 cells was performed to identify the target antigen of UNA337 to UNA345. The result is shown in Figure 3-26, B. For UNA337 to UNA340, still no specific protein was identified. Modified FIP was not able to identify the target antigen of UNA337 to UNA340, regardless of Western blot reaction. On the other hand, a specific band at around 120 kDa was detected in each IP eluate of UNA341 to UNA345 with strong to mild Western blot reaction of the particular serum with the IP eluate. These bands (band 13 to 17) were sent to MALDI-TOF-MS and KIF11 was detected in every sample (Table 3-14).

Band	Annotation	Cut off	Score	Seq. cov.	Pep-tides	Mass /Da	Database
13	Kinesin-like protein KIF11 OS=Homo sapiens OX=9606 GN=KIF11 PE=1 SV=2	56	121	15	18	120111	SwissProt _Homo _sapiens
14	Kinesin-like protein KIF11 OS=Homo sapiens OX=9606 GN=KIF11 PE=1 SV=2	56	188	21	23	120111	SwissProt _Homo _sapiens
15	Kinesin-like protein KIF11 OS=Homo sapiens OX=9606 GN=KIF11 PE=1 SV=2	56	230	24	27	120111	SwissProt _Homo _sapiens
16	Kinesin-like protein KIF11 OS=Homo sapiens OX=9606 GN=KIF11 PE=1 SV=2	56	214	27	28	120111	SwissProt _Homo _sapiens
17	Kinesin-like protein KIF11 OS=Homo sapiens OX=9606 GN=KIF11 PE=1 SV=2	56	228	27	32	120111	SwissProt _Homo _sapiens
17	Kinesin-like protein KIF11 OS=Homo sapiens OX=9606 GN=KIF11 PE=1 SV=2	27	48	2	2	120111	SwissProt _Homo _sapiens

Table 3-14 Mass spectrometry analysis of UNA341 to UNA345.
Peptide-mass-fingerprinting results are in black and tandem mass spectrometry results are in blue.

3.10 Verification of KIF11 with transfected HEK293 cells in IFA

Recombinant HEK293 cell-based IFA was performed to verify the identification of KIF11 with UNA341 to UNA345. All index sera showed strong specific immunoreaction against HEK-KIF11 expressing cells, which was no observed in HEK-control cells. RC-IFA pictures of UNA341 and UNA345 are presented as examples in Figure 3-27, A and B, where red arrows indicates some specific reactions. This confirmed that KIF11 was the target antigen of UNA341 to UNA345.

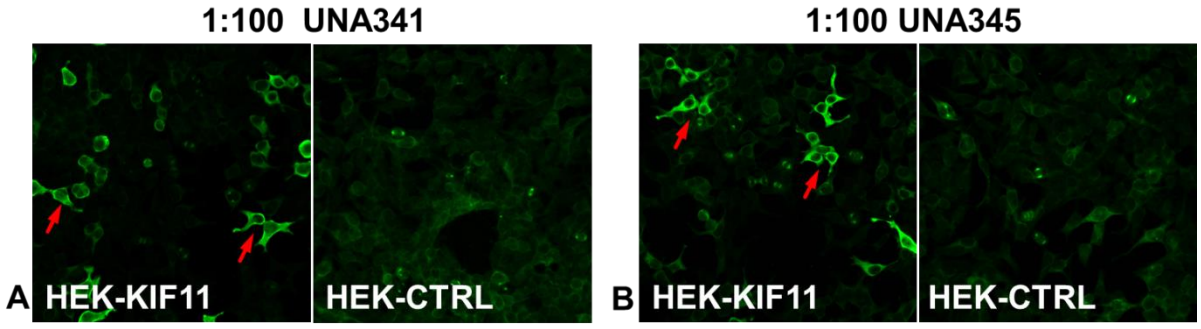

Figure 3-27 IFA with transfected HEK293 cells expressing KIF11.
Sera were diluted 1:100 and tested with transfected HEK293 cells expressing KIF11 in IFA. Anti-human-IgG-Alexa488 (1:500) was applied as secondary antibody. Red arrows indicate specific fluorescence signal. **A)** UNA341 and **B)** UNA345 (magnification 200x)

4 Discussion

The application of ANA test is increased in diagnostic laboratories. A negative HEp-2-IFA indicates a probable absence of a SARD while a positive finding requires further monospecific analysis for precise diagnose and personalized treatment. Currently, the established ANAs could not fully explain the observed patterns on HEp-2 cells. This urges the identification of novel ANA antigens and the development of new immunoassays. In this work, unknown nuclear autoantigens were identified by immunoprecipitation experiments and two types of immunoassays were developed.

4.1 Modification of immunoprecipitation and identification of KIF11

The strategy to identify the ANA target antigens was established in a previous master project [32]. Using the same strategy, nine additional candidate antigens were successfully identified and will be discussed in detail in section 4.2. However, the immunocomplexes formed by autoantibodies and HEp-2 cells lysate were occasionally not extractable using RIPA buffer. Part b of the result demonstrated a modified immunoprecipitation method using synchronized cells and a harsher buffer (RIPA-4U) containing different detergents and additional chaotropic salt. Surprisingly, the insoluble immunocomplexes were stable in this buffer and could be extracted. In combination with the standard downstream process, KIF11 was successfully identified. Interestingly, in 1996, two groups had independently reported KIF11 as the target antigen of anti-HsEg5 (anti-NuMA2) [37, 38]. The established method in this work requires fewer steps compared to the previous methods and could be easily applied for the identification of other antigen-antibody complexes.

KIF11 is a motor protein that belongs to the kinesin-like protein family. It is widely expressed in many tissues and especially in cells that actively proliferate [39]. KIF11 localizes to spindle microtubules with an enrichment at the centrosomes during mitosis and shows a cell cycle dependent cytoplasmic distribution [39]. It contains an N-terminal motor domain, a tail domain at the C-terminus and a stalk domain in between [39, 40, 41]. KIF11 plays an essential role in mitotic spindle dynamics of eukaryotic cells and is functional as homotetramer, which has a bipolar structure with two motor domains on each end, and stalk domain and tail domain in the middle as central stalk [39, 40]. Two antiparallel microtubules can be crosslinked by KIF11 homotetramers and be slide apart from plus-end to minus-end [39, 40, 41, 42]. In this

way, the separation of spindle-pole is driven by KIF11. Posttranslational modifications, like phosphorylation, are of importance for its activity and interaction with microtubules [39, 43, 44]. Additionally, it was found that KIF11 may also play a role in non-dividing cells, like neurons [39]. Overexpression of KIF11 was reported in various cancers, like oral cancer, glioblastoma and carcinoma [45, 46, 47]. It is a prognostic biomarker for these cancers and a potential therapeutic target.

These autoantibodies were first detected in patients with SLE and then also in patients with other systemic autoimmune rheumatic diseases [37, 38, 48, 49]. The detection of anti-HsEg5 was concluded as very uncommon and the potential of application of anti-HsEg5 seemed limited [49]. However, it should be mentioned that the analysis of anti-HsEg5 autoantibodies with large cohorts relied only on the detection of a specific ANA pattern on HEp-2 cells, which was “strong staining of spindle poles and spindle fibers with no dateable nuclear stain”. Without an established monospecific immunoassay, the importance of anti-HsEg5 may be significantly underestimated. In this work, a recombinant cell-based assay showed the potential to fill this gap (see section 3.10) and an additional lineblot development is also of interest.

4.2 Candidate antigens and established immunoassays

Fourteen candidate antigens were identified using fractionated immunoprecipitation (FIP) with HEp-2 cells and MALDI-TOF-MS. Nine of the candidate antigens, NVL, TFAP2A, TDP43, SMCHD1, XRN2, PELP1/SENP3, CD2BP2, MATR3 and TJP1, were novel antigens with unknown clinical association. In contrast, the association of the other five candidate antigens, PSME3, POLR2A, DHX9, RuvBL1/2 and RPA1/2/3, with autoimmune diseases was reported earlier by other researchers [50, 51, 52, 53, 54].

Two research slides for RC-IFA, UFO-ANA clinical association 1 and 2, were developed for eleven candidate antigens. Additionally, a lineblot, UFO-ANA profile 1, was assembled for eight candidate antigens. The available assays for the candidate antigens are summarized in Table 4-1. Six candidate antigens could be tested with both immunoassays, while only one assay is currently available for the other seven candidate antigens. Both immunoassays were analyzed with healthy controls and index sera. All the index sera showed strong positive reactions while no positive result was detected in the healthy control group (section 3.5.3). These results proof

that the positive reactions observed were specific. The further analysis of the immunoassays with 529 sera from 488 patients of the SARD cohort showed that 34 samples from 32 patients were positive in RC-IFA and 87 samples from 79 patients were positive in lineblot. Positive sera against selected four candidate antigens, NVL, PSME3, CD2BP2 and TJP1, were further examined in Western blot with purified recombinant antigen. In the following paragraphs, the candidate antigens are evaluated from different aspects.

Immunoassay type	Immunoassay name	Candidate antigens
RC-IFA	UFO-ANA clinical association 1	PSME3, TFAP2A, TDP43, DHX9, POLR2A, RPA1+2+3, RuvBL1+2
	UFO-ANA clinical association 2	SMCHD1, PELP1+SENP3, NVL, XRN2
Lineblot	UFO-ANA profile 1	PSME3, POLR2A aa1475-1970, TJP1 aa1-575, TFAP2A, TDP43, NVL, CD2BP2, SMCHD1

Table 4-1 Developed immunoassays for candidate antigens
Candidate antigens marked with underline are only available in RC-IFA, while the ones with square are only available in lineblot. The others could be tested with both immunoassays.

4.2.1 Candidate antigens analyzed with two immunoassays

SMCHD1, PSME3 and POLR2A, were described in a previous master project and thus only the new findings will be discussed.

4.2.1.1 Nuclear valosin-containing protein-like (NVL)

As the name of NVL indicates, it shows a high level of amino acid similarity to valosin-containing protein and locates exclusively in nucleus. NVL belongs to ATPase associated with various cellular activities or the AAA protein family. The major isoform of NVL contains two tandem AAA domains, a nuclear localization signal and a nucleolar localization signal [55]. It is ubiquitously expressed and mainly localized in the nucleolus and involved in biogenesis of the 60 S ribosomal subunit [55]. Additionally, it has also essential functions in telomerase biogenesis and pre-mRNA processing [56, 57]. It was reported that mutations in NVL may play a role in mental illness like major depressive disorder and schizophrenia [58, 59].

The sera from five SSc patients and one myositis patients revealed positive reactions against NVL in immunoassays. The sera from four patients were positive in both RC-IFA and lineblot, while the other two were positive in only RC-IFA. According to the analysis with Western blot, all the positive reactions observed in RC-IFA were

confirmed. The two lineblot negative sera showed weak Western blot reactivity, which was not observed in negative control sera. The weaker reaction detected in lineblot and Western blot may be due to the lower antibody titer in serum or recognition of a different epitope. At this point one can conclude that, RC-IFA showed the same specificity but higher sensitivity than the lineblot for anti-NVL autoantibodies. Clinically, the anti-NVL autoantibodies were detected in 1.3% (5/378) of SSc and 6.6% (1/15) of myositis patients. However, due to the small number of myositis patients, it should be carefully analyzed with a larger myositis cohort. In five of the six patient sera, other relevant ANAs were detected additionally (anti-centromere, anti-Scl70, anti-PM75, anti-PM100 and anti-NOR90). As it is mentioned in section 1.4, some ANAs are biomarkers for the clinical disease subset classification and prediction of prognosis. Therefore, the association of anti-NVL autoantibodies with SSc can further contribute to the precision diagnosis of patients and personalized treatment.

4.2.1.2 Transcription factor AP-2-alpha (TFAP2A)

TFAP2A has an ubiquitous expression and locates predominantly in the nucleus [60]. It can bind to GC-rich DNA sequences and thereby regulates the transcription of selected target genes, which play a regulatory role in apoptosis, cell cycle and gene expression [61]. TFAP2A is crucial during embryogenesis, as the activity of TFAP2A controls the formation of the neural crest [62, 63]. It is reported that the TFAP2A mutation is one of the causes for branchio-oculo-facial syndrome, which is a rare autosomal-dominant cleft palate-craniofacial disorder [64]. There are evidences that deregulation of TFAP2A is implicated in various cancer, like melanoma, breast tumours, gliomas and ovarian carcinomas [60].

Totally, 35 sera were anti-TFAP2A positive in lineblot while only two of them showed positive reaction in RC-IFA. The lineblot-positive sera illustrated many different ANA patterns on HEp-2 cells and the patients were with various diagnoses. No conclusion could be drawn with these results. A possible explanation might be an insufficient quality of recombinant TFAP2A or cross-reaction of other ANAs present in the samples. Additional experiments are needed in order to understand the importance of these results.

4.2.1.3 TAR DNA-binding protein 43 (TDP43)

TDP43 is a highly conserved and ubiquitously expressed nuclear protein [65]. Similar to MATR3, it contains two RNA-binding domains, a nuclear localization signal, a nuclear export signal and additionally a glycine-rich region at the C-terminus [65, 66, 67]. Normally, TDP43 is localized in the nucleus with a small amount in the cytoplasm [65, 67]. It has multiple functions in nucleus and cytoplasm in transcription, pre-mRNA splicing, mRNA processing including transport, translation, stabilization and degradation [65, 67, 68, 69, 70]. The association of TDP43 with neurodegenerative diseases has been studied intensively for decades. Abnormal aggregation of TDP43 in inclusion bodies in the cytoplasm is a hallmark of affected cells in amyotrophic lateral sclerosis (ALS), frontotemporal lobar degeneration-ubiquitin type (FTLD-U) and inclusion body myositis (IBM) [68, 71, 72, 73]. Additionally, TDP43 proteinopathy has been reported in other neurodegenerative diseases including Alzheimer's disease, hippocampal sclerosis, Picks disease and Parkinson's disease [65, 74, 75]. It was reported that mutations of TDP43 is one of the reasons that triggers abnormal accumulation of TDP43 aggregates in cytoplasm [76]. The level of TDP43 is elevated in blood or CSF of ALS patients [72]. However, an autoimmune reaction against TDP43 is so far not been reported.

Six positive samples against TDP43 were found in the lineblot while no positive case was detected using RC-IFA. The observed discrepancy could be due to differences in the conformation or accessibility of the recombinant antigens, which will be discussed in more detail in section 4.4.

4.2.1.4 Structural maintenance of chromosomes flexible hinge domain-containing protein 1 (SMCHD1)

Two sera were anti-SMCHD1 positive, one only in RC-IFA and one only in lineblot. Further analysis is necessary to evaluate the result. It is possible that anti-SMCHD1 antibodies in the two sera target conformational and linear epitope, respectively. Thus, no consistent positive reaction was observed.

4.2.1.5 Proteasome activator complex subunit 3 (PSME3)

All together anti-PSME3 positive samples from nine patients were identified (five SSc, three SLE, one myositis). The results of anti-PSME3 detection illustrated a higher discrepancy between the immunoassays compared to NVL. Sera from six patients were positive in RC-IFA and lineblot, while sera from three patients were

only positive in one immunoassay. The Western blot analysis was able to confirm the positive reactions of one double-positive serum (SARD297, SLE patient) but the other eight sera were negative. Seven sera (including SARD297) showed a homogeneous pattern on HEp-2 cells, which is differed from a granular pattern detected in the index serum [32]. This might be due to the other ANAs detected in the sera, like anti-Scl70 autoantibodies. It was previously reported that PSME3 is unspecifically related with connective tissue diseases [32], which was confirmed in this study. The discrepancy between different immunoassays needs to be further analyzed. One possible explanation is that the antigen amount applied on Western blot was not enough. SARD297 showed the highest ANA titer and the highest intensity among the nine positive patients. It is believed that the anti-PSME3 autoantibodies are present in six patients, which showed positive reaction in both immunoassays. Further Western blot experiments with different amounts of purified antigen should be implemented to select an optimum antigen amount.

4.2.1.6 DNA-directed RNA polymerase II subunit RPB1 (POLR2A)

For POLR2A, samples from six patients were positive in RC-IFA and four were positive in lineblot. However, the two immune assays showed no agreement. On the one hand, due to high density of HEK-POLR2A cells, the interpretation of RC-IFA was difficult, especially for samples with strong homogeneous or centromere pattern. Therefore, RC-IFA is not suitable for screening POLR2A before the substrate is optimized. Experiments with different seeding densities of the recombinant HEK293 cells and expression time may worth being done. Moreover, it is reported that the phosphorylated form of RNA polymerase II is prone to be the target of ANA [77]. Therefore, co-expression of phosphatase with POLR2A may increase the specificity of this assay. On the other hand, the lineblot applied aa1475-1970 of POLR2A, which may not represent all possible epitopes. More experiments with full-length POLR2A and its fragments need to be done, for example, to apply prepared full-length and fragment in lineblot or ELISA with these ten sera and compare the reactivity.

4.2.2 Candidate antigens analyzed exclusively with RC-IFA

As it is shown in section 3.4.4, Figure 3-16, some candidate antigens required co-expression of interaction partners (PEL1 and SENP3), homologs (RuvBL1 and RuvBL2) or subunits (RPA1, RPA2 and RPA3) to ensure the optimum detection of autoantibodies. Meanwhile, due to the time limit, the preparation of purified DHX9

and XRN2 was not achieved. Therefore, the mentioned candidate antigens were only analyzed with RC-IFA. The positive results should be further confirmed with a second method. DHX9 was described in a previous master project and thus only the new findings will be discussed.

4.2.2.1 5'-3' exoribonuclease 2 (XRN2)

In human, XRN2 functions predominantly in the nucleus and is located mainly in the nucleolus [78, 79]. It interacts with NKRF/NFκB factor and DEAH-box helicase DHX15 to form a nucleolar subcomplex, which is important for maintaining nucleolar homeostasis [79, 80]. XRN2 plays a key role in termination of RNA polymerase II transcription [81, 82]. It is also essential in regulation of nuclear RNAs, including degradation of structured RNAs and processing of rRNA [83]. Additionally, XRN2 responses to DNA damage under stress and relocates into the nucleus. It prevents transcription-related DNA damage, like double strand breaks by resolving RNA:DNA hybrids [84].

Interestingly, no sample was found anti-XRN2 positive. It could be that anti-XRN2 autoantibodies are very rare or that it is associated to other diseases.

4.2.2.2 ATP-dependent RNA helicase A (DHX9)

Four patients were anti-DHX9 positive. They all showed a granular pattern on HEp-2 cells but had distinct diagnoses. It was reported that anti-DHX9 autoantibodies are potential biomarker for SLE [52]. However, two SSc patients were observed anti-DHX9 positive in this study. It is possible that anti-DHX9 autoantibodies are closely associated with the ANA pattern but are not specific for a certain disease. As it is shown in Table 1-2, anti-Ro52 autoantibodies are related with SARD and clinical symptoms but less specifically associated with certain disease. A more comprehensive study with a SLE cohort might be implemented.

4.2.2.3 Proline-, glutamic acid- and leucine-rich protein 1 (PELP1) and sentrin-specific protease 3 (SENP3)

PELP1 is expressed in most tissues and has critical functions in the nucleus [85, 86]. It provides multiple binding sides for nuclear receptors and transcription factors, and thus controls the progression of cell cycle, by regulating apoptosis, proliferation and metastasis [87]. It is reported that over-expression of PELP1 can support tumor progression [86]. It serves as a prognostic biomarker for breast cancer survival and is a potential therapy target [85].

Small ubiquitin-like modifier (SUMO) proteases are involved in various biochemical processes in cells by deconjugating SUMO modifications from proteins [88]. SENP3 is one of these proteases. It is widely expressed in tissues and localizes in the nucleolus [88]. SENP3 has a critical function in ribosome maturation by interacting with the NPM1 and PELP1-TEX10-WDR18 complex [88, 89]. There is evidence that the distribution of PELP1 in the nucleolus and nucleoplasm is regulated by SENP3 [89, 90]. Figure 3-16, A demonstrates that co-expression of PELP1 and SENP3 results in elevated fluorescence signal. This might be the indirect evidence that SENP3 is important for the stabilization and localization of PELP1. It is also possible that the autoantibodies recognize the PELP1-SENP3 complex. But as the index serum (UNA26) showed Western blot reaction against both candidate antigens (Figure 3-4, C1), it is less likely that these autoantibodies are targeting the complex.

The serum of one patient with ASS (1/10) was positive against PELP1+SENP3. It is worth to examine these interaction partners with a larger cohort of patients with ASS.

4.2.2.4 RuvB-like 1 (RuvBL1) and RuvB-like 2 (RuvBL2)

RuvBL1 and RuvBL2 are two homologs that belong to the AAA protein family [91]. They share 43% sequence identity and 65% sequence similarity [92]. They are ubiquitously expressed and mainly located in the nucleus [91]. RuvBL1 and RuvBL2 can form homo-and hetero-hexamers, even dodecamers [91, 92, 93]. In this study, with the help of a recombinant cell-based assay, it was observed that the co-presence of RuvBL1 and RuvBL2 is important for the stabilization of each other (Figure 3-16, B). They have diverse functions in cellular processes, including chromatin remodeling, regulation of transcription, assembly and maturation of snRNP, DNA damage signaling and repair, regulation of cell cycle and mitosis, etc. [91, 92, 93, 94]. With all these functions, RuvBL1 and RuvBL2 show central roles in regulatory networks for cell survival and proliferation. It is not surprising that overexpression of both proteins was found in various cancers, for example breast, lung, gastric, esophageal, pancreatic, kidney, bladder as well as lymphatic, and leukemic cancers [91]. This made them to important biomarkers for the diagnosis and prognosis of various cancers and to potential therapeutic targets. On the other hand, RuvBL1 and RuvBL2 were identified as target antigens of ANA previously and showed a potential in the diagnosis of systemic autoimmune rheumatic diseases. Firstly, anti-RuvBL1 autoantibodies were detected in sera of patients with SLE, polymyositis/dermatomyositis, rheumatoid arthritis and autoimmune hepatitis [95].

Later, more studies show evidences that anti-RuvBL1/2 autoantibodies are potential SSc biomarkers with a prevalence of approximately 2% by using immunoblot and ELISA with recombinant RuvBL1 and RuvBL2 [53, 96, 97]. However, till now the autoantibodies against RuvBL1/2 are not well-established and no commercial test kit is available.

The sera of two SSc patients (2/378, 0.5%) were positive against RuvBL1+2. One of the patients showed no additional ANA while the other showed a weak positive reaction against NOR90. These results confirmed that anti-RuvBL1/2 is associated with SSc but with very low prevalence.

4.2.2.5 Replication protein A (RPA)

RPA is a heterotrimeric protein complex, which consists of RPA1 (70 kDa subunit), RPA2 (32 kDa subunit) and RPA3 (14 kDa subunit). It provides six oligosaccharide/oligonucleotide-binding domains, where four are in RPA1 and each of RPA2 and RPA3 contains one [98, 99]. RPA can bind to single-stranded DNA and has essential functions in DNA metabolism, including DNA replication, DNA repair, DNA recombination and cell cycle and DNA damage checkpoints [98, 99]. Autoantibodies against subunits of RPA were detected in sera from patients with systemic autoimmune rheumatic diseases. The prevalence of anti-RPA autoantibodies is around 1.4% to 2% of SLE patients [54, 100, 101]. It was reported that the autoantibodies were most reactive against RPA2 and sometimes also RPA1 in Western blot; and until now, no reactivity against RPA3 was reported [54, 100].

Three anti-RPA positive samples were detected in RC-IFA with the SARD cohort. All positive patients had SSc but not SLE. Other SSc-markers were presented in the sera as well. Anti-RPA autoantibodies could have been associated with both SLE and SSc with a low prevalence.

4.2.3 Candidate antigens analyzed exclusively with lineblot

Two candidate antigens were analyzed with lineblot only. As it is shown in Figure 3-15, RC-IFA was not functional for the detection of anti-CD2BP2 because no specific reaction was observed with the index serum; and the detection of anti-TJP1 required a 1:10 dilution, which is not the same as the designed screening dilution. The positive reactions observed in lineblot were confirmed in Western blot. An additional verification with RC-IFA is worth being done for anti-TJP1 positive sera.

4.2.3.1 CD2 antigen cytoplasmic tail-binding protein 2 (CD2BP2)

CD2BP2 is ubiquitously expressed in cells and dependent on the cell type, it has important functions in the nucleus and the cytoplasm [102]. In CD2 receptor expressing cells, like T cells, thymocytes and natural killer cells, the GYF-domain in CD2BP2 can interact with CD2 through the proline-rich motifs in cytoplasmic tail of CD2, which signals production of interleukin-2 [102, 103]. Besides the function in immune response, CD2BP2 plays a role in pre-mRNA processing. CD2BP2 is also known as U5 snRNP 52K protein (U5-52K), because it is a component of U5 small nuclear ribonucleoprotein (snRNP), which together with other snRNPs forms the spliceosome [102]. It was also reported that CD2BP2 is crucial for embryogenesis [104].

To our knowledge, there is no report about CD2BP2/U5-52K associated with autoimmune disease. However, detection of autoantibodies against snRNPs is not unusual for patients with connective tissue diseases [105]. For example, anti-Smith autoantibodies are targeting seven proteins (B/B', D1, D2, D3, E, F, G) that construct the core of U1, U2, U4 and U5 snRNP particles with a prevalence between 5 and 30% in SLE patients [106, 107]. The frequency of anti-RNP autoantibodies, which are directed against proteins (70 kDa, A, C) that are associated with U1 RNA forming U1 snRNP, is around 25-47% in SLE patients [106, 107].

Eleven sera from ten patients were anti-CD2BP2 positive, of which eight had SSc, one MCTD and one myositis. With exception of one SSc patient, all others have additional ANAs. Anti-CD2BP2 showed an association with SSc with prevalence of 2.1%. It is likely that these autoantibodies are syndrome related and reflect disease activity. A more comprehensive study to identify the clinical character of the anti-CD2BP2 positive patients may reveal the importance of this ANA.

4.2.3.2 Tight junction protein ZO-1 (TJP1)

TJP1 aa1-575 was applied in lineblot. Anti-TJP1 autoantibodies were detected in 16 sera. Most of the patients had SSc except one with UCTD. Additional ANAs were detected in 14 Sera (13 SSc, 1 UCTD). Anti-TJP1 showed an association with SSc with a prevalence of 4.0%. These autoantibodies could be useful in further subclassification of the patients. The potential pathogenesis of anti-TJP1 autoantibodies is discussed in section 4.3.

4.2.4 Candidate antigen with no established immunoassay

Matrin-3 (MATR3) is a major component of the nuclear matrix, which is called also nuclear scaffold or skeleton [108]. It connects the nuclear membrane to intranuclear compartments and supports the structure of the nucleus. MATR3 has two DNA-binding domains and two RNA-binding domains along with a nuclear localization signal and a nuclear export signal [108]. It is localized in the nucleoplasm but not the nucleolus. Because of the interaction of MATR3 with multiple nuclear proteins, it has important functions in the regulation of transcription, pre-mRNA splicing, stabilization of mRNA, DNA damage repair insulation of genomic domains and facilitating DNA replication [108, 109, 110]. Interestingly, the interaction partner of MATR3 include newly identified candidate antigens, like TDP43, DHX9 and POLR2A; and well-established ANA targets, like Ku70 and Ku80 [108, 111]. It is possible that certain autoantibodies target the complexes of MATR3 with one or more of these proteins. Under condition of HIV infection, MATR3 is recruited and serves as Rev protein co-regulator, where Rev is essential in HIV-1 biogenesis. Inherited mutations of MATR3 are associated with the neurodegenerative disease amyotrophic lateral sclerosis (ALS). In this disease, aggregation of MATR3 is often observed, as well as distal myopathy [108, 111, 112, 113]. As it is shown in Figure 3-15, D, RC-IFA is not suitable for detection of anti-MATR3 autoantibodies. The solid phase-based immunoassays, like lineblot, should be further developed as described in section 3.5.

4.2.5 An overview of the candidate antigens

The fifteen candidate antigens discussed above in section 4.1 and 4.2 are shortly summarized in this section. All the candidate antigens have important roles in various cellular processes and many show multiple functions. An overview of all identified candidate antigens in this work and previous master project is given in Table 4-2. Most of the candidate antigens are associated with DNA replication (RPA), DNA repair (XRN2, DHX9, RuvBL and RPA), DNA transcription (TFAP2A, TDP43, POLR2A, XRN2, PELP1, RuvBL and MATR3), RNA processing (NVL, TDP43, XRN2, DHX9, PELP1, RuvBL and CD2BP2) and RNA translation (NVL and TDP43). The current functional picture of the well-established ANA target antigens is most related to DNA metabolism (dsDNA, histone, Scl-70, Ku and Mi-2); and RNA metabolism (DFS70, RNP/Sm, Ro, La, RNA polymerase, TIF1, fibrillarin, NOR90, PM-Scl and Th/To) [25]. Structurally, two candidate antigens, NVL and RuvBL homologs, are belonging to AAA protein family and contain AAA domains, which

hydrolyze ATPs. In this work, the characterization of NVL, CD2BP2 and TJP1 revealed that these three candidate antigens were potential SSc marker and could be helpful in subclassification of patients or in monitoring the disease activity. However, a screening analysis with a cohort containing more diversity and more numbers of SARD patients should be further implemented. Besides of that, it is described in section 1.2.1 that many ANAs are associated with cancers. It is possible that the identified candidate antigens are biomarker for only cancer or for SARD patients with cancer but not for SARD alone. Thus, it is worth to implement an analysis with a large cancer cohort.

Candidate antigens	ANA pattern	Established assays	Function	Remark
KIF11	Mitotic spindles and a cell-circle dependent cytoplasmic fine speckled	none	Motor protein, splicing antiparallel microtubules	Known to be associated with SLE; antigen overexpressed in various cancer
NVL	Nucleolar	RC-IFA and lineblot	AAA protein family, ribosome biogenesis, mRNA processing	Novel antigen; may associated with SSc
TFAP2A	Pseudo-dense fine speckled	RC-IFA and lineblot	Transcription regulation	Novel antigen; unknown clinical association
TDP43	Granular	RC-IFA and lineblot	mRNA processing	Novel antigen; unknown clinical association
SMCHD1	Granular	RC-IFA and lineblot	Chromatin organization and epigenetic regulation	Novel antigen; unknown clinical association
PSME3	Granular	RC-IFA and lineblot	Subunit of proteasome activator 11s, regulation of proteasome	Known to be associated with SARD; low disease specificity
POLR2A	Granular	RC-IFA and lineblot	Subunit of RNA polymerase II, mRNA biosynthesis	Known to be associated with SLE and SSc
XRN2	Nucleolar and granular	RC-IFA	Transcription termination and alternative splicing	Novel antigen; unknown clinical association
DHX9	Granular	RC-IFA	DNA metabolism, RNA processing	Known to be associated with SLE; suspected low disease specificity
PELP1	Nucleolar and granular	RC-IFA	Transcription coregulator, ribosomal biogenesis	Novel antigen; unknown clinical association; antigen as prognostic marker for breast cancer
SENP3	Nucleolar and granular	RC-IFA	SUMO-specific proteases, deconjugation of SUMO2 and SUMO3	Novel antigen; unknown clinical association

RuvBL1 and 2	Granular	RC-IFA	AAA protein family, regulation in cell growth and proliferation	Known to be associated with SLE and SSc; antigen overexpressed in various cancer
RPA1/2/3	Pleomorphic	RC-IFA	Subunits of replication protein A, DNA metabolism	Known to be associated with SLE
CD2BP2	Pseudo-dense fine speckled	Lineblot	Nucleus: Component of U5 snRNP complex, spliceosome assembly Cytoplasm: regulation of CD2-triggered T lymphocyte activation	Novel antigen; may associated with SSc
TJP1	none	Lineblot	Regulation of tight junctions and anchor of the tight junctions	Novel antigen; may associated with SSc
MATR3	Granular	None	Major component of nuclear skeleton, regulation of transcription, mRNA processing	Novel antigen; unknown clinical association

Table 4-2 Accumulative table for candidate antigens
The five antigens already reported in the previous master project [32] are in grey.
AAA: ATPase associated with various cellular activities; SUMO: Small ubiquitin-like modifier; SLE: Systemic lupus erythematosus; SSc: Systemic sclerosis; SARD: systemic autoimmune rheumatic disease

4.3 Potential pathogenesis of anti-TJP1 autoantibodies

The identification of TJP1 as a candidate antigen was previously reported in a master project [32]. In this work, further experiments were conducted and verified that TJP1 was the target antigen of the index serum (UNA25) (Figure 3-13 and 3-15, I). However, it showed some distinct character compared to the other candidate antigens. Firstly, though with a high titer of ANA reaction (1:3200), UNA25 showed only a moderate reaction in RC-IFA with recombinant HEK-TJP1 cells with a 1:10 dilution, which was absent with 1:100 diluted UNA25 (Figure3-15, I). Secondly, the neutralization test failed (Figure 3-14, I), which implied that the ANA pattern might be caused by another undetected autoantibody but not by anti-TJP1 autoantibodies in UNA25. Thus, a colocalization experiment with an anti-TJP1 antibody (see section 3.4.5) was performed to examine the hypothesis. The result revealed that anti-TJP1 autoantibodies target endogenous TJP1 with a diffuse staining of the cytoplasm but not staining of the nucleus of HEp-2 cells was observed. Additionally, a colocalization experiment with HEK293 cells was performed. Here the commercial anti-TJP1 antibody stained regions at cell-cell contacts of adjacent HEK293 cells. Remarkably, besides of the nuclear signal UNA25 showed, a similar pattern at intercellular

contacts, colocalizing with the anti-TJP1 antibody signal (Figure 3-17). It was reported that the tight junction molecules could be up- or down-regulated in cancer cells, which results in the dysregulation of tight junction [114]. The observation, that tight junctions are visible in HEK293 but not in HEp-2 cells, might be due to the different origins of the two cells lines. HEp-2 cells are a HeLa derived cancer cell line, while HEK293 cells origin from embryonic kidney cells.

TJP1 is specifically enriched at the tight junctions of epithelial and endothelial cells. It belongs to the membrane associated guanylate kinase (MAGUK) protein family and shuffles between the nucleus and tight junctions [115]. A schematic picture is present in Figure 4-1. TJP1 is a sub-membranous protein and functions as tight junction plaque that anchors transmembrane molecules, including claudin, occludin and junctional adhesion molecules to the cytoskeleton [115, 116, 117]. Manetti et al. showed that the abnormal expression of junctional adhesion molecules, like JAM-A and JAM-C, was related to microvascular endothelial cell activation and inflammatory process, which contribute to onset of SSc [118]. On the other hand, the autoantibodies targeting desmosomes, which belong to junctional complexes, are well studied and a pathologic effect of anti-desmoglein autoantibodies was reported in patients with autoimmune bullous dermatoses [119, 120]. In short, the presence of anti-desmoglein autoantibodies results in blisters in the skin by deconstruction of desmosome. However, it is currently unclear how are the autoantibodies get in touch with sub-membranous TJP1. It was reported that some autoantibodies can be internalized by cells by different mechanisms: Fc receptors at cell surface are able to initiate the internalization of antibodies, which are afterwards degraded or released but not bind to intracellular component [121]. A Fc receptor independent mechanism requires vehicle molecules, for example penetration peptides or molecules, like nucleoside, or Fab-binding cell surface protein, like myosin 1, which allow the bound antibody to be transported across the membrane [121, 122]. It was reported that anti-dsDNA, anti-Sm and anti-ribosomal P autoantibodies penetrated the cell membrane *in vivo* and attacked the nuclear components, which resulted in cellular damage and apoptosis [121, 122, 123]. It is possible that anti-TJP1 autoantibodies penetrate the membrane by a Fc independent mechanism, or sub-membranous TJP1s could be presented on the cell surface under certain situations, like cellular damage or stress.

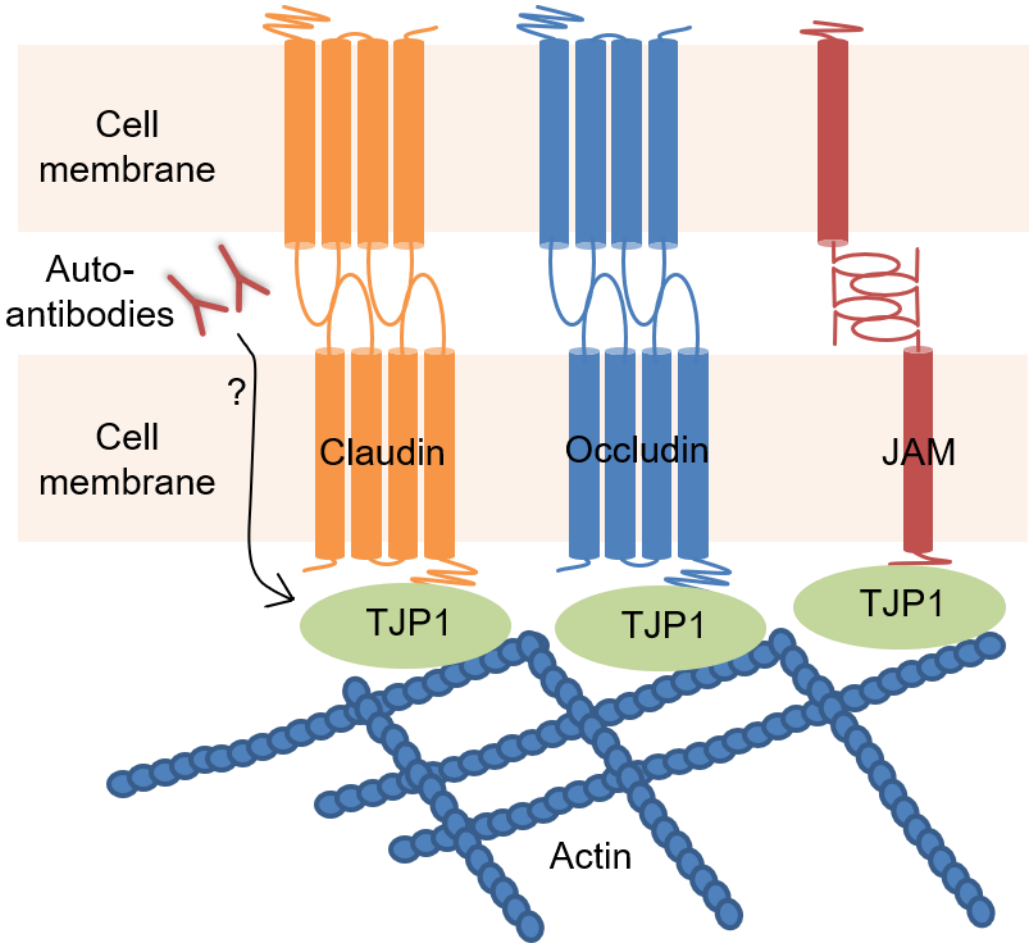

Figure 4-1 Schematic structure of different tight junctions (modified from Schneeberger et al [124])
TJP1 interacts with different transmembrane molecules and anchors them to the cell skeleton. Anti-TJP1 autoantibodies might target sub-membranous TJP1 and cause disassembly of tight junction. JAM: junctional adhesion molecule; TJP1: tight junction protein 1

Autoantibodies against TJP1 might affect the assembly of tight junction. In this study, 15/378 (4%) SSc patients and 1/10 (10%) UCTD patients were anti-TJP1 positive (section 3.6.4). SSc includes symptoms, like fibrosis, vascular wall damage, skin sclerosis and renal crisis [125]. All the involved organs have adequate tight junctions and it can be suspected that anti-TJP1 autoantibodies play a role in the disease progress. The pathogenesis of anti-TJP1 autoantibodies should be further studied in more detail. *In vitro* experiments using tight junction building cells are necessary to evaluate the influence of anti-TJP1 antibodies on cells and pathogenic mechanism.

4.4 Potential application of candidate antigens in diagnosis of ANA-associated autoimmune diseases

4.4.1 Application of lineblot

As it is mentioned in section 1.3, in complement to standard IFA with HEp-2 cells, the application of lineblot or immunoblot is essential for monospecific differentiation of ANA. It has the advantages of uncomplicated handling and interpretation of results. Currently, there are different profiles containing various combinations of disease-specific antigens. For example, one of the most used SSc immunoblot contains SSc-specific target antigens (Scl-70, centromere, RNA polymerase III, fibrillarin, Th/To, NOR90, PDGFR) and the indicators (PM-Scl, Ku and Ro52) for overlap syndromes [126]. However, the identity of ANAs in approximately 5-15% of SSc patients are is still unknown. As it is summarized in section 4.2.5, the novel candidate antigens presented in this work, like NVL, CD2BP2 and TJP1, are closely related to SSc and could narrow the gap. These three candidate antigens could be added to the SSc immunoblot and thus increase the specificity of the overall finding. Autoantibodies against these three candidate antigens added up to 7.4% (28/379) of SSc patients. 10.7% (3/28) of them showed no reaction against other established ANAs, while 17.9% (5/28) showed additional positive reactions against Ro52. Ro52, which is also known as tripartite motif containing-21 (TRIM21), shows low specificity to SSc and could be frequently detected also in SLE and SjS [127]. The other positive sera belong to patients with myositis (2), MCTD (1) and UCTD (1), which display shared clinical characters. On the other hand, these autoantigens could enlarge the spectrum of monospecific ANA analysis. This is crucial, when the patients show atypical syndrome but indeed should be treated because of the elevated autoimmune condition. A broader test spectrum and specific clinical associations of autoantibodies aid the physicians to make subclassifications of the patients and to take measures in time. In conclusion, it is suggested to include the newly identified candidates, especially NVL, CD2BP2 and TJP1 in the current monospecific ANA tests and to further study the association of disease activity and clinical syndromes with these novel candidate antigens.

4.4.2 Application of cell-based assay

The RC-IFA is based on recombinant HEK293 cells overexpressing candidate antigens. It is successfully applied in the detection of autoantibodies, like anti-

neuronal autoantibodies and anti-desmoglein autoantibodies, for a decade [128, 129]. In practice, RC-IFA supports the diagnosis of neurological autoimmune diseases or autoimmune bullous diseases. In this work, RC-IFA was combined with ANA diagnostics for the first time and showed surprising results. Unlike the tissue specific neuronal antigens or desmogleins, ANA antigens are mostly ubiquitously expressed and thus, are also endogenously expressed in HEK293 cells. It was suspected that the interference of the endogenous antigens with recombinant antigens might lead to strong background reaction. Unexpectedly, the index sera showed a clear positive reaction in RC-IFA in most cases. This is probably the case, because recombinantly overexpressed antigens do not seem to locate exclusively in the nucleus but also in the cytoplasm of the transfected cells. Therefore, RC-IFA showed very good compatibility with ANA detection (section 3.4.4). When compared to the conventional monospecific ANA tests, like lineblot and ELISA, RC-IFA has the advantage of presenting the target antigens in a less manipulated condition. In RC-IFA, it is more likely that the proteins hold their conformational structure and provide binding-sites for the autoantibodies targeting both linear and conformational epitopes. The development of this cell-based assay gives the opportunity for fast conversion of identified novel candidate antigens into test immunoassays, which enables early evaluation of candidate antigens by skipping the time- and resource-costing preparation of recombinant or native antigens. However, it has to be mentioned that the interpretation and standardization of RC-IFA is more complicated compared to lineblot or ELISA.

In this work, HEK-RuvBL1+2 was a perfect example for the detection of conformational epitopes recognizing autoantibodies. The autoantibodies against RuvBL1 and 2 were reported as potential SSc biomarker (see section 4.2.2.4). However, due to the lack of suitable screening tools, the value of autoantibodies targeting RuvBL proteins was possibly underestimated. It is proofed in this work that the co-presence of the homologs is crucial for the autoimmune reaction (Figure 3-16, B). One possible explanation is that the co-expression of RuvBL homologs stabilizes the correctly folded structure of both proteins, thereby providing a high-affinity epitope.

Last but not least, the application of recombinant HEK cells in parallel to HEp-2 cells and monkey liver in IFA could be a new trend in the near future for ANA diagnostics. By design and customization of a BIOCHIP Mosaic, it is possible to have a specific

profile that can be used to test the related autoantibodies in one incubation. Though, it is not yet clear, whether all the well-established ANAs are compatible with RC-IFA, it is considered that after optimization some of them may have high potential in ANA RC-IFA analysis.

4.4.3 Application of candidate antigens in combination with automation and artificial intelligence

Due to the increasing number of autoantigens it is questionable how the high number of possible autoantibody tests should be handled by diagnostic laboratories in the future. The assistance of automated test systems and artificial intelligence might be indispensable in this context, so that the newly established immunoassays can bring additional benefits in subclassification of patients and personalized medical care.

Many clinical laboratories have experiences with automated ANA test systems for various immunoassays, including IFA, ELISA, lineblot and CLIA, which dramatically increase the analysis efficiency with high specificity and sensitivity [130, 131]. On the other hand, the application of artificial intelligence in the diagnosis of different diseases is currently intensively studied and rapidly developed [132, 133, 134, 135]. With the combination of automation, big data analysis and artificial intelligence, more capacity for the analysis of multiple parameters might be available.

4.5 Possible therapy based on the candidate antigens

To achieve precision medicine, further developments of diagnostic and treatment opportunities are both required. The application of B cell eliminator/suppressor, like rituximab, in the treatment of systemic autoimmune rheumatic diseases, like RA, SLE, SSc and more, is proofed to be effective and is increasingly used in the practice [125, 136, 137]. However, in several patients, relapses were observed. Because of the unspecific elimination of B cells and the side effects, the demand for a specific B cell elimination technology is increased.

Revolutionary chimeric antigen receptor (CAR) technology is being applied in cancer therapy for a few years. It showed inspiring success in treating leukemias by engineering the T cells, which express CARs with an extracellular single-chain variable fragment (scFv) targeting CD19 [138]. The engineered cytotoxic T cells eliminate specifically $CD19^+$ B cells. Adapting the term in the autoimmune field, chimeric autoantibody receptor (CAAR) was brought up. Ellebrecht and colleagues

have applied this principle in creating a treatment for the anti-desmoglein 3 (Dsg3) antibody-mediated autoimmune disease pemphigus vulgaris [139, 140]. The idea was to design cytotoxic T cells that can eliminate the autoreactive B cells by recognizing their B cell receptor. CAAR T cell technology requires the identification of the autoantibodies, in order to design the corresponding T cells according to the individual autoreactive B cell repertoire. Therefore, the identification of novel candidate antigens is not only important for a precise diagnostic, but also to realize the personalized treatment regarding elimination of specific autoreactive B cells.

5 Conclusions and future perspectives

In conclusion, besides of the five candidate antigens previously described in a master project, ten additional candidate antigens were identified, seven of which are novel ANA antigens. All of the candidate antigens were verified with one or more methods. Two kinds of immunoassays, RC-IFA and lineblot were established for eleven and eight candidate antigens, respectively. Application of the established immunoassay in screening a SARD cohort revealed that autoantibodies against NVL, CD2BP2 and TJP1 are potential biomarkers for SSc.

This study includes a cohort of 488 patients with systemic autoimmune rheumatic diseases, where the majority are SSc patients. A more comprehensive study with larger cohorts of patients with other systemic autoimmune rheumatic diseases, like SLE and SjS, may reveal the additional value of the identified candidate antigens. On the other hand, because of the close association of ANAs with various cancers, it is interesting to analyze these candidate antigens with different cancer cohorts in order to evaluate the utility of the candidate antigens in cancers.

Moreover, TDP43 and MATR3 showed associations with neurodegenerative diseases in the literature. Though the connection between autoimmunity and neurodegenerative diseases is not yet clear, a pioneer study with an amyotrophic lateral sclerosis (ALS) and/or a frontotemporal lobar degeneration (FTD) cohort is worth being done. The application of the immunoassay in analyzing neurodegenerative diseases may be different from ANA test for systemic autoimmune rheumatic diseases. A different start dilution (1:10 or less) or recruitment of cerebrospinal fluid needs to be considered.

Additionally, TJP1 as a potential pathogenic target urges further investigation. As it is the first protein discovered at tight junctions, the character and functions of TJP1 in tight junctions are well-established. An *in vitro* study using living cells that form tight junctions could be the first step to enlighten the question if autoantibodies can directly bind to this sub-membranous protein and if yes, what is the mechanism of that.

Last but not least, it is important to continue the identification of novel autoantibodies in serological negative patients with autoimmune disorders. The novel antigens with

aid of big data analysis and innovative therapies will contribute to better understanding of autoimmune diseases and improve precision medicine.

Reference

[1] K. Murphy, Janeway's Immunobiology (8th Edition), NY: Garland Science, Taylor & Francis Group, LLC, 2012.

[2] A. B. Poletaev, L. P. Churilov, Y. I. Stroev and M. M. Agapov, "Immunophysiology versus immunopathology: Natural autoimmunity in human health and disease," *Pathophysiology,* pp. 221-231, July 2012.

[3] L. Moroni, I. Bianchi and A. Lleo, "Geoepidemiology, gender and autoimmune disease," *Autoimmunity Reviews,* pp. A386-A392, May 2012.

[4] A. Lleo, P. Invernizzi, B. Gao, M. Podda and M. E. Gershwin, "Definition of human autoimmunity — autoantibodies versus autoimmune disease," *Autoimmunity Reviews,* pp. A259-A266, March 2010.

[5] P. S. Ramos, A. M. Shedlock and C. D. Langefeld, "Genetics of autoimmune diseases: insights from population genetics," *J Hum Genet.,* p. 60(11): 657–664, November 2015.

[6] S. M. Hayter and M. C. Cook, "Updated assessment of the prevalence, spectrum and case definition of autoimmune disease," *Autoimmunity Reviews,* pp. 754-765, August 2012.

[7] Y. Kochi, A. Suzuki, R. Yamada and K. Yamamoto, "Genetics of rheumatoid arthritis: Underlying evidence of ethnic differences," *Journal of autoimmunity,* pp. 158-162, February 2009.

[8] D. Daneman, "Type 1 diabetes," *Lancet,* pp. 367(9513):847-58, March 2006.

[9] C. A. Janeway Jr, P. Travers, M. Walport and e. al., Immunobiology: The Immune System in Health and Disease. 5th edition., New York: Garland Science, 2001.

[10] R. J. Ludwig, K. Vanhoorelbeke, F. Leypoldt, Z. Kaya, K. Bieber, S. M. McLachlan, L. Komorowski, J. Luo, O. Cabral-Marques, C. M. Hammers, J. M. Lindstrom, P. Lamprecht, A. Fischer, G. Riemekasten, C. Tersteeg, P. Sondermann, B. Rapoport, K.-P. Wandinger, C. Probst, A. E. Beidaq, E.

Schmidt, A. Verkman, R. A. Manz and F. Nimmerjahn, "Mechanisms of autoanibody-induced pathology," *Frontiers in Immunology,* p. 8:603, 31 May 2017.

[11] R. Bei, L. Masuelli, C. Palumbo, M. Modesti and A. Modesti, "A common repertoire of autoantibodies is shared by cancer and autoimmune disease patients: Inflammation in their induction and impact on tumor growth," *Cancer Letters,* pp. 8-23, 18 August 2009.

[12] P. S. Leung, L. Rossaro, P. A. Davis, O. Park, A. Tanaka, K. Kikuchi, H. Miyakawa, G. L. Norman, W. Lee, M. E. Gershwin and Acute Liver Failure Study Group, "Antimitochondrial Antibodies in Acute Liver Failure: Implications for Primary Biliary Cirrhosis," *Hepatology,* pp. 46(5):1436-42, November 2007.

[13] A. McKeon, "Paraneoplastic and Other Autoimmune Disorders of the Central Nervous System," *Neurohospitalist,* p. 3(2): 53–64, April 2013.

[14] J. A. Bluestone, K. Herold and G. Eisenbarth, "Genetics, pathogenesis and clinical interventions in type 1 diabetes," *Nature,* pp. 464(7293), 1293-1300, 2010.

[15] K. Didier, L. Bolko, D. Giusti, S. Toquet, A. Robbins, F. Antonicelli and A. Servettaz, "Autoantibodies Associated With Connective Tissue Diseases: What Meaning for Clinicians?," *Front. Immunol,* 26 March 2018.

[16] A. T. Maria, L. Partouche, R. Goulabchand, S. Rivière, P. Rozier, C. Bourgier, A. L. Quellec, J. Morel, D. Noël and P. Guilpain, "Intriguing Relationships Between Cancer and Systemic Sclerosis: Role of the Immune System and Other Contributors," *Front. Immunol.,* p. 9:3112, 10 January 2019.

[17] S. Lv, J. Zhang, J. Wu, X. Zheng, Y. Chu and S. Xiong, "Origin and Anti-Tumor Effects of anti-dsDNA Autoantibodies in Cancer Patients and Tumor-Bearing Mice," *Immunol Lett,* pp. 99(2):217-27, 15 July 2005.

[18] M. W. Saif, A. Zalonis and K. Syrigos, "The clinical significance of autoantibodies in gastrointestinal malignancies: an overview," *Expert Opinion on Biological Therapy,* pp. 493-507, March 2007.

[19] A. V. Kozyr, A. V. Kolesnikov, E. S. Aleksandrova, L. P. Sashchenko, N. V.

Gnuchev, P. V. Favorov, M. A. Kotelnikov, E. I. Iakhnina, I. A. Astsaturov, T. B. Prokaeva, Z. S. Alekberova, S. V. Suchkov and A. G. Gabibov, "Novel functional activities of anti-dna autoantibodies from sera of patients with lymphoproliferative and autoimmune diseases," *Applied Biochemistry and Biotechnology volume,* pp. 75, pages45–61, October 1998.

[20] R. B. Conn, "Practice Parameter—The Lupus Erythematosus Cell Test: An Obsolete Test Now Superseded by Definitive Immunologic Tests," *American Journal of Clinical Pathology,* pp. 65-66, 1 Juanuary 1994.

[21] A. Kavanaugh, R. Tomar, J. Reveille, D. H. Solomon and H. A. Homburger, "Guidelines for Clinical Use of the Antinuclear Antibody Test and Tests for Specific Autoantibodies to Nuclear Antigens," *Archives of Pathology & Laboratory Medicine,* vol. 124, no. 1, pp. 71-81, August 2000.

[22] E. M. Tan and H. G. Kunkel, "Characteristics of a Soluble Nuclear Antigen Precipitating with Sera of Patients with Systemic Lupus Erythematosus," *J Immunol,* pp. 96(3):464-471, 1 March 1966.

[23] J. Damoiseaux, L. E. Andrade, O. G. Carballo, K. Conrad, P. L. Francescantonio, M. J. Fritzler, I. G. de la Torre, M. Herold, W. Klotz, W. de Melo Cruvinel, T. Mimori, C. von Muhlen, M. Satoh and E. K. Chan, "Clinical relevance of HEp-2 indirect immunofluorescent patterns: the International Consensus on ANA patterns (ICAP) perspective," *Ann Rheum Dis,* pp. 78:879-889, 12 March 2019.

[24] M. Aringer, K. Costenbader, D. Daikh, R. Brinks, M. Mosca, R. Ramsey-Goldman, J. S. Smolen, D. Wofsy, D. T. Boumpas, D. L. Kamen, D. Jayne, R. Cervera, N. Costedoat-Chalumeau, B. Diamond, D. D. Gladman, B. Hahn, F. Hiepe, S. Jacobsen, D. Khanna, K. Lerstrøm, E. Massarotti, J. McCune, G. Ruiz-Irastorza, J. Sanchez-Guerrero, M. Schneider, M. Urowitz, G. Bertsias, B. F. Hoyer, N. Leuchten, C. Tani, S. K. Tedeschi, Z. Touma, G. Schmajuk, B. Anic, F. Assan, T. M. Chan, A. E. Clarke, M. K. Crow, L. Czirják, A. Doria, W. Graninger, B. Halda-Kiss, S. Hasni, P. M. Izmirly, M. Jung, G. Kumánovics, X. Mariette, I. Padjen, J. M. Pego-Reigosa, J. Romero-Diaz, Í. Rúa-Figueroa Fernández, R. Seror, G. H. Stummvoll, Y. Tanaka, M. G. Tektonidou, C. Vasconcelos, E. M. Vital, D. J. Wallace, S. Yavuz, P. L. Meroni, M. J. Fritzler,

R. Naden, T. Dörner and S. R. Johnson, "2019 European League Against Rheumatism/ American College of Rheumatology classification criteria for systemic lupus erythematosus," *Ann Rheum Dis,* p. 78:1151–1159, September 2019.

[25] K. Conrad, W. Schößler, F. Hiepe and M. J. Fritzler, Autoantibodies in Systemic Autoimmune Diseases: A diagnostic Reference (Autoantigens, autoantibodies, autoimmunity Volume 2, third edition), K. Conrad and U. Sack, Eds., Germany: Pabst Science Publishers, 2015.

[26] M. J. Fritzler, "Perspective: Widening Spectrum and Gaps in Autoantibody Testing for Systemic Autoimmune Diseases," *J Rheumatol Res,* pp. 1(1): 10-18, 13 January 2019.

[27] M. R. Arbuckle, M. T. McClain, M. V. Rubertone, R. H. Scofield, G. J. Dennis, J. A. James and J. B. Harley, "Development of Autoantibodies before the Clinical Onset of Systemic Lupus Erythematosus," *N Engl J Med,* pp. 349:1526-33, 2003.

[28] J. B. Carter, S. Carter, S. Saschenbrecker and B. E. Goeckeritz, "Recognition and Relevance of Anti-DFS70 Autoantibodies in Routine Antinuclear Autoantibodies Testing at a Community Hospital," *Front. Med.,* p. 5:88, 09 April 2018.

[29] A. Stochmal, J. Czuwara, M. Trojanowska and L. Rudnicka, "Antinuclear Antibodies in Systemic Sclerosis: an Update.," *Clinic Rev Allerg Immunol,* pp. 58, 40–51, 2020.

[30] N. J. Olsen, M. Y. Choi and M. J. Frizler, "Emerging Technologies in Autoantibody Testing for Rheumatic Diseases," *Arthritis Res Ther,* p. 19(1):172., 24 July 2017.

[31] G. Yaniv, G. Twig, D. B.-A. Shor, A. Furer, Y. Sherer, O. Mozes, O. Komisar, E. Slonimsky, E. Klang, E. Lotan, M. Welt, I. Marai, A. Shina, H. Amital and Y. Shoenfeld, "A Volcanic Explosion of Autoantibodies in Systemic Lupus Erythematosus: A Diversity of 180 Different Antibodies Found in SLE Patients," *Autoimmun Rev,* pp. 14: 75-79, January 2015.

[32] Z. Zeng, Characterization of cryptic antinuclear autoantibody target antigens (master thesis), Lübeck: Lübeck University of Applied Sciences, 2017.

[33] Euroimmun AG, Euroline ANA profile 23 (IgG) test instruction, Germany, 2016.

[34] Euroimmun AG, Instructions for the indirect immunofluorescence test, Germany, 2016.

[35] H. T. Ma and R. Y. Poon, "Synchronization of HeLa Cells," in *G. Banfalvi (ed.), Cell Cycle Synchronization: Methods and Protocols*, Springer - Humana Press , 2011, pp. 151-161.

[36] T. D. Pollard, W. C. Earnshaw, J. Lippincott-Schwartz and G. T. Johnson, Eds., "Chapter 43 - G2 Phase, Responses to DNA Damage, and Control of Entry Into Mitosis," in *Cell Biology (Third Edition)*, Elsevier, 2017, pp. 743-754.

[37] L. E. Andrade, E. K. Chan, C. L. Peebles and E. M. Tan, "TWO MAJOR AUTOANTIGEN-ANTIBODY SYSTEMS OF THE MITOTIC SPINDLE APPARATUS," *ARTHRITIS & RHEUMATISM,* vol. 39, no. 10, pp. 1673-1653, October 1996.

[38] C. M. Whitehead, R. J. Winkfein, M. J. Fritzler and J. B. Rattner, "THE SPINDLE KINESIN-LIKE PROTEIN HsEg5 IS AN AUTOANTIGEN IN SYSTEMIC LUPUS ERYTHEMATOSUS," *ARTHRITIS & RHEUMATISM,* vol. 39, no. 10, pp. 1635-1642, October 1996.

[39] E. J. Wojcik, R. S. Buckley, J. Richard, L. Liu, T. M. Huckaba and S. Kim, "Kinesin-5: Cross-bridging mechanism to targeted clinical therapy," *Gene,* pp. 531:133-149, 2013.

[40] N. P. Ferenz, A. Gable and P. Wadsworth, "Mitotic Functions of Kinesin-5," *Semin Cell Dev Biol.,* pp. 21(3):255-259, May 2010.

[41] S. K. Singh, H. Pandey, J. Al-Bassam and L. Gheber, "Bidirectional motility of kinesin-5 motor proteins: structural determinants, cumulative functions and physiological roles," *Cellular and Molecular Life Sciences,* pp. 1757-1771, 2018.

[42] A. S. Kashina, R. J. Baskin, D. G. Cole, K. P. Wedaman, W. M. Saxton and J. M. Scholey, "A bipolar kinesin," *Nature,* pp. 379(6562):270-272, 18 January

1996.

[43] B. J. Mann and P. Wadsworth, "Kinesin-5 Regulation and Function in Mitosis," *Trends in cell biology,* vol. 29, no. 1, pp. 66-79, 1 January 2019.

[44] A. Blangy, H. A. Lane, P. d'Hérin, M. Harper, M. Kress and E. A. Nigg, "Phosphorylation by p34cdc2 regulates spindle association of human Eg5, a kinesin-related motor essential for bipolar spindle formation in vivo.," *Cell,* pp. 83(7):1159-69, 29 December 1995.

[45] M. Venere, C. M. Horbinski, J. F. Crish, X. Jin, A. Vasanji, J. Major, A. Burrows, C. Chang, J. Prokop, Q. Wu, P. A. Sims, P. Canoll, M. K. Summers, S. S. Rosenfeld and J. N. Rich, "The Mitotic Kinesin KIF11 is a Central Driver of Invasion, Proliferation, and Self Renewal in Glioblastoma," *Sci Transl Med.,* p. 7(304):304ra143, 9 September 2015.

[46] K. Daigo, A. Takano, P. M. Thang, Y. Yoshitake, M. Shinohara, I. Tohnai, Y. Murakami, J. Maegawa and Y. Daigo, "Characterization of KIF11 as a novel prognostic biomarker and therapeutic target for oral cancer.," *Int J Oncol.,* pp. 52(1):155-165, January 2018.

[47] C. Liu, N. Zhou, J. Li, J. Kong, X. Guan and X. Wang, "Eg5 Overexpression Is Predictive of Poor Prognosis in Hepatocellular Carcinoma Patients," *Disease markers ,* pp. 2017(26):1-9, June 2017.

[48] P. Grypiotis, A. Ruffatti, M. Tonello, C. Winzler, C. Radu, S. Zampieri, M. Favaro, A. Calligaro and S. Todesco, "Significato clinico dei quadri fluoroscopici specifici per il fuso mitotico in pazienti affetti da malattie reumatiche," *Reumatismo,* pp. 54(3):232-237, 2002.

[49] R. Szalat, P. Ghillani-Dalbin, M. Jallouli, Z. Amoura, L. Musset, P. Cacoub and D. Sène, "Anti-NuMA1 and anti-NuMA2 (anti-HsEg5) antibodies: Clinical and immunological features: A propos of 40 new cases and review of the literature," *Autoimmunity Reviews,* vol. 9, no. 10, pp. 652-656, August 2010.

[50] H. P. Seelig, "Other autoantibodies to nuclear antigens," in *Autoantibodies*, Netherlands, Elsevier Science B.V., 1996, pp. 582-594.

[51] M. Hirakata, Y. Okano, U. Pati, A. Suwa, T. A. Medsger, J. A. Hardin and J.

Craft, "Identification of autoantibodies to RNA polymerase II. Occurrence in systemic sclerosis and association with autoantibodies to RNA polymerases I and III.," *Journal of Clinical Investigation,* pp. 2665-2672, 1993.

[52] R. H. Scofield, "Do we need new antoantibodies in lupus?," *Arthritis research and therapy,* p. 12:120, 2010.

[53] K. Kaji, N. Fertig, T. A. Medsger Jr., T. Satoh, K. Hoshino, Y. Hamaguchi, M. Hasegawa, M. Lucas, A. Schnure, F. Ogawa, S. Sato, K. Takehara, M. Jujimoto and M. Kuwana, "Autoantibodies to RuvBL1 and RuvBL2: A Novel Systemic Sclerosis–Related Antibody Associated With Diffuse Cutaneous and Skeletal Muscle Involvement," vol. 66, no. 4, pp. 575-84, April 2014.

[54] Y. Yamasaki, S. Narain, L. Hernandez, T. Barker, K. Ikeda, M. S. Segal, H. B. Richards, E. K. Chan, W. H. Reeves and M. Satoh, "Autoantibodies against the replication protein A complex in systemic lupus erythematosus and other autoimmune diseases," *Arthritis Research & Therapy,* p. R111, 17 July 2006.

[55] Y. Fujiwara, K.-i. Fujiwara, N. Goda, N. Iwaya, T. Tenno, M. Shirakawa and H. Hiroaki, "Structure and Function of the N-terminal Nucleolin Binding Domain of Nuclear Valosin-containing Protein-like 2 (NVL2) Harboring a Nucleolar Localization Signal," *JOURNAL OF BIOLOGICAL CHEMISTRY,* pp. pp21732-21741, 17 June 2011.

[56] J. Her and I. K. Chung, "The AAA-ATPase NVL2 is a telomerase component essential for holoenzyme assembly," *Biochemical and Biophysical Research Communications,* pp. pp1086-1092, 20 January 2012.

[57] Y. Yoshikatsu, Y.-i. Ishida, H. Sudo, K. Yuasa, A. Tsuji and M. Nagahama, "NVL2, a nucleolar AAA-ATPase, is associated with the nuclear exosome and is involved in pre-rRNA processing," *Biochemical and Biophysical Research Communications,* pp. pp780-786, 28 August 2015.

[58] M. Wang, J. Chen, K. He, Q. Wang, Z. Li, J. Shen, Z. Wen, Z. Song, Y. Xu and Y. Shi, "The NVL gene confers risk for both major depressive disorder and schizophrenia in the Han Chinese population," *Progress in Neuro-Psychopharmacology and Biological Psychiatry,* pp. 7-13, 1 October 2015.

[59] S. Ripke, N. Wray, C. Lewis, S. Hamilton, M. Weissman, G. Breen, E. Byrne, D. Blackwood, D. Boomsma, S. Cichon, A. Heath, F. Holsboer, S. Lucae, P. Madden, N. Martin, P. McGuffin, P. Muglia, M. M. Noethen, B. W. Penninx, M. L. Pergadia, J. B. Potash, M. Rietschel, D. Lin, B. Müller-Myhsok, J. Shi, S. Steinberg, H. J. Grabe, P. Lichtenstein, P. Magnusson, R. H. Perlis, M. Preisig, J. W. Smoller, K. Stefansson, R. Uher, Z. Kutalik, K. E. Tansey, A. Teumer, A. Viktorin, M. R. Barnes, T. Bettecken, E. B. Binder, R. Breuer, V. M. Castro, S. E. Churchill, W. H. Coryell, N. Craddoc, I. W. Craig, D. Czamara, E. J. de Geus, F. Degenhardt, A. E. Farmer, M. Fava, J. Frank, V. S. Gainer, P. J. Gallagher, S. D. Gordon, S. Goryachev, M. Gross, M. Guipponi, A. K. Henders, S. Herms, I. B. Hickie, S. Hoefels, W. J. Hoogendijk, J. J. Hottenga, D. V. Iosifescu, M. Ising, I. Jones, L. Jones, T. Jung-Ying, J. A. Knowles, I. S. Kohane, M. A. Kohli, A. Korszun, M. Landen, W. B. Lawson, G. Lewis, D. J. MacIntyre, W. Maier, M. Mattheisen, P. J. McGrath, A. McIntosh, A. McLean, C. M. Middeldorp, L. Middleton, G. M. Montgomery, S. N. Murphy, M. Nauck, W. A. Nolen, D. Nyholt, M. O'Donovan, H. Oskarsson, N. Pedersen, W. A. Scheftner, A. Schulz, T. G. Schulze, S. I. Shyn, E. Sigurdsson, S. L. Slager, J. H. Smit, H. Stefansson, M. Steffens, T. E. Thorgeirsson, F. Tozzi, J. Treutlein, M. Uhr, E. J. van den Oord, G. Grootheest, H. Völzke, J. B. Weilburg, G. Willemsen, . F. G. Zitman, B. Neale, M. Daly, D. F. Levinson and P. F. Sullivan, "A mega-analysis of genome-wide association studies for major depressive disorder," *Molecular Psychiatry,* pp. 497-511, April 2013.

[60] F. Orso and D. Taverna, "TFAP2A (transcription factor AP-2 alpha (activating enhancer binding protein 2 alpha))," *Atlas of Genetics and Cytogenetics in Oncology and Haematology,* pp. 14(8):735-738, 2010.

[61] K. Hilger-Eversheim, M. Moser, H. Schorle and R. Buettner, "Regulatory roles of AP-2 transcription factors in vertebrate development, apoptosis and cell-cycle control," *Gene,* vol. 260, no. 1-2, pp. 1-12, 30 December 2000.

[62] N. de Crozé, F. Maczkowiak and A. H. Monsoro-Burq, "Reiterative AP2a activity controls sequential steps in the neural crest gene regulatory network," *PNAS,* vol. 108, no. 1, pp. 155-160, 4 January 2011.

[63] E. V. Otterloo, W. Li, A. Garnett, M. Cattell, D. M. Medeiros and R. A. Cornell,

"Novel Tfap2-mediated control of soxE expression facilitated the evolutionary emergence of the neural crest," *Development,* pp. 139(4): 720-730, 15 Febuary 2012.

[64] J. M. Milunsky, T. A. Maher, G. Zhao, A. E. Roberts, H. J. Stalker, R. T. Zori, M. N. Burch, M. Clemens, J. B. Mulliken, R. Smith and A. E. Lin, "TFAP2A Mutations Result in Branchio-Oculo-Facial Syndrome," *The American Journal of Human Genetics,* p. 1171–1177, May 2008.

[65] S. T. Warraich, S. Yang, G. A. Nicholson and I. P. Blair, "TDP-43: A DNA and RNA binding protein with roles in neurodegenerative diseases," *The International Journal of Biochemistry & Cell Biology,* vol. 42, no. 10, pp. 1606-1609, October 2010.

[66] Y. A. T. Kasu, S. Alemu, A. Lamari, N. Loew and C. S. Brower, "The N Termini of TAR DNA-Binding Protein 43 (TDP43) C-Terminal Fragments Influence Degradation, Aggregation Propensity, and Morphology," *molecular and Cellular Biology,* pp. 38:e00243-18, 9 July 2018.

[67] Y. M. Ayala, P. Zago, A. D'Ambrogio, Y.-F. Xu, L. Petrucelli, E. Buratti and F. E. Baralle, "Structural determinants of the cellular localization and shuttling of TDP-43," *Journal of Cell Science,* pp. 121:3778-3785, 2008.

[68] M. Sendtner, "TDP-43: multiple targets, multiple disease mechanisms?," *Nature Neuroscience,* vol. 14, no. 4, pp. 403-405, April 2011.

[69] E. Buratti and F. E. Baralle, "The multiple roles of TDP-43 in pre-mRNA processing and gene expression regulation," *RNA Biology,* pp. 420-429, 1 July 2010.

[70] L.-L. Jiang, W. Xue, J.-Y. Hong, J.-T. Zhang, M.-J. Li, S.-N. Yu, J.-H. He and H.-Y. Hu, "The N-terminal dimerization is required for TDP-43 splicing activity," *Scientific Reports,* p. 7:6196, 21 July 2017.

[71] B. A. Berning and A. K. Walker, "The Pathobiology of TDP-43 C-Terminal Fragments in ALS and FTLD," *Frontiers in Neuroscience,* p. 13:335, 11 April 2019.

[72] L. T. Vu and R. Bowser, "Fluid-Based Biomarkers for Amyotrophic Lateral

Sclerosis," *Neurotherapeutics,* pp. 14:119-134, 2017.

[73] M. Salajegheh, J. L. Pinkus, J. P. Taylor, A. A. Amato, R. Nazareno, R. H. Baloh and S. A. Greenberg, "Sarcoplasmic Redistribution of Nuclear TDP-43 in Inclusion Body Myositis," *Muscle Nerve.,* pp. 40(1): 19-31, July 2009.

[74] K. A. Josephs, J. L. Whitwell, S. D. Weigand, M. E. Murray, N. Tosakulwong, A. M. Liesinger, L. Petrucelli, M. L. Senjem, D. S. Knopman, B. F. Boeve, R. J. Ivnik, G. E. Smith, C. R. Jack Jr., J. E. Parisi, R. C. Petersen and D. W. Dickson, "TDP-43 is a key player in the clinical features associated with Alzheimer's disease," *Acta Neuropathologica,* pp. 811-824, 23 March 2014.

[75] N. Aoki, M. E. Murray, K. Ogaki, S. Fujioka, N. J. Rutherford, R. Rademakers, O. A. Ross and D. W. Dickson, "Hippocampal sclerosis in Lewy body disease is a TDP-43 proteinopathy similar to FTLD-TDP Type A," *Acta Neuropathol,* pp. 129(1):53-64, January 2015.

[76] W. Guo, Y. Chen, X. Zhou, A. Kar, P. Ray, X. Chen, E. J. Rao, M. Yang, H. Ye, L. Zhu, J. Liu, M. Xu, Y. Yang, C. Wang, D. Zhang, E. H. Bigio, M. Mesulam, Y. Shen, Q. Xu, K. Fushimi and J. Y. Wu, "An ALS-associated mutation affecting TDP-43 enhances protein aggregation, fibril formation and neurotoxicity," *Nature Structural & Molecular Biology,* pp. 822-830, 12 June 2011.

[77] M. Satoh, M. Kuwana, T. Ogasawara, A. K. Ajmani, J. J. Langdon, D. Kimpel, J. Wang and W. H. Reeves, "Association of autoantibodies to topoisomerase I and the phosphorylated (IIO) form of RNA polymerase II in Japanese scleroderma patients.," *J Immunol,* pp. 153:5838-5848, 1994.

[78] S. Xiang, A. Cooper-Morgan, X. Jiao, M. Kiledjian, J. L. Manley and L. Tong, "Structure and function of the 5'->3' exoribonuclease Rat1 and its activating partner Rai1," *Nature,* pp. 784-8, 9 April 2009.

[79] R. Tomecki, P. J. Sikorski and M. Zakrzewska-Placzek, "Comparison of preribosomal RNA processing pathways in yeast, plant and human cells - focus on coordinated action of endo- and exoribonucleases.," *FEBS Letters,* pp. 1801-1850, July 2017.

[80] I. Memet, C. Doebele, K. E. Sloan and M. T. Bohnsack, *Nucleic Acids*

Research, vol. 45, no. 9, pp. 5359-5374, 04 January 2017.

[81] S. West, N. Gromak and N. Proudfoot, "Human 5′ → 3′ exonuclease Xrn2 promotes transcription termination at co-transcriptional cleavage sites," *Nature,* vol. 432, pp. 522-525, 25 November 2004.

[82] N. Fong, K. Brannan, B. Erickson, H. Kim, M. Cortazar, R. M. Sheridan, T. Nguyen, S. Karp and D. L. Bentley, "Effects of transcription elongation rate and Xrn2 exonuclease activity on RNA polymerase II termination suggest widespread kinetic competition," *Molecular cell,* pp. 60(2):256-267, 15 October 2015.

[83] M. Wang and D. G. Pestov, "50-end surveillance by Xrn2 acts as a shared mechanism for mammalian pre-rRNA maturation and decay," *Nucleic Acids Research,* vol. 39, no. 5, pp. 1811-1822, 2011.

[84] J. C. Morales, P. Richard, P. L. Patidar, E. A. Motea, T. T. Dang, J. L. Manley and D. A. Boothman, "XRN2 Links Transcription Termination to DNA Damage and Replication Stress," *PLoS Genetics,* p. 12(7)e1006107, 20 Jul 2016.

[85] G. R. Sareddy and R. K. Vadlamudi, "PELP1: Structure, biological function and clinical significance," *Gene,* vol. 585, pp. 128-134, 2016.

[86] B. J. Girard, A. R. Daniel, C. A. Lange and J. H. Ostrander, "PELP1: A review of PELP1 interactions, signaling, and biology," *Molecular and Cellular Endocrinology,* vol. 382, no. 1, pp. 642-651, 25 January 2014.

[87] N. Raman, W. Elisabath and S. Müller, "The AAA ATPase MDN1 Acts as a SUMO-Targeted Regulator in Mammalian Pre-ribosome Remodeling," *Molecular cell,* vol. 64, pp. 607-615, 3 November 2016.

[88] C. M. Hickey, N. R. Wilson and M. Hochstrasser, "Function and Regulation of SUMO Proteases," *Nature Reviews Molecular Cell Biology,* pp. 13 (12):755-766, December 2012.

[89] E. Finkbeiner, M. Haindl and S. Muller, "The SUMO system controls nucleolar partitioning of a novel mammalian ribosome biogenesis complex," *The EMBO Journal,* vol. 30, no. 6, pp. 1067-1078, 2011.

[90] N. Raman, A. Nayak and S. Müller, "mTOR Signaling Regulates Nucleolar Targeting of the SUMO-Specific Isopeptidase SENP3," *Molecular and Cellular Biology,* pp. 34 (24):4474-4484, November 2014.

[91] Y.-Q. Mao and W. A. Houry, "The Role of Pontin and Reptin in Cellular Physiology and Cancer Etiology," *Frontiers in Molecular Biosciences,* p. 4:58, 24 August 2017.

[92] S. Gorynia, Structure and Function of the human AAA+ proteins RuvBL1 and RuvBL2 (Doctoral dissertation), Berlin: Fachbereich Biologie, Chemie, Pharmazie der Freien Universität Berlin, 2007.

[93] T. Puri, P. Wendler, B. Sigala, H. Saibil and I. R. Tsaneva, "Dodecameric Structure and ATPase Activity of the Human TIP48/TIP49 Complex," *Journal of Molecular Biology,* vol. 366, no. 1, pp. 179-192, 9 February 2007.

[94] S. Jha and A. Dutta, "RVB1/RVB2: running rings around molecular biology," *Molecular cell,* pp. 34(5):521-533, 12 June 2009.

[95] Y. Makino, T. Mimori, C. Koike, Kanemaki, Masato, Y. Kurokawa, S. Inoue, T. Kishimoto and T.-a. Tamura, "TIP49, Homologous to the Bacterial DNA Helicase RuvB, Acts as an Autoantigen in Human," *BIOCHEMICAL AND BIOPHYSICAL RESEARCH COMMUNICATIONS,* pp. 819-823, 1998.

[96] J. D. Pauling, G. Salazar, H. Lu, Z. E. Betteridge, S. Assassi, M. D. Mayes and N. J. McHugh, "Presence of anti-eukaryotic initiation factor-2B, anti-RuvBL1/2 and anti-synthetase antibodies in patients with anti-nuclear antibody negative systemic sclerosis," *Rheumatology (Oxford),* pp. 57(4):712-717, 1 April 2018.

[97] H. Kokubu, N. Fujimoto, T. Kato, T. Nakanishi, Y. Hamaguchi and T. Tanaka, "Anti-RuvBL1/2 Autoantibody-positive Systemic Sclerosis," *Hifu no kagaku,* vol. 18, no. 4, pp. 226-230, 13 December 2019.

[98] Y. S. Krasikova, N. I. Rechkunova and O. I. Lavrik, "Replication protein A as a major eukaryotic single-stranded DNA-binding protein and its role in DNA repair," *Molecular Biology,* pp. 649-662, 2016.

[99] Y. Zou, Y. Liu, X. Wu and S. M. Shell, "Functions of Human Replication Protein A (RPA): From DNA Replication to DNA Damage and Stress Responses," *J*

Cell Physiol., 208(2): 267-273 August 2006.

[100] R. Garcia-Lozano, I. Wichmann, A. Garcia, J. Sanchez-Roman, F. Gonzalez-Escribano and A. Nunez-Roldan, "Presence of antibodies to replication protein A in some patients with systemic lupus erythematosus (SLE)," *Clinical &Experimental Immunology,* pp. 103(1):74-76, January 1996.

[101] R. Garcia-Lozano, F. Gonzalez-Escribano, J. Sanchez-Roman, I. Wichmann and A. Nunez-Roldan, "Presence of antibodies to different subunits of replication protein A in autoimmune sera," *PNAS,* pp. 92(11): 5116-5120, 23 May 1995.

[102] T. K. Nielsen, S. Liu, R. Lührmann and R. Ficner, "Structural Basis for the Bifunctionality of the U5 snRNP 52K Protein (CD2BP2)," *Journal of Molecular Biology,* pp. 369(4):902-908, 04 April 2007.

[103] M. Heinze, M. Kofler and C. Freund, "Investigating the functional role of CD2BP2 in T cells," *International Immunology,* vol. 19, no. 11, pp. 1313-1318, November 2007.

[104] G. I. Albert, C. Schell, K. M. Kirschner, S. Schäfer, R. A. Müller, B. Kuropka, M. Girbig, N. Hübner, E. Krause, H. Scholz, T. B. Huber, K.-P. Knobeloch and C. Freund, "The GYF domain protein CD2BP2 is critical for embryogenesis and podocyte function," *Journal of Molecular Cell Biology,* pp. 7(5),402-414, 16 June 2015.

[105] G. G. Williamson, J. Pennebaker and J. A. Boyle, "Clinical characteristics of patients with rheumatic disorders who possess antibodies against ribonucleoprotein particles," *Arthritis & Rheumatology,* vol. 26, no. 4, pp. 509-515, April 1983.

[106] P. Migliorini, C. Baldini, V. Rocchi and S. Bombardieri, "Anti-Sm and anti-RNP antibodies," *Autoimmunity,* pp. 38:1, 47-57, 07 Jul 2005.

[107] B. Dema and N. Charles, "Autoantibodies in SLE: Specificities, Isotypes and Receptors," *Antibodies (Basel),* p. 5(1):2, March 2016.

[108] M. B. Coelhe, J. Attig, J. Ule and C. W. Smith, "Matrin3: connecting gene expression with the nuclear matrix," *WIREs RNA,* pp. 7:303-315, 2016.

[109] M. Salton, R. Elkon, T. Borodina, A. Davydov, M.-L. Yaspo, E. Halperin and Y. Shiloh, "Matrin 3 Binds and Stabilizes mRNA," *PLoS ONE,* p. 6(8): e23882, 2011.

[110] M. Gallego-Iradi, H. Strunk, A. M. Crown, R. Davila, H. Brown, E. Rodriguez-Lebron and D. R. Borchelt, "N-terminal sequences in matrin 3 mediate phase separation into droplet-like structures that recruit TDP43 variants lacking RNA binding elements," *Laboratory Investigation ,* pp. 1030-1040, 24 April 2019.

[111] O. Hardiman, A. Al-Chalabi, A. Chio, E. M. Corr, G. Logroscino, W. Robberecht, P. J. Shaw, Z. Simmons and L. H. van den Berg, "Amyotrophic lateral sclerosis," *Nature Reviews Disease Primers,* vol. 3, p. 17071, 5 October 2017.

[112] A. Mensch, B. Meinhardt, N. Bley, S. Hüttelmaier, I. Schneider, G. Stoltenburg-Didinger, T. Kraya, T. Müller and S. Zierz, "The p.S85C-mutation in MATR3 impairs stress granule formation in Matrin-3 myopathy," *Experimental Neurology,* pp. 222-231, 2018.

[113] M. Gallego-Iradi, A. M. Clare, H. H. Brown, C. Janus, J. Lewis and D. R. Borchelt, "Subcellular Localization of Matrin 3 Containing Mutations Associated with ALS and Distal Myopathy," *PLoS ONE,* p. 10(11):e0142144, 2015.

[114] T. A. Martin and W. G. Jiang, "Loss of tight junction barrier function and its role in cancer metastasis," *Biochimica et Biophysica Acta (BBA) - Biomembranes,* vol. 1788, no. 4, pp. 872-891, April 2009.

[115] J. Hou, "Paracellular Channel Formation," in *The Paracellular Channel*, Academic Press, 2019, pp. 9-27.

[116] L. González-Mariscal, A. Betanzos and A. Avila-Flores , "MAGUK proteins: structure and role in the tight junction.," *Semin Cell Dev Biol.,* vol. 11, pp. 315-24, Aug 2000.

[117] K. Ebnet, M. Aurrand-Lions, A. Kuhn, F. Kiefer, S. Butz, K. Zander, M.-K. M. zu Brickwedde, A. Suzuki, B. A. Imhof and D. Vestweber, "The junctional adhesion molecule (JAM) family members JAM-2 and JAM-3 associate with the cell polarity protein PAR-3: a possible role for JAMs in endothelial cell polarity," *Journal of Cell Science,* vol. 116, no. Pt 19, pp. 3879-3891, 2003.

[118] M. Manetti, S. Guiducci, E. Romano, I. Rosa, C. Ceccarelli, T. Mello, A. F. Milia, M. L. Conforti, L. Ibba-Manneschi and M. Matucci-Cerinic, "Differential Expression of Junctional Adhesion Molecules in Different Stages of Systemic Sclerosis," *ARTHRITIS & RHEUMATISM,* vol. 65, no. 1, pp. 247-257, January 2013.

[119] K. Bieber, S. Sun, N. Ishii, M. Kasperkiewicz, E. Schmidt, M. Hirose, J. Westermann, X. Yu, D. Zillikens and R. J. Ludwig, "Animal models for autoimmune bullous dermatoses," *Experimental Dermatology,* pp. 19:2-11, January 2010.

[120] C. M. Hammers and J. R. Stanley, "Mechanisms of Disease: Pemphigus and Bullous Pemphigoid," *Annu. Rev. Pathol. Mech. Dis.,* pp. 11:175-197, 2016.

[121] S. X. Deng, E. Hanson and I. Sanz, "In vivo cell penetration and intracellular transport of anti-Sm and anti-La autoantibodies," *International Immunology,* vol. 12, no. 4, pp. 415-423, April 2000.

[122] M. P. Madaio and K. Yanase, "Cellular Penetration and Nuclear Localization of Anti-DNA Antibodies: Mechanisms, Consequences, Implications and Applications," *Journal of Autoimmunity,* pp. 535-538, October 1998.

[123] M. Reichlin, "Cellular Dysfunction Induced by Penetration of Autoantibodies into Living Cells: Cellular Damage and Dysfunction Mediated by Antibodies to dsDNA and Ribosomal P Proteins," *Journal of Autoimmunity,* pp. 557-561, October 1998.

[124] E. E. Schneeberger and R. D. Lynch, "The tight junction: a multifunctional complex," *Am J Physiol Cell Physiol,* pp. 286:C1213-1228, 1 June 2004.

[125] P. Sobolewski, M. Maslinska, M. Wieczorek, Z. Lagun, A. Malewska, M. Roszkiewicz, R. Nitskovich, E. Szymanska and I. Walecka, "Systemic sclerosis – multidisciplinary disease: clinical features and treatment," *Reumatologia.,* pp. 57(4):221-233, 2019.

[126] EUROIMMUN AG, Test instruciton for Systemic Sclerosis (Nucleoli) Profile, Lübeck, 2016.

[127] A. Robbins, M. Hentzien, S. Toquet, K. Didier, A. Servettaz, B.-N. Pham and D.

Giusti, "Diagnostic Utility of Separate Anti-Ro60 and Anti-Ro52/TRIM21 Antibody Detection in Autoimmune Diseases," *Front Immunol.,* p. 10:444, 12 March 2019.

[128] C. Probst, S. Saschenbrecker, W. Stoecker and L. Komorowski, "Anti-neuronal autoantibodies: Current diagnostic challenges," *Multiple Sclerosis and Related Disorders,* pp. 3(3):303-320, 1 May 2014.

[129] N. van Beek, K. Rentzsch, C. Probst, L. Komorowski, M. Kasperkiewicz, K. Fechner, I. M. Boecker, D. Zillikens, W. Stöcker and E. Schmidt, "Serological diagnosis of autoimmune bullous skin diseases: prospective comparison of the BIOCHIP mosaic-based indirect immunofluorescence technique with the conventional multi-step single test strategy.," *Orphanet journal of rare diseases,* p. 7:49, 9 Augest 2012.

[130] C. D. Hawker, J. R. Genzen and C. T. Wittwer, "Automation in the Clinical Laboratory," in *Tietz Textbook of Clinical Chemistry and Molecular Diagnostics*, N. Rifai, A. R. Horvath and C. T. Wittwer, Eds., Elsevier, 2017, pp. 370.e1-e24.

[131] J. Voigt, C. Krause, E. Rohwäder, S. Saschenbrecker, M. Hahn, M. Danckwardt, C. Feirer, K. Ens, K. Fechner, E. Barth, T. Martinetz and W. Stöcker, "Automated Indirect Immunofluorescence Evaluation of Antinuclear Autoantibodies on HEp-2 Cells," *Clinical and Developmental Immunology,* p. 651058, Oct 2012.

[132] Amisha, P. Malik, M. Pathania and V. K. Rathaur, "Overview of artificial intelligence in medicine," p. 8(7): 2328–2331., July 2019.

[133] P. Hamet and J. Tremblay, "Artificial Intelligence in Medicine," *Metabolism,* pp. 69S:S36-S40, April 2017.

[134] D. D. Miller and E. W. Brown, "Artificial Intelligence in Medical Practice: The Question to the Answer?," *Am J Med,* pp. 131(2):129-133, February 2018.

[135] S. Rauschert, K. Raubenheimer, P. E. Melton and R. C. Huang, "Machine Learning and Clinical Epigenetics: A Review of Challenges for Diagnosis and Classification," *Clin Epigenetics,* p. 12(1):51, 3 April 2020.

[136] J. C. Edwards, L. Szczepanski, J. Szechinski, A. Filipowicz-Sosnowska, P.

Emery, D. R. Close, R. M. Stevens and T. Shaw, "Efficacy of B-Cell–Targeted Therapy with Rituximab in Patients with Rheumatoid Arthritis," *N Engl J Med,* pp. 350:2572-2581, 17 June 2004.

[137] F. Alshaiki, E. Obaid, A. Almuallim, R. Taha, H. El-haddad and H. Almoallim, "Outcomes of rituximab therapy in refractory lupus: A meta-analysis," *Eur J Rheumatol.,* pp. 5(2):226-126, June 2018.

[138] K. Newick, E. Moon and S. M. Albelda, "Chimeric antigen receptor T-cell therapy for solid tumors," *Molecular Therapy - Oncolytics,* p. 3:16006, 13 April 2016.

[139] C. T. Ellebrecht, V. G. Bhoj, A. Nace, E. J. Choi, X. Mao, M. J. Cho, G. Di Zenzo, A. Lanzavecchia, J. T. Seykora, G. Cotsarelis, M. C. Milone and A. S. Payne, "Reengineering chimeric antigen receptor T cells for targeted therapy of autoimmune disease," *Science,* pp. 353(6295):179-84, 8 July 2016.

[140] C. T. Ellebrecht, D. K. Lundgren and A. S. Payne, "On the mark: genetically engineered immunotherapies for autoimmunity," *Current Opinion in Immunology,* vol. 61, pp. 69-73, December 2019.

Appendix 1 List of UNA sera

UNA No.	Volume /ml	estimate titer	ANA Pattern
1	>0.4	1:1000	Granular (mitosis positive)
2	>0.4	1:3200	Granular and nucleolar
3	>0.4	1:1000	Granular and few nuclear dots
4	<0.4	1:320	Granular
5	<0.4	1:1000	Granular (partly stronger)
6	>0.4	1:320	Granular
7	<0.4	1:320	Granular (partly stronger)
8	<0.4	1:1000	Granular
14	<0.4	1:320	Nucleolar
15	<0.4	1:320	Nucleolar
16	>0.4	1:320	Dense fine speckled
17	>0.4	1:1000	Granular and nucleolar
23	>0.4	1:3200	Granular
25	>0.4	1:3200	Homogeneous
26	>0.4	1:3200	Granular and nucleolar
27	<0.4	1:1000	Dense fine speckled
29	>0.4	1:100	Nuclear envelope and nucleolar
30	<0.4	1:1000	Nucleolar
31	<0.4	1:3200	Nucleolar and granular
32	>0.4	1:3200	Granular
33	>0.4	1:1000	Granular
34	>0.4	1:320	Granular
35	>0.4	1:1000	Granular
36	>0.4	1:320	Granular (mitosis positive)
38	>0.4	1:3200	Granular
41	>0.4	1:3200	Granular
43	>0.4	1:1000	Granular
44	>0.4	1:320	Granular and nuclear dots
45	<0.4	1:1000	Dense fine speckled
49	>0.4	1:320	Granular (mitosis positive)
50	<0.4	1:320	Granular (mitosis positive)
51	<0.4	1:1000	Dense fine speckled
52	<0.4	1:10000	Nucleolar and granular (mitosis positive)
53	>0.4	1:3200	Granular (mitosis positive)
54	>0.4	1:320	Granular
56	<0.4	1:320	Dense fine speckled
57	<0.4	1:1000	Granular
61	>0.4	1:3200	Granular
62	>0.4	1:3200	Dense fine speckled
63	>0.4	1:3200	Granular
64	<0.4	1:1000	Nucleolar
65	>0.4	1:3200	Granular
66	<0.4	1:1000	Granular
67	<0.4	1:3200	Granular
68	<0.4	1:1000	Granular
70	>0.4	1:3200	Granular and nuclear dots
71	>0.4	1:1000	Granular
72	>0.4	1:3200	Homogeneous and granular
73	<0.4	1:1000	Granular (partly stronger)
74	>0.4	1:3200	Granular and nucleolar
75	>0.4	1:320	Nucleolar
79	<0.4	1:3200	Nucleolar and granular

81	>0.4	1:1000	Nucleolar
85	<0.4	1:1000	Granular and few nuclear dots
86	>0.4	1:320	Granular
87	>0.4	1:1000	Nucleolar
88	<0.4	1:1000	Granular and nucleolar
92	>0.4	1:3200	Granular
93	<0.4	1:1000	Granular (partly stronger)
94	<0.4	1:1000	Homogeneous
96	>0.4	1:1000	Granular (mitosis positive)
98	<0.4	1:320	Homogeneous
102	>0.4	1:1000	Granular and nucleolar
103	>0.4	1:320	Granular
104	<0.4	1:3200	Nucleolar
105	>0.4	1:1000	Homogeneous and nuclear envelope
106	<0.4	1:320	Granular and nucleolar
108	>0.4	1:1000	Granular and few nuclear dots
110	<0.4	1:1000	Nucleolar
111	>0.4	1:1000	Granular (partly stronger)
112	>0.4	1:1000	Few nuclear dots
116	<0.4	1:1000	Nucleolar
118	<0.4	1:1000	Granular (mitosis positive)
119	>0.4	1:320	Granular (mitosis positive)
121	<0.4	1:1000	Granular (mitosis positive)
123	>0.4	1:1000	Nuclear envelope and granular
124	<0.4	1:100	Nucleolar
125	>0.4	1:1000	Granular and nucleolar
126	<0.4	1:3200	Granular and nucleolar
127	>0.4	1:3200	Homogeneous
128	>0.4	1:320	Nucleolar
129	>0.4	1:3200	Nucleolar
131	>0.4	1:1000	Homogeneous
132	>0.4	1:1000	Homogeneous and nucleolar
133	>0.4	1:1000	Granular
134	>0.4	1:1000	Granular and nucleolar
140	<0.4	1:100	Granular
144	<0.4	1:3200	Dense fine speckled
147	<0.4	1:3200	Granular
148	<0.4	1:3200	Granular
149	<0.4	1:10000	Granular
150	<0.4	1:3200	Granular
151	<0.4	1:3200	Granular
152	<0.4	1:10000	Granular
155	<0.4	1:3200	Granular
157	<0.4	1:1000	Granular
160	<0.4	1:3200	Nucleolar
161	<0.4	1:1000	Homogeneous
162	>0.4	1:10000	Dense fine speckled
163	>0.4	1:100	Granular (mitosis positive)
166	<0.4	1:32000	Nucleolar
167	<0.4	1:1000	Dense fine speckled
168	>0.4	1:1000	Granular (mitosis positive)
169	>0.4	1:1000	Dense fine speckled
170	>0.4	1:10000	Granular and nucleolar
171	<0.4	1:100	Nuclear dots
172	>0.4	1:1000	Dense fine speckled
173	>0.4	1:1000	Homogeneous
174	>0.4	1:1000	Homogeneous

176	>0.4	1:1000	Nucleolar
177	>0.4	1:10000	Granular and nucleolar
178	>0.4	1:1000	Nucleolar
179	>0.4	1:1000	Granular
180	>0.4	1:3200	Granular
183	<0.4	1:1000	Nucleolar
187	<0.4	1:3200	Nuclear envelope and nucleolar
189	>0.4	1:3200	Granular
190	>0.4	1:320	Granular (mitosis positive)
191	<0.4	1:3200	Granular
193	<0.4	1:1000	Nucleolar
194	>0.4	1:3200	Few nuclear dots and Granular
195	>0.4	1:1000	Few nuclear dots
196	<0.4	1:320	Granular (partly stronger)
197	<0.4	1:1000	Granular and nuclear envelope
198	>0.4	1:3200	Homogeneous
199	<0.4	1:320	Homogeneous
200	>0.4	1:3200	Nucleolar
202	>0.4	1:3200	Granular and nucleolar
204	<0.4	1:1000	Nucleolar and homogeneous
205	<0.4	1:1000	Granular and few nuclear dots
206	>0.4	1:1000	Granular and nuclear dot
208	<0.4	1:1000	Granular and homogeneous
209	>0.4	1:320	Granular (mitosis positive)
211	>0.4	1:3200	Granular
214	>0.4	1:320	Centromere
216	>0.4	1:3200	Homogeneous
218	>0.4	1:320	Granular
219	>0.4	1:320	Granular (mitosis positive)
220	>0.4	1:3200	Granular (partly stronger) and centromere
336	>0.4	1:1000	G2-specific nucleolar and granular
337	>0.4	1:320	G2-specific nucleolar
338	>0.4	1:320	G2-specific nucleolar
339	>0.4	1:320	G2-specific nucleolar
340	>0.4	1:1000	G2-specific nucleolar
341	>0.4	1:1000	Spindle apparatus associated granular cytoplasm in G2-cells
342	>0.4	1:1000	Spindle apparatus associated granular cytoplasm in G2-cells
343	>0.4	1:1000	Spindle apparatus associated granular cytoplasm in G2-cells
344	>0.4	1:320	Spindle apparatus associated granular cytoplasm in G2-cells
345	>0.4	1:1000	Spindle apparatus associated granular cytoplasm in G2-cells

Appendix 2 Intensity of healthy control sera in UFO-ANA profile 1

	Poly-Ig control	M	G	A	SMCHD1	CD2BP2	NVL	TDP43	TFAPA2A	TJP1 aa1-575	POLR2A aa1475-1970	PSME3
HC1	89	0	44	0	2	5	5	1	10	2	3	1
HC2	86	0	45	0	1	2	2	1	4	9	4	1
HC3	86	0	42	0	2	1	1	3	4	1	1	1
HC4	87	0	43	0	2	2	2	1	7	5	1	0
HC5	85	0	44	0	1	3	0	1	3	5	0	1
HC6	87	0	46	0	1	0	1	1	1	1	1	1
HC7	89	0	46	0	0	2	0	1	1	0	3	1
HC8	88	0	46	0	1	3	5	0	2	1	2	1
HC9	88	0	45	0	0	2	2	0	3	1	5	0
HC10	88	0	46	0	0	0	0	1	1	0	2	0
HC11	87	0	46	0	2	2	0	1	2	0	1	1
HC12	88	0	45	0	2	2	1	1	12	3	2	1
HC13	88	0	45	0	0	2	0	1	8	2	1	1
HC14	86	0	45	0	1	9	6	1	4	2	3	1
HC15	87	0	46	0	1	1	1	0	6	3	2	0
HC16	86	0	44	0	1	0	0	1	1	2	1	0
HC17	86	0	44	0	4	2	3	1	3	20	4	1
HC18	83	0	44	0	3	3	1	0	2	0	2	0
HC19	87	0	44	0	1	1	1	1	4	0	1	1
HC20	87	0	42	0	1	3	1	1	6	1	5	2
HC21	83	0	42	0	0	1	1	1	2	0	1	1

HC22	81	0	42	0	0	1	0	1	0	0	2	0
HC23	84	1	42	0	0	2	2	1	1	1	1	1
HC24	80	0	43	0	3	5	4	1	7	2	4	1
HC25	83	0	43	0	0	1	0	1	0	0	1	1
HC26	81	0	42	0	0	1	0	1	11	2	1	1
HC27	84	0	43	0	1	1	0	1	4	2	1	1
HC28	82	0	43	0	1	1	0	0	6	0	1	0
HC29	81	1	43	0	1	1	2	0	2	0	2	0
HC30	80	0	43	0	3	1	1	0	4	1	2	1
HC31	86	0	45	0	0	2	2	1	7	1	1	0
HC32	84	0	45	0	1	2	1	1	5	2	1	0
HC33	87	0	46	0	0	1	0	1	3	1	1	1
HC34	85	0	45	0	2	1	0	1	2	0	0	0
HC35	82	0	45	0	1	4	4	1	16	1	2	1
HC36	84	0	44	0	1	1	0	1	1	1	1	0
HC37	78	0	43	0	1	1	4	0	1	0	1	0
HC38	79	0	46	0	0	1	2	1	2	3	2	1
HC39	82	0	46	0	1	0	1	0	2	0	1	0
HC40	83	0	47	0	2	2	2	1	0	0	3	0
HC41	89	0	51	0	1	2	3	1	20	1	1	1
HC42	90	0	49	0	1	2	0	0	5	0	1	0
HC43	89	0	52	0	0	2	1	1	7	1	1	0
HC44	91	0	50	0	0	2	3	1	5	0	1	1
HC45	87	0	47	0	0	2	1	0	5	2	7	2
HC46	85	0	49	0	0	0	0	1	3	0	5	2
HC47	88	0	49	0	1	2	1	0	6	1	1	1

Appendix 2 Intensity of healthy control sera in UFO-ANA profile 1

HC48	88	0	48	0	1	1	0	0	5	3	1	0
HC49	87	0	50	0	2	1	3	1	2	0	2	0
HC50	84	0	49	0	4	3	2	1	7	2	2	1

Appendix 3 List of positive cases in systemic rheumatic disease (SARD) cohort

Levels of RC-IFA: 0=negative, 0.5=borderline, 1-5= weakest positive to strongest positive. Lineblot cut-off for NVL, CD2BP2, TJP1 and AP2A is 20 and for the others is 10.

Target antigen	RC-IFA /level	Lineblot /intensity	Sample No.	Diagnosis	ANA pattern and estimated titer	Additional established ANA
NVL	2	88	SARD34	SSc	Nucleolar 1:1000 and granular cytoplasm 1:1000	Anti-Ro52
	2	90	SARD35			Anti-Ro52
	4	105	SARD361			Anti-Ro52
	4	97	SARD37	SSc	Nucleolar and granular 1:1000	Anti-Ro52
	3	55	SARD210	SSc	Nucleolar, granular and centromere 1:1000	Anti-CenpB and anti-CenpA
	2	8	SARD230	Myositis	Nucleolar and granular 1:320	Anti-PM75
	3	15	SARD309	SSc	Nucleolar and homogenous 1:1000	Anti-Scl70
	4	87	SARD407	SSc	Nucleolar and granular 1:1000	Anti-Ro52 and anti-PM100
PELP1 and SENP3	1	-	SARD305	ASS	Granular and granular cytoplasm 1:320	Anti-Ro52 and anti-NOR90
CD2BP2	-	50	SARD66	SSc	Pseudo-DFS 1:1000	Anti-Ro52 and anti-Scl-70
	-	45	SARD67			
	-	41	SARD128	SSc	Granular 1:320	None
	-	23	SARD146	SSc	Homogeneous 1:1000	Anti-Scl-70 and anti-Th/To
	-	34	SARD210	SSc	Nucleolar, granular and centromere 1:1000	Anti-CenpB and anti-CenpA
	-	25	SARD309	SSc	Nucleolar and homogenous 1:1000	Anti-Scl-70
	-	64	SARD320	SSc	Centromere 1:1000 and granular 1:100	Anti-Ro52, anti-CenpB and anti-CenpA
	-	49	SARD399	SSc	Homogeneous 1:1000	Anti-PM100 and anti-Scl-70
	-	29	SARD490	SSc	Granular cytoplasm 1:1000	Anti-Ro52
	-	37	SARD516	MCTD	Granular 1:3200	Anti-Scl-70
	-	24	SARD518	Myositis	Pseudo-DFS 1:1000	Anti-Ro52 and anti-Ku

Appendix 3 List of positive cases in systemic rheumatic disease (SARD) cohort

Target antigen	RC-IFA /level	Lineblot /intensity	Sample No.	Diagnosis	ANA pattern and estimated titer	Additional established ANA
DHX9	2	-	SARD24	SSc	Granular 1:320 and centromere 1:1000	Anti-CenpB and anti-CenpA
	1	-	SARD295	UCTD	Granular 1:1000	None
	1	-	SARD301	SLE	Granular 1:1000	None
	3	-	SARD333	SSc	Granular 1:320	None
SMCHD1	0	11	SARD179	SSc	Centromere 1:1000	Anti-CenpB
	3	4	SARD312	SSc	Centromere 1:1000 and granular 1:100	Anti-CenpB and anti-CenpA
PSME3	3	16	SARD63	SSc	Homogeneous 1:3200	Anti-Ro52 and anti-Scl-70
	3	11	SARD112	SSc	Pseudo-DFS 1:1000	Anti-Scl-70
	2	2	SARD239	Myositis	Granular and granular cytoplasm 1:100	Anti-Ro52
	4	83	SARD297	SLE	Homogeneous1:3200 and granular cytoplasm 1:100	Anti-Ku and anti-RP11
	0	11	SARD319	SSc	Homogenous 1:1000	Anti-Scl-70
	3	19	SARD349	SSc	Homogenous 1:1000	Anti-Scl-70
	4	49	SARD480	SSc	Homogenous 1:1000	Anti-Ro52, anti-Scl-70 and anti-NOR90
	0	14	SARD515	SLE	Granular 1:3200	Anti-Ro52 and anti-Fibrillarin
	1	32	SARD527	SLE	Homogenous 1:3200	Anti-Ku, anti-PM75 and anti-CenpA
RuvBL1+2	3	-	SARD134	SSc	Granular 1:1000	Anti-NOR90
	3	-	SARD214	SSc	Granular 1:1000	None
RPA1+2+3	2	-	SARD112	SSc	Pseudo-DFS 1:1000	Anti-Scl-70
	3	-	SARD168	SSc	Homogenous 1:3200	Anti-Ro52 and anti-Scl70
	3	-	SARD380	SSc	Centromere 1:1000	Anti-Ro52, anti-CenpB and anti-CenpA
POLR2A	2	4	SARD124	SSc	Pseudo-DFS 1:1000	Anti-Scl-70
	1	1	SARD259	RA	Granular 1:1000	Anti-Ro52 and anti-PM100
	2	1	SARD321	SSc	Centromere 1:1000	Anti-CenpB and anti-CenpA
	2	3	SARD443	SSc	Granular and nucleolar 1:3200	None

Appendix 3 List of positive cases in systemic rheumatic disease (SARD) cohort

Target antigen	RC-IFA /level	Lineblot /intensity	Sample No.	Diagnosis	ANA pattern and estimated titer	Additional established ANA
POLR2A	3	2	SARD510	SLE	Granular 1:1000 and granular cytoplasm 1:320	Anti-Ro52 and anti-CenpA
	1	1	SARD512	SLE	Granular 1:1000	Anti-Ro52
	0	16	SARD440	SSc	Centromere 1:3200	Anti-CenpB and anti-CenpA
	0	12	SARD471	UCTD	Granular 1:100	Anti-Scl-70
	0.5	17	SARD489	SSc	Granular 1:1000	Anti-Ku
	0	15	SARD497	Myositis	Granular 1:1000 and granular cytoplasm 1:320	Anti-Ro52
TDP43	0	17	SARD59	SSc	Homogeneous 1:1000	Anti-Scl70 and anti-PM100
	0	34	SARD141	SSc	Centromere 1:1000	Anti-CenpB and anti-CenpA
	0	51	SARD142			
	0	26	SARD146	SSc	Homogeneous 1:1000	Anti-Scl70 and anti-Th/To
	0	30	SARD418	SSc	Homogeneous 1:1000	Anti-Scl70
	0	61	SARD433	SSc	Homogeneous 1:320 and nucleolar 1:1000	Anti-PM100
TJP1	-	41	SARD4	SSc	Granular 1:100	None
	-	27	SARD19	SSc	Granular and nucleolar 1:320	None
	-	23	SARD72	SSc	Granular and granular cytoplasm 1:320	Anti-Ro52
	-	30	SARD80	SSc	Homogeneous 1:1000	Anti-Scl70
	-	49	SARD89	SSc	Homogeneous 1:1000	Anti-Scl70
	-	27	SARD120	SSc	Centromere 1:320 and granular cytoplasm 1:320	Anti-CenpB and anti-CenpA
	-	60	SARD135	SSc	Homogeneous 1:3200	Anti-Scl70
	-	27	SARD153	SSc	Homogeneous 1:1000	Anti-Ro52 and anti-Scl70
	-	60	SARD159	SSc	Homogeneous 1:1000and granular cytoplasm 1:320	Anti-Ro52 and anti-Scl70
	-	37	SARD196	SSc	Homogeneous 1:3200	Anti-Scl70
	-	29	SARD324	SSc	Granular 1:320 and granular cytoplasm 1:1000	Anti-Ro52
	-	28	SARD337	SSc	Centromere 1:1000 and granular cytoplasm 1:320	Anti-CenpB, anti-CenpA and anti-

Appendix 3 List of positive cases in systemic rheumatic disease (SARD) cohort

Target antigen	RC-IFA /level	Lineblot /intensity	Sample No.	Diagnosis	ANA pattern and estimated titer	Additional established ANA
TJP1						PM100
	-	60	SARD353	SSc	Centromere 1:320, nuclear envelope 1:100 and granular cytoplasm 1:100	Anti-Ro52 and anti-CenpB, anti-CenpA
	-	50	SARD372	SSc	Homogeneous 1:1000	Anti-Scl70 and RP155
	-	26	SARD385	SSc	Homogeneous 1:1000	Anti-Scl70
	-	60	SARD502	UCTD	Homogeneous 1:1000 and granular cytoplasm 1:320	Anti-Ku and anti-NOR90
TFAP2A	3	81	SARD518	Myositis	Pseudo-DFS 1:100	Anti-Ro52 and anti-Ku
	1	84	SARD259	RA	Granular 1:1000 and granular cytoplasm 1:100	Anti-Ro52 and anti-PM100
	0	93	SARD7	SSc	Centromere 1:1000 and granular cytoplasm 1:100	Anti-Ro52, anti-CenpB and anti-CenpA
	0	50	SARD1	SSc	Granular 1:1000	Anti-Ro52 and anti-Scl70
	0	50	SARD21			
	0	50	SARD22			
	0	23	SARD29	SSc	Centromere and granular cytoplasm 1:320	Anti-CenpB and anti-CenpA
	0	78	SARD34	SSc	Nucleolar 1:1000 and granular cytoplasm 1:1000	anti-Ro52
	0	69	SARD35			
	0	81	SARD361			
	0	29	SARD90	SSc	Nucleolar and granular 1:1000	Anti-PM100 and anti-RP11
	0	23	SARD91	SSc	Homogeneous and nucleolar1:1000	Anti-PM100 and anti-Scl70
	0	25	SARD102	SSc	Homogeneous 1:3200	Anti-CenpB and anti-Scl70
	0	83	SARD118	SSc	Pseudo-DFS 1:1000	anti-Scl70
	0	35	SARD141	SSc	Centromere 1:1000	Anti-CenpB and anti-CenpA
	0	47	SARD142			
	0	21	SARD155	SSc	Homogeneous 1:1000	Anti-Ro52, anti-Ku and anti-Scl70
	0	22	SARD186	SSc	Granular 1:100	none

Target antigen	RC-IFA /level	Lineblot /intensity	Sample No.	Diagnosis	ANA pattern and estimated titer	Additional established ANA
TFAP2A	0	23	SARD189	SSc	Granular 1:1000	Anti-Ro52 and anti-CenpA
	0	42	SARD223	SSc	Granular 1:1000	Anti-Ro52 and anti-Scl-70
	0	43	SARD229	pSS	Granular 1:1000	Anti-Ro-52 and anti-Scl70
	0	30	SARD238	ASS	Granular 1:320 and granular cytoplasm 1:1000	Anti-Ro-52
	0	25	SARD297	SLE	Homogeneous1:3200 and granular cytoplasm 1:100	anti-Ku and anti-RP11
	0	29	SARD335	SSc	Centromere 1:1000	Anti-CenpB and anti-CenpA
	0	29	SARD370	SSc	Homogeneous 1:1000	Anti-Scl70
	0.5	49	SARD379	SSc	Granular and nucleolar 1:1000	Anti-PM75
	0	57	SARD438	SSc	Granular and nucleolar 1:1000	Anti-Ro-52, anti-Th/To and anti-PM100
	0	30	SARD440	SSc	Centromere 1:3200 and granular cytoplasm 1:100	Anti-CenpB and anti-CenpA
	0	47	SARD448	SSc	Centromere and granular cytoplasm 1:1000	Anti-CenpB and anti-CenpA
	0	30	SARD462	SSc	Homogeneous 1:3200	Anti-Scl70 and anti-Th/To
	0	29	SARD482	SSc	Homogeneous 1:3200	Anti-Scl70
	0	64	SARD486	SSc	Centromere and granular cytoplasm 1:320	Anti-Ro52, anti-CenpB and anti-CenpA
	0	45	SARD495	SSc	Centromere 1:1000 and granular cytoplasm 1:100	Anti-CenpB and anti-CenpA
	0	21	SARD521	MCTD	Granular 1:3200	Anti-Ku and anti-NOR90
	0	74	SARD523	RA	Granular and nucleolar 1:1000	Anti-Ro52